Numerical and experimental investigation of high-performance sonochemical reactors

Zheng XU

Contents

Chapter 1 Introduction 1

1.1 Acoustics 2

1.2 Acoustic cavitation 2

1.3 Sonochemical reaction 4

1.4 Application of sonochemistry 5

1.5 Related works (Experimental) 5

1.5.1 Ambient temperature 6

1.5.2 Ultrasonic frequency 6

1.5.3 Ultrasound intensity 7

1.5.4 Enhancement of sonochemical effects 7

1.5.5 Advanced oxidation processes (AOPs) 10

1.6 Related works (Theoretical) 12

1.7 Research objectives and structure of this thesis 13

1.7.1 Research objectives 13

1.7.2 Structure of this thesis 13

References 15

Chapter 2 Numerical simulation of liquid velocity distribution in a sonochemical reactor 22

2.1 Introduction 23

2.2 Calculation modeling 23

2.2.1 Acoustic pressure distribution 23

2.2.2 The flow field 27

2.3 Results and discussion 29

2.3.1 Acoustic pressure distribution 29

2.3.2 Liquid velocity distribution 31

2.4 Conclusions 43

References 45

Chapter 3 Numerical simulation of sonochemical reaction field in a sonochemical reactor 47

3.1 Introduction 48

3.2 Calculation modeling 49

3.3 Results and discussion 51

3.3.1 The threshold of a transient cavitation bubble 51

3.3.2 The absorption coefficient 52

3.3.3 Setting of liquid surface 53

3.3.4 Dual transducer irradiation 56

3.3.5 Influence of reflection plate 58

3.4 Conclusions 59

References 60

Chapter 4 Enhancement of sonochemical reaction by dual-pulse ultrasound 61

4.1 Introduction 62

4.2 Experiment methods 62

4.2.1 Apparatus 62

4.2.2 Sample 63

4.2.3 Visualization 64

4.2.4 Power-modulated pulsed wave 64

4.3 Results and discussion 65

4.3.1 Oxidation of KI solution 65

4.3.2 Degradation of AO7 solution 74

4.4 Conclusions 75

References 76

Chapter 5 Advanced oxidation processes for wastewater treatment 77

5.1 Introduction 78

5.2 Dynamical properties of iodine release under combination of ultrasound and light irradiations 78

5.2.1 Introduction 78

5.2.2 Apparatus and methods 79

5.2.3 Results and discussion 81

5.2.4 Conclusions 90

5.3 Effects of operational conditions on 1,4-dioxane degradation by combined use of ultrasound and ozone microbubbles 92

5.3.1 Introduction 92

5.3.2 Experimental procedure 93

5.3.3 Results and discussion 95

5.3.4 Conclusions 106

References 107

Chapter 6 Conclusions and future works 110

6.1 Conclusions 111

6.2 Future works 113

Chapter 1

Introduction

1.1 Acoustics

Sound is a mechanical wave that is an oscillation of pressure transmitted through a solid, liquid or gas by vibrations. Sound pressure is the local pressure deviation from ambient atmospheric pressure caused by a sound wave. In air, it can be measured by using a microphone and in water by using a hydrophone.

Sound pressure in a lossless medium can be governed by the following equation:

$$\frac{1}{\rho_0 c_s^{\,2}} \frac{\partial^2 p}{\partial t^2} + \nabla^2 \cdot \left(-\frac{p}{\rho_0}\right) = 0 . \tag{1-1}$$

Here ρ_0 refers to the density of the media, and c_s denotes the speed of sound. p and t represent acoustic pressure and irradiation time, respectively.

Ultrasound is defined as sound above the upper threshold of human hearing (>20 kHz). It has several characteristics which make it useful in many applications.

- It is inaudible to humans.
- Ultrasound waves can be produced with high directivity.
- It is a compressional vibration of matter.

Power ultrasound can be used in chemistry. Ultrasound does not interact directly with molecules to induce the chemical change, as its typical wavelength is too long compared to molecules. Instead, it causes cavitations which induce extremely high temperature and pressure in a liquid.

1.2 Acoustic cavitation

Acoustic cavitation is the formation and immediate implosion of cavities in a liquid. It occurs when the liquid is subjected to rapid changes of an acoustic field, and causes the formation of cavities where pressure is relatively low.

The formation, growth, and implosive collapse of cavitation bubbles are the origin for sonochemistry. These gas bubbles will alternately expand and compress under

the mechanical influence of the sound wave.

The bubble oscillating motion can be numerically calculated by using the RPNNP equation [1]:

$$R\frac{d^2R}{dt^2}+\frac{3}{2}(\frac{dR}{dt})^2=\frac{1}{\rho}[(p_0+\frac{2\tau}{R_0}-p_v)(\frac{R_0}{R})^3+p_v-\frac{2\tau}{R_0}-\frac{4\eta}{R}\frac{dR}{dt}-p_0-p], \qquad (1\text{-}2)$$

where R is the radius of the cavitation bubble, ρ is the density of the medium, p_0 is the static pressure in the medium, τ is the surface tension of the cavitation bubble, R_0 is the equilibrium radius of the cavitation bubble, p_v is vapor pressure, p is pressure imposed on a fluid, and η is the shear viscosity.

As the amount of material entering the bubble during the expansion half cycle is more than that expelled during the compression cycle, these cavitation bubbles grow over many acoustic cycles, and finally reach a critical size at which a resonance condition is met. These critical sized bubbles become extremely unstable, and grow to the maximum size, where they finally violently implosion. The scheme is depicted in Fig. 1-1.

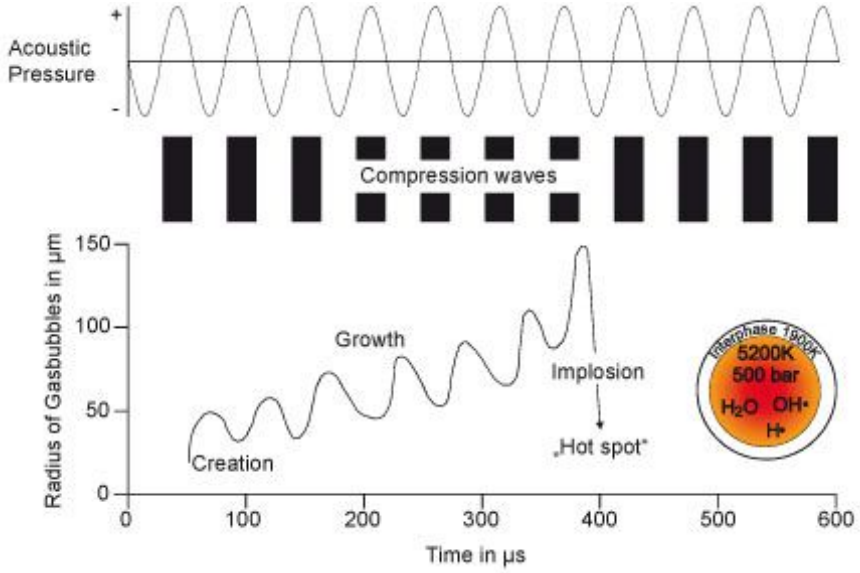

Fig. 1-1 Creation, growth and implosion of a cavity in a liquid.

With a known initial cavitation bubble radius and ultrasonic frequency, the

pressure threshold for bubble implosion could be calculated [2].

During implosion, extremely high pressure and temperature is generated inside the bubble leading to the formation of highly active hydrogen and hydroxide radicals, which play a critical role in the chemical effects of ultrasound. At the same time, the physical effects of cavitation (e.g., micro-streaming, micro-jetting shockwave, and turbulence) also contribute to the enhancement of the chemical reaction performance.

Due to its unique chemical and physical effects, acoustic cavitations have been applied to a number of areas, including: therapeutic applications, contrast imaging, electrochemistry, food technology, nano-materials synthesis, materials extraction, phase separation, surface cleaning and sonochemical reaction.

1.3 Sonochemical reaction

Sonochemistry is a field that deals with chemistry produced and enhanced by ultrasound via cavitation bubbles. Sonochemical treatment typically operates at ambient conditions and does not require the addition of extra chemicals. Generally, sonochemistry has many unique characteristics:

- Extremely high temperature and pressure achieved at the final stage of bubble collapse provides a means of ‘hot spot’ substances in a liquid. This unusual phenomenon makes it possible to produce highly reactive oxidizing agent OH radicals directly from water, and to initiate and enhance reactions that require high temperature and pressure. In addition, the rapid heating and cooling process associated with bubble oscillations makes it also possible to synthesize new materials with extraordinary properties that cannot be realized by conventional means.
- Sonochemical reactions occur locally on particle surfaces when reactions

involve solid particles. In response to a sound field, a fluid tends to move faster than solid particles due to its relatively low density. As a result, a low pressure region is created on particle surfaces in the rarefaction cycle of the sound. Cavitation bubbles form at the crevices on particles and collapse locally when the compression cycle of the wave arrives. This characteristic makes ultrasonic cavitation a very useful candidate for treating dilute contaminated streams.

- The rapid collapse of bubbles in sonochemistry induces very strong shear flows. In additions to enhance mixing and mass transfer in the solution, these shear flows can disrupt the phase boundary between immiscible liquids and increase reaction area.
- When a bubble undergoes asymmetric collapse near a solid boundary or other bubbles, the forming and impingement of a micro-jet result in surface cleaning and pitting. This mechanism is very useful in processing materials and enhancing reactions involving metals, power or other particulate reagents.

1.4 Application of sonochemistry

Sonochemical reactions have been used in wastewater treatment. The generation of highly reactive primary radicals during cavitation and the presence of extreme conditions inside the bubbles provided the conditions to degrade almost all organic compounds around or inside the cavitation bubbles.

Sonochemical reactions have also been extensively used in materials synthesis, specifically for a broad range of inorganic materials. One of these sonochemical synthesis processes is the preparation of very narrow size distribution for metal particles.

1.5 Related works (Experimental)

The first work of sonochemistry was reported by Richards and Loomis [3], ‘The

chemical effects of high frequency sound waves'. They described two types of chemical reactions: 1. the acceleration of conventional reactions by ultrasound. 2. redox processes in aqueous solution, such as the oxidation of sulphite.

According to the summary by Thompson and Doraiswamy [4], the sonochemical reaction rate is mostly affected by ambient temperature, the ultrasonic frequency and the ultrasonic intensity.

1.5.1 Ambient temperature

Contrary to chemical reactions in general, an increase in ambient reaction temperature results in an overall decrease in the sonochemical effect. The follows was summarized by Adewuyi [5]:

- The lowing temperature decreases the solvent vapor pressure which increases the intensity of cavitation. At low vapor pressure, fewer vapors have an opportunity to diffuse into the bubble and thus cushion the cavitational collapse, therefore making the implosion more violent.
- As liquid temperature decreases, the amount of gas dissolved increases and the vapor pressure of the liquid decreases.

1.5.2 Ultrasonic frequency

The frequency of ultrasound has a significant effect on the cavitation process because it alters the critical size of the cavitation bubbles. At very high frequencies, the cavitational effect is reduced because:

- The rarefaction cycle of the sound wave produces a negative pressure which is insufficient in its duration and/or intensity to initiate cavitation.
- The compression cycle occurs faster than the time required for the microbubble to collapse.

However, current research finds out that high frequencies may lead to higher

reaction performances. In the work by Entezari et al. [6], the rate of sonochemical oxidation of iodide was 31 times greater when operating at a frequency of 900 kHz compared to 20 kHz. They ascribed the increase of reaction to the formation of hydroxyl radicals from the air-water mixture was accelerated because of the larger number of useful cavitational events at 900 kHz. The similar results have also been carried out by Petrier et al. [7] and Hua et al. [8]. Petrier et al. reasoned that because bubble lifetimes were shorter at higher frequencies, the OH radicals have an opportunity to escape the cavitation bubble before undergoing any reaction or recombination. Koda et al. [9] standardized the sonochemical efficiency (SE) for many sonochemical reactors. The maximum of sonochemical effects were observed around 300 kHz. The SE values in the range of frequency of 200-500 kHz are 10 times higher than those in the low and high frequency regions.

1.5.3 Ultrasound intensity

Chendke et al. [10] concluded that the reaction performance increase with increasing acoustic pressure of the system due to the magnified effect of cavitation implosions. An increase in the ultrasound intensity means an increase in the acoustic pressure amplitude. The collapse time, the released temperature, and the pressure on collapse are all dependent on the acoustic amplitude. The cavitation bubble collapse will be more violent at higher acoustic amplitudes. Therefore, as the power is increased, the reaction rate also increases in most cases. However, as pressure increases, the intensity must be increased to obtain cavitation in the first place. Too much pressure reduces the rate of reaction by decreasing the frequency or efficiency of bubble formations [11].

1.5.4 Enhancement of sonochemical effects

(1) Pulsed wave

When ultrasound waves are generated with a certain pulsed mode, some cavitational effects may occur to a greater degree than when the same acoustic signal is applied in continuous wave. Leighton clarified aspects opened by many papers, including the “activity” of the system, the recycling periodic cavities through resonance, the survival of unstabilized nuclei, the transient excitation, and the bubble migration.

Henglein et al. [12,13] investigated the effects of the pulsed on and off times on the oxidation of potassium iodide (KI) solution. The mechanism for pulsed wave was discussed in terms of the relative contributions of “stable” and “transient” cavitation. Casadonte et al. [14] explored the effects of pulse waveform and frequency on the oxidation of potassium iodide and the degradation of acid orange at 500 kHz. The power-modulated pulsed ultrasound was used. An oxidation rate increased by a factor of 3 as compared with a continuous irradiation was observed under conditions of equivalent acoustic input power. Sonochemical reaction fields visualized by luminal sonoluminescence were increased under the pulsed conditions. Tuziuti et al. [15] also examined the effect of liquid volume on sonochemical reaction. Enhancement of reaction performance was observed and they ascribed the enhancement to the residual pressure amplitude during the pulsed off time and the spatial enlargement of active reaction sites.

(2) Superposition of ultrasonic fields

In order to enhance reaction performances, superposition of ultrasonic fields with dual frequency to enhance sonochemical reactions has been widely investigated. Tatake and Pandit [16] investigated the use of dual frequency sound source experimentally and theoretically. They compared numerical results of bubble motions for dual frequency source to that of a single frequency source at equal level

of energy dissipation per unit volume. Servant et al. [17] modified the CAMUS code originally developed for a single frequency sonication to include the dual frequency sonication effects. They pointed out that the dual frequency sonication involves more intense cavitation bubble field. Sivakumar et al. [18] have experimentally proved that the energy efficiency as well as cavitational effects for dual frequency sonication is higher than the single frequency sonication. Zhu et al. [19] carried out ultrasonic irradiation at 28 kHz combined with 0.87 MHz sound sources and reported that the dual source irradiation resulted into more iodine liberation than the arithmetic sum of the quantity produced by two individual sonication modes. Suzuki et al. [20] examined the effect of superposition of two ultrasonic fields on the KI solution. In this case, the enhancement of sonochemical effect for dual frequency irradiation was evident below 100 kHz. Yasuda et al. [21] used an ultrasonic dual frequency reactor, and investigated the fluorescence intensity of terephthalate ion in the frequency range from 176 kHz to 635 kHz. When the frequency of transducer attached at the bottom wall was comparable in magnitude to that at the side wall, a high enhancement of fluorescence intensity was observed compared with the sum of fluorescence intensities when using a single transducer. Furthermore, the enlargement of reaction field was also observed using luminal solution.

(3) Liquid flow

Liquid flow and liquid mixing enhance sonochemical reaction rate. Yasuda et al. [22] reported that the sonochemical decomposition conversion of 5, 10, 15, 20-Tetrakis (4-sulfotophenyl) porphyrin was enhanced by liquid mixing with a stirring device. Hatanaka et al. [23] have investigated the effects of ultrasonic frequency (20-131 kHz) and power on the intensity of the sonochemical luminescence of luminal, when liquid mixing was applied. They reported that fluid

flow can cause the enhancement of multibubble sonoluminescence under suitable conditions. Kojima et al. [24] used a rectangular sonochemical reactor at a frequency of 490 kHz with a stirrer to examine the effect of liquid flow on the sonochemical efficiency and the area of chemical lunimnescence in the reactor. Results indicate that the sonochemical efficiency increases with the rotational speed of the stirrer. Some researches indicate the enhancement by liquid flow is due to the acceleration of mass transfer [25,26].

In recent years, the quantificational measurement of a flow field and the relationship between flow field and sonochemical reaction performance have been drawn attention by many researchers. Chouvellon et al. [27] measured the liquid velocity distribution by using a particle image velocimeter, and they found out that the liquid velocity increased with viscosity. Mandroyan et al. [28,29] used the sonochemical reactor with an electrode and a horn type transducer to visualize the cavitation bubbles by laser tomography technique. They also measured the flow velocity distribution by use of a particle image velocimeter.

1.5.5 Advanced oxidation processes (AOPs)

All AOPs are characterized by a common chemical feature: the capability of exploiting the high reactivity of OH radicals in driving oxidation processes which are suitable for achieving complete abatement and through mineralization of even less reactive pollutants. One of the problems with sonolysis is the low decomposition efficiency. In order to increase reaction efficiency, many researchers reported the combination of sonolysis and any other AOPs is necessary.

Generally, these methods involve various combinations of ozone, hydrogen peroxide, sonolysis, ultraviolet radiation, and photocatalytic treatments [30].

(1) Ultrasound + Light treatment

Gaplovsky et al. [31] investigated the effect of ultrasound on the photochemical reaction of diphenyl ether. They indicated that ultrasound enhanced the rate of phenol formation, especially at higher concentrations of diphenyl ether. Rashid et al. [32] checked the photolysis, sonolysis and photosonolysis of common groundwater contaminants (1,1,1-trichloroethane, trichloroethylene, and tetrachloro-ethylene). The process using photosonolysis exhibited higher degradation efficiencies than that with sonolysis and photolysis separately in most cases. To enhance reaction efficiencies, researchers added catalyst [33] or photocatalyst [34]. However, ultraviolet light accounts for only 4% of the incoming solar energy, which leads to the too low efficiency in degrading organic pollutants, and fails to the practical application. In recent years, some works have been carried out by using ultrasound and visible light irradiation. However, the addition of photocatalyst is necessary [35,36]. In many researches, the synergistic effect was observed by the combined use of ultrasound and light. This effect was explained by the direct photolysis of the hydrogen peroxide produced during the ultrasound treatment [37,38]:

$$H_2O_2 \text{ (generated by ultrasound process)} + h\gamma \rightarrow \cdot OH + \cdot OH \qquad (1\text{-}3)$$

(2) Ultrasound+Ozone

The combination use of ozone and ultrasound in degradation of compounds has been widely investigated [39-42]. Tezcanli-Güyer and Ince [43] investigated the individual and the combined effects of ultrasound and ozone using acid orange 7 (C.I. 15510). They analyzed the decay of absorbance at maximum absorption of the dye. The result showed that decolorization by US/O_3 was 272% faster than that by ultrasound alone.

The use of ozone in AOPs is widely popular with the advantage that ozone reacts with organic compounds either directly and/or indirectly by decomposition at highly

pH [44]. Combined operation of sonolysis and ozonation renders synergistic effects in organic matter destruction. The synergy is partly due to excess hydroxyl radicals formed upon thermal decomposition of ozone in the gas phase:

$$O_3(g) +))) \rightarrow O_2(g) + O(3P)(g), \quad (1\text{-}4)$$

$$O(3P)(g) + H_2O(g) \rightarrow 2{\cdot}OH(g), \quad (1\text{-}5)$$

and partly to increased mass transfer of ozone in solution by mechanical effects of ultrasound [45,46].

1.6 Related works (Theoretical)

(1) Pressure field

Since the cavitation is driven by an acoustic pressure field, studies of pressure field distributions in sonochemical reactor are very important in understanding and improvement of sonochemical reactors.

Ando et al. [47] and Liu et al. [48] reported the FEM calculation of an acoustic field in an ultrasonic cleaning vessel taking into account the effect of the vibration of the vessel wall. However, the effect of bubbles in the acoustic field was neglected. Dähnke et al. [49] modeled linear pressure fields in sonochemical reactors with homogeneous and inhomogeneous density distributions of cavitation bubbles. They considered gas bubbles in a liquid lead to a heavy change of phase velocity and sound attenuation. Furthermore, they compared their theoretical results to the experiment results [50]. Servant et al. calculated pressure fields in sonochemical reactor with (28.2 kHz) low frequency ultrasound [51] and (477 kHz) high frequency ultrasound [52]. Yasui et al. [53] numerically calculated spatial distributions of the acoustic amplitude in a sonochemical reactor using the finite element method (FEM). The boundary condition, attenuation coefficient and standing wave pattern of an acoustic field have been investigated.

(2) Acoustic streaming

Acoustic streaming is forced by the action of the Reynolds stress, defined as the mean value of the acoustic momentum flux.

The classical treatment of acoustic streaming due to the action of Reynolds stress forcing resisted by viscosity was carried out by Nyborg [54]. Rudenko and Soluyan confirmed that the streaming velocity is a function of propagation distance in their theoretical work [55]. Wu et al. [56] developed the theory of deriving the approximate solution to the Nyborg equation. Mitome et al. [57] investigated the acoustic nonlinearity in acoustic streaming. As the distance from transducer became longer, the streaming velocity increased near sound source and deceased at far distance. Kamakura et al. [58] theoretically and experimentally investigated the streaming velocity along the axis of ultrasonic propagation for the 5 MHz transducer. They simulated the liquid flow in ultrasonic fields.

1.7 Research objectives and structure of this thesis

1.7.1 Research objectives

The first objective of this research is to understand the mechanisms of the enhancement of the sonochemical reaction. The acoustic pressure and liquid flow distribution influence has been investigated, and the methods to enhance sonochemical reaction performance have been suggested.

In addition, we experimentally checked the enhancement of superposition of pressure field by using dual-pulsed wave. The combinations of AOPs have also been experimentally investigated. The synergistic effect analysis indicates the liquid flow is important in sonochemical reaction performance.

1.7.2 Structure of this thesis

In this thesis, the sonochemical reaction performance, the combined use of

ultrasound and ultraviolet/visible light, dual-pulsed ultrasound, combined use of ultrasound and ozone microbbles, the ultrasound induced flow field and dual-ultrasound have been investigated. Specifically, this thesis will address the following issues of the sonochemical phenomenon:

- The liquid velocity distribution induced by ultrasound in a sonochemical reactor
- The pressure distribution induced by single and dual ultrasound in a sonochemical reactor
- The enhancement of sonochemical reaction by use of power-modulated dual pulsed waves
- The dynamic process of iodine release under the irradiations of ultrasound and visible light, respectively and simultaneously
- The operational conditions on 1,4-dioxane degradation by combined use of ultrasound and ozone microbubbles and the mechanism discussion

References

[1] C. Wu, J. Tsao, The ultrasonic weak short-pulse responses of microbubbles based on a two-frequency approximation. *J. Acoust. Soc. Am.*, **114**, 2662-2671 (2003).

[2] J. Šponser, Dependence of the cavitation threshold on the ultrasonic frequency. *Czech. J. Phys.*, **40**, 1123-1132 (1990).

[3] W. T. Richards, A. L. Loomis, The chemical effects of high frequency sound waves I. A preliminary survey. *J. Am. Chem. Soc.*, **49**, 3086-3100 (1927).

[4] L. H. Thompson, L. K. Doraiswamy, Sonochemistry, science and engineering. *Ind. Eng. Chem. Res.*, **38**, 1215-1249 (1999).

[5] Y. G. Adewuyi, Sonochemistry: environmental science and engineering applications. *Ind. Eng. Chem. Res.*, **40**, 4681-4715 (2001).

[6] M. H. Entezari, P. Kruus, Effect of frequency on sonochemical reactions. I: Oxidation of iodide. *Ultrason. Sonochem.*, **1**, S75-S79 (1994).

[7] C. Petrier, A. Jeunet, J. L. Luche, G. Reverdy, Unexpected frequency effects on the rate of oxidative processes induced by ultrasound. *J. Am. Chem. Soc.*, **114**, 3148-3150 (1992).

[8] I. Hua, M. R. Hoffmann, Optimization of ultrasonic irradiation as an advanced oxidation technology. *Environ. Sci. Technol.*, **31**, 2237-2243 (1997).

[9] S. Koda, T. Kimura, T. Kondo, H. Mitome, A standard method to calibrate sonochemical efficiency. *Ultrason. Sonochem.*, **10**, 149-156 (2003).

[10] P. K. Chendke, H. S. Fogler, Second-order sonochemical phenomena ─ extensions of previous work and applications in industrial processing. *Chem. Eng. J.*, **8**, 165-178 (1974).

[11] J. P. Lorimer, T. J. Mason, Sonochemistry, part 1- The physical aspects, *Chem. Soc. Rev.*, **16**, 239-247 (1987).

[12] A. Henglein, Chemical effects of continuous and pulsed ultrasound in aqueous solutions. *Ultrason. Sonochem.*, **2**, S115-S121 (1995).

[13] A. Henglein, R. Ulrich, J. Lilie, Luminescence and chemical action by pulsed ultrasound. *J. Am. Chem. Soc.*, **111**, 1974-1979 (1989).

[14] D. J. Casadonte Jr, M. Flores, C. Petrier, Enhancing sonochemical activity in aqueous media using power-modulated pulsed ultrasound: an initial study. *Ultrason. Sonochem.*, **12**, 147-152 (2005).

[15] T. Tuziuti, K. Yasui, J. Lee, T. Kozuka, A. Towata, Y. Iida, Mechanism of enhancement of sonochemical-reaction efficiency by pulsed ultrasound. *J. Phys. Chem. A*, **112**, 4875-4878 (2008).

[16] P. A. Tatake, A. B. Pandit, Modeling and experimental investigation into cavity dynamics and cavitational yield: influence of dual frequency ultrasound sources. *Chem. Eng. Sci.*, **57**, 4987-4995 (2002).

[17] G. Servant, J. L. Laborde, A. Hita, J. P. Caltagirone, A. Gerad, On the interaction between ultrasound waves and bubble clouds in mono- and dual-frequency sonoreactors. *Ultrason. Sonochem.*, **10**, 347-355 (2003).

[18] M. Sivakumar, P. A. Tatake, A. B. Pandit, Kinetics of p-nitrophenol degradation: effect of reaction conditions and cavitational parameters for a multiple frequency system. *Chem. Eng. J.*, **85**, 327-338 (2002).

[19] C. P. Zhu, R. Feng, Y. Y. Zhao, Sonochemical effect of bifrequency irradiation. *Chin. Sci. Bull.*, **45**, 142-145 (2000).

[20] T. Suzuki, K. Yasui, K. Yasuda, Y. Iida, T. Tuziuti, T. Torii, M. Nakamura, Effect of dual frequency on sonochemical reaction rates. *Res. Chem. Intermed.*, **30**, 703-711 (2004).

[21] K. Yasuda, T. Torii, K. Yasui, Y. Iida, T. Tuziuti, M. Nakamura, Y. Asakura,

Enhancement of sonochemical reaction of terephthalate ion by superposition of ultrasonic fields of various frequencies. *Ultrason. Sonochem.*, **14**, 699-704 (2007).

[22] K. Yasuda, M. Tachi, Y. Bando, M. Nakamura, Effect of liquid mixing on performance of porphyrin decomposition of organic material by ultrasonic irradiation. *J. Chem. Eng. Jpn.*, **32**, 347-349 (1999).

[23] S. Hatanaka, H. Mitome, K. Yasui, S. Hayashi, Multibubble sonoluminescence enhancement by fluid flow. *Ultrasonics*, **44**, e435-e438 (2006).

[24] Y. Kojima, Y. Asakura, G. Sugiyama, S. Koda, The effects of acoustic flow and mechanical flow on the sonochemical efficiency in a rectangular sonochemical reactor. *Ultrason. Sonochem.*, **17**, 978-984 (2010).

[25] D. V. Sakharov, R. T. Hekkenberg, D. C. Rijken, Acceleration of fibrinolysis by high-frequency ultrasound: the contribution of acoustic streaming and temperature rise. *Thromb. Res.*, **100**, 333-340 (2000).

[26] A. Simon, L. Penpenic, N. Gondrexon, S. Taha, G. Dorange, A comparative study between classical stirred and ultrasonically assisted dead-end ultrafiltration. *Ultrason. Sonochem.*, **7**, 183-186 (2000).

[27] M. Chouvellon, A. Largillier, T. Fournel, P. Boldo, Y. Gonthier, Velocity study in an ultrasonic reactor. *Ultrason. Sonochem.*, **7**, 207-211 (2000).

[28] A. Mandroyan, R. Viennet, Y. Bailly, M. L. Doche, J. Y. Hihn, Modification of the ultrasound induced activity by the presence of an electrode in a sonoreactor working at two low frequencies (20 and 40 kHz). Part I: active zone visualization by laser tomography. *Ultrason. Sonochem.*, **16**, 88-96 (2009).

[29] A. Mandroyan, M. L. Doche, J. Y. Hihn, R. Viennet, Y. Bailly, L. Simonin, Modification of the ultrasound induced activity by the presence of an electrode in

a sonoreactor working at two low frequencies (20 and 40 kHz). Part II: mapping flow velocities by particle image velocimetry (PIV). *Ultrason. Sonochem.*, **16**, 97-104 (2009).

[30] C. G. Joseph, Sonophotocatalysis in advanced oxidation process: a short review. *Ultrason. Sonochem.*, **16**, 583-589 (2009).

[31] A. Gáplovský, J. Donovalova, Š. Toma, B. Jakubikova, R. Mracnova, The effect of ultrasound on diphenyl ether photochemistry. *Chem. Pap.*, **57**, 250-254 (2003).

[32] M. M. Rashid, C. Sato, Photolysis, sonolysis, and photosonolysis of trichloroethane (TCA), Trichloroethylene (TCE), and tetracloroethylene (PCE) without catalyst. *Water, Air, & Soil Pollution*, **216**, 429-440 (2011).

[33] T. Zhou, T. Lim, X. Wu, Sonophotolytic degradation of azo dye reactive black 5 in an ultrasound/UV/ferric system and the roles of different organic ligands. *Wat. Res.*, **45**, 2915-2924 (2011).

[34] S. Na, Y. Ahn, M. Cui, J. Khim, Significant diethyl phthalate (DEP) degradation by combined advanced oxidation process in aqueous solution. *J. Environ. Manage.*, **101**, 104-110 (2012).

[35] S. Tangestaninejad, M. Moghadam, V. Mirkhani, I. Mohammadpoor-Baltork, H. Salavati, Sonochemical and visible light induced photochemical and sonophotochemical degradation of dyes catalyzed by recoverable vanadium-containing polyphosphomolybdate immobilized on TiO_2 nanoparticles. *Ultrason. Sonochem.*, **15**, 815-822 (2008).

[36] K. Zhang, W. Oh, Kinetic study of the visible light-induced sonophotocatalytic degradation of MB solution in the presence of Fe/TiO2-MWCNT catalyst. *Bull. Korean Chem. Soc.*, **31**, 1589-1595 (2010).

[37] R. Kidak, N. Ince, Catalysis of advanced oxidation reactions by ultrasound, a case study with phenol. *J. Haz. Mat.*, **146**, 630-635 (2007).

[38] O. Hamdaoui, E. Naffrechoux, Sonochemical and photosonochemical degradation of 4-chlorophenol in aqueous media. *Ultrason. Sonochem.*, **15**, 981-987 (2008).

[39] L. Weavers, F. Ling, M. Hoffmann, Aromatic compound degradation in water using a combination of sonolysis and ozonolysis. *Environ. Sci. Technol.*, **32**, 2727-2733 (1998).

[40] V. Abramov, O. Abramov, A. Gekhman, V. Kuznetsov, G. Price, Ultrasonic intensification of ozone and electrochemical destruction of 1,3-dinitrobenzene and 2,4-dinitrotoluene. *Ultrason. Sonochem.*, **13**, 303-307 (2000).

[41] H. Destaillats, A. Colussi, J. Joseph, M. Hoffmann, Synergistic effects of sonolysis combined with ozonolysis for the oxidation of azobenzene and methyl orange. *J. Phys. Chem.*, **104**, 8930-8935 (2000).

[42] S. Song, Z. He, J. Chen, US/O_3 combination degradation of aniline in aqueous solution. *Ultrason. Sonochem.*, **14**, 84-88 (2007).

[43] G. Tezcanli-Güyer, N. Ince, Individual and combined effects of ultrasound, ozone and UV irradiation: a case study with textile dyes. *Ultrasonics*, **42**, 603-609 (2004).

[44] W. Chu, C. W. Ma, Quantitative prodiction of direct and indirect dye ozonation kinetics. *Water Res.*, **34**, 3153-3160 (2000).

[45] T. Olson, P. Barbier, Oxidation kinetics of natural organic matter by sonolysis and ozone. *Water Res.*, **28**, 1383-1391 (1994).

[46] J. Kang, M. Hoffmann, Kinetics and mechanism of the sonolytic destruction of methyl tert-butyl ether by ultrasonic irradiation in the presence of ozone. *Environ.*

Sci. Technol., **32**, 3194-3199 (1998).

[47] E. Ando, Y. Kagawa, Finite element simulation for the design of an ultrasonic cleaning tank. *Electron. Commun. Jpn.*, **72**, 43-57 (1989).

[48] Y. Liu, T. Yamabuchi, T. Yoshizawa, S. Hirobayashi, Finite element simulation of coupled vibration modes in an ultrasonic cleaning tub: Effect of the presence of a washing object. *Acoust. Sci. Technol.*, **25**, 173-176 (2004).

[49] S. Dähnke, F. J. Keil, Modeling of three-dimensional linear pressure fields in sonochemical reactors with homogeneous and inhomogeneous density distributions of cavitation bubbles. *Ind. Eng. Chem. Res.*, **37**, 848-864 (1998).

[50] S. Dähnke, K. Swamy, F. J. Keil, A comparative study on the modeling of sound pressure field distributions in a sonoreactor with experimental investigation. *Ultrason. Sonochem.*, **6**, 221-226 (1999).

[51] G. Servant, J. Laborde, A. Hita, J. Caltagirone, A. Gėrard, Spatio-temporal dynamics of cavitation bubble clouds in a low frequency reactor: comparison between theoretical and experimental results. *Ultrason. Sonochem.*, **8**, 163-174 (2001).

[52] G. Servant, J. Caltagirone, A. Gėrard, J. Laborde, A. Hita, Numerical simulation of cavitation bubble dynamics induced by ultrasound waves in a high frequency reactor. *Ultrason. Sonochem.*, **7**, 217-227 (2000).

[53] K. Yaui, T. Kozuka, T. Tuziuti, A. Towata, T. Iida, J. King, FEM calculation of an acoustic field in a sonochemical reactor. *Ultrason. Sonochem.*, **14**, 605-614 (2007).

[54] W. Nyborg, Acoustic streaming due to attenuated plane waves. *J. Acoust. Soc. Am.*, **25**, 68-75 (1953).

[55] O. Rudenko, S. Soluyan, Theory of non-stationary acoustic streaming. *Sov. Phys.*

Acoust., **17**, 97-101 (1971).

[56] J. Wu, G. Du, Acoustic streaming generated by focused Gaussian beam and finite amplitude toneburst. *Ultrasound Med. Biol.*, **19**, 167-176 (1993).

[57] H. Mitome, T. Kozuka, T. Tuziuti, Effect of nonlinearity in development of acoustic streaming. *Jpn. J. Appl. Phys.*, **34**, 2584-2589 (1995).

[58] T. Kamakura, K. Matsuda, Y. Kumamoto, Acoustic streaming induced in focused Gaussian beams. *J. Acoust. Soc. Am.*, **97**, 2740-2746 (1995).

Chapter 2

Numerical simulation of liquid velocity distribution in a sonochemical reactor

2.1 Introduction

It is widely confirmed that the flow field accelerates sonochemical reactions. To optimize the sonochemical reactor geometry, the flow distribution in reactors has been investigated.

In this chapter, acoustic pressure distributions in a sonochemical reactor have been numerically calculated. Liquid velocity distributions in a sonochemical reactor for low (input power to transducer: 10W), middle (30 W) and high (50 W) acoustic power have been simulated from the acoustic pressure distribution.

Results have been compared with experimental data reported previously. The sound absorption coefficient was evaluated. The fountain shape at liquid surface has been properly included into calculation domain. Moreover, effects of the liquid height and transducer plate radius on the liquid velocity distribution have been discussed.

2.2 Calculation modeling

2.2.1 Acoustic pressure distribution

The time harmonic wave equation (inhomogeneous Helmholtz equation) in media can be ascribed as

$$\nabla \cdot (-\frac{1}{\rho_c}\nabla p) - \frac{\omega^2}{\rho_c c_c^{\,2}} p = 0, \qquad (2\text{-}1)$$

where p represents acoustic pressure. The angular frequency ω is defined as $\omega = 2\pi f$, where f is the ultrasound frequency.

The absorption coefficient is expressed by the complex density ρ_c and complex sound speed $c_c(=\frac{\omega c_s}{\omega - i\alpha c_s})$ included absorption.

$$\rho_c = \frac{Z_c k_c}{\omega}, \quad c_c = \frac{\omega}{k_c}. \qquad (2\text{-}2)$$

The complex wave number k_c and the impedance Z_c are expressed as follows.

$$k_c = \frac{\omega}{c_s} - i\alpha \,, \quad Z_c = \rho_0 c_s \,, \tag{2-3}$$

where α is the absorption coefficient, c_s and ρ_0 denote sound speed in the media without absorption and density of the media, respectively.

Calculations have been performed in a cylindrical vessel with 0.100 m in radius and 0.100 m in height filled with water. The cylindrical vessel was made from quartz glass with 10 mm in thickness. A transducer operated at 490 kHz is mounted at the bottom of reactor centre with radius of 0.025 m. We set that *r* is the radial distance from transducer centre and *z* is the height from the vessel bottom. The geometry with boundary conditions for acoustic pressure field calculations is shown in Fig. 2-1(a). To save calculation time and memory, the right half of the reactor in two dimensions was calculated under the assumption of axial-symmetry against transducer centre because acoustic pressure distributions were originated from the transducer. Thus, transducer centre (r = 0) along the propagation direction was set as axial symmetry.

Impedance boundaries were utilized to specify the boundary condition of water – air and quartz glass – air interfaces. The impedance boundary is written as

$$\vec{n} \cdot (-\frac{1}{\rho_c} \nabla p) = \frac{i\omega p}{Z_e} \,, \tag{2-4}$$

where $Z_e = \rho_e c_e$ is the acoustic input impedance of the external domain (ρ_e and c_e is the density and sound speed of the external domain) and $\vec{n}$ is the unit normal vector against the wall.

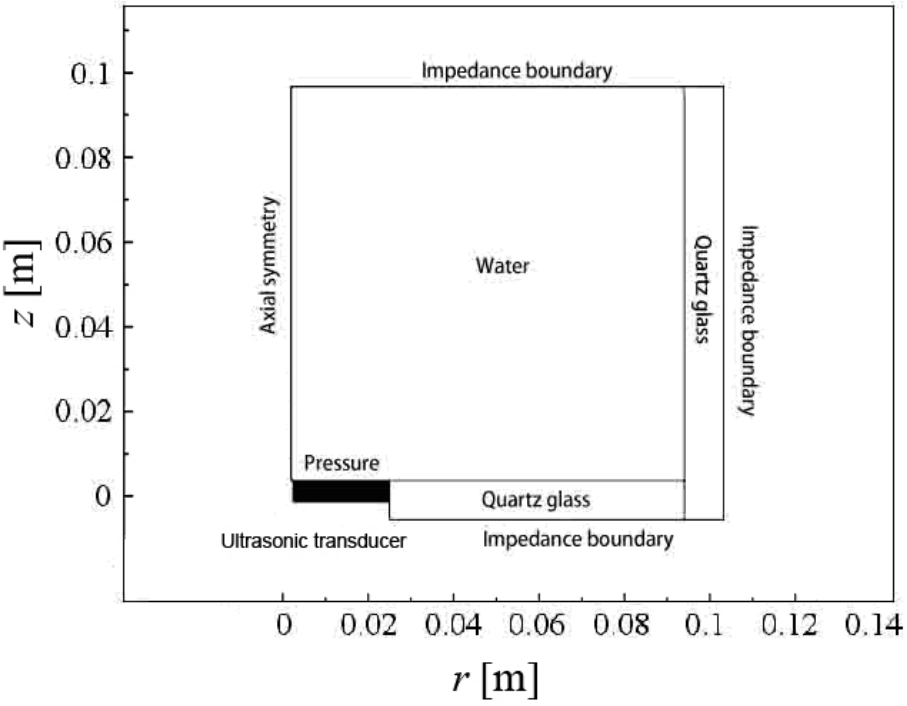
Impedance boundary
Axial symmetry
Water
Quartz glass
Impedance boundary
Pressure
Quartz glass
Ultrasonic transducer
Impedance boundary
z [m]
r [m]
0.1
0.08
0.06
0.04
0.02
0
0.02
0.04
0.06
0.08
0.1
0.12
0.14

(a)

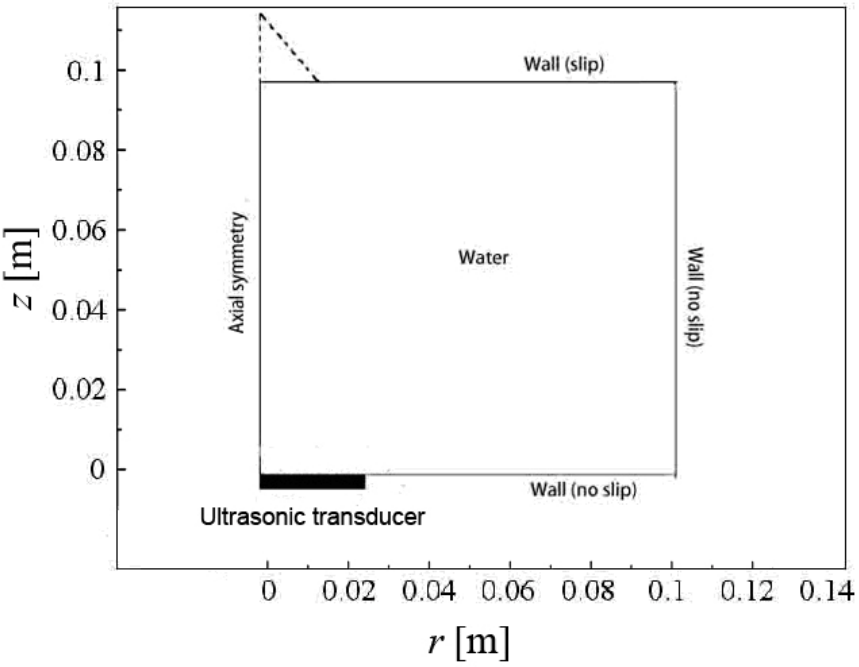
Wall (slip)
Axial symmetry
Water
Wall (no slip)
Wall (no slip)
Ultrasonic transducer
z [m]
r [m]
0.1
0.08
0.06
0.04
0.02
0
0.02
0.04
0.06
0.08
0.1
0.12
0.14

(b)

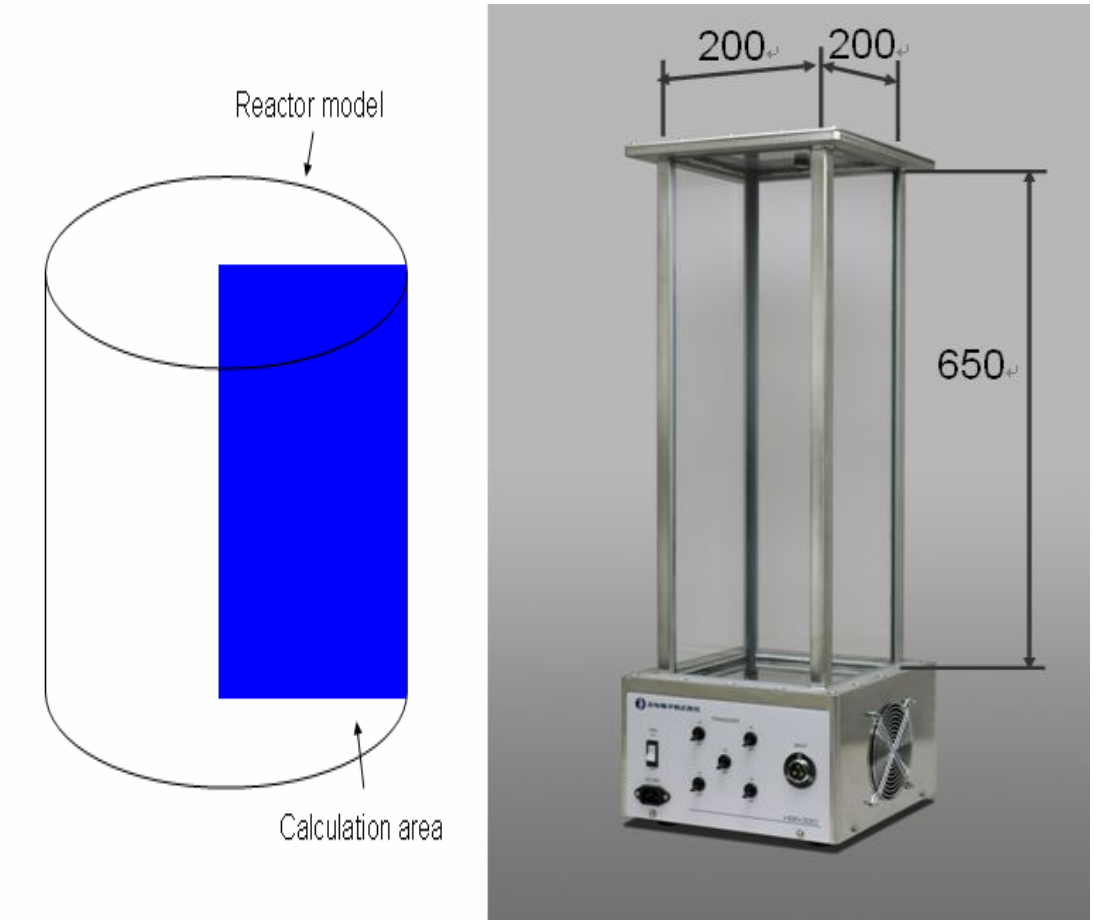

(c) (d)

Figure 2-1 Boundary and subdomain conditions of (a) pressure and (b) flow field model, (c) calculation modeling, and (d) Experiment apparatus.

For the transducer surface, the boundary was set as acoustic pressure. Pressure values at the transducer surface were not uniform. As pressure distributions at transducer surface with low, middle and high input powers, experimental data [1] for input powers of the transducer at 10, 30 and 50 W were used, respectively. They used a rectangular sonochemical reactor (0.2 m × 0.2 m × 0.1 m (height)). A transducer with 0.025 m in radius was set at the bottom centre of the reactor. The experiment apparatus is shown in Fig. 2-1(c). Initial values of acoustic pressure in water and quartz glass were set as 0. Calculations were carried out by COMSOL

Multiphysics™ (COMSOL AB, Stockholm, Sweden). The length of elements has been set to be less than the 1/12 of the ultrasound wavelength in water at 490 kHz. Triangle element has been employed in our calculation. The calculation area consists of about 400,000 elements and in calculation the degree of freedom is about 800,000.

2.2.2 The flow field

Since the liquid flow is a second order effect of ultrasound propagation, its velocity is very low (Experiment result shown in Fig. 2-3(c)). Therefore, the laminar flow equation was used.

The flow field was calculated by two equations, the momentum transport equation:

$$-\nabla\cdot(-p\vec{I}-\tau)+\rho_0(\vec{u}\cdot\nabla)\vec{u}=\vec{F}\,, \tag{2-5}$$

and the continuity equation:

$$\nabla\cdot\vec{u}=0\,, \tag{2-6}$$

where ($\tau = -\mu(\nabla\vec{u}+(\nabla\vec{u})^T)$) is the viscous stress tensor, $\vec{I}$ is the unit matrix, $\vec{u}$, μ and $\vec{p}_L$ are the particle velocity, liquid viscosity and pressure in liquid, respectively. $\vec{F}$ represents the force per unit volume that causes streaming. Superscript *T* denotes the transpose matrix. The equation presumes constant density of a liquid throughout the reactor.

Equations (2-5) and (2-6) are written as [2]:

$$<F>=\nabla\cdot\vec{p}_2-\mu\nabla^2\vec{u}_2-[\mu_b+(1/3)\mu]\nabla\nabla\cdot\vec{u_2}\,, \tag{2-7}$$

the volume force <*F*> is expressed as:

$$<F>=-\rho_0<(\vec{u}_{ac}\cdot\nabla)\vec{u}_{ac}+\vec{u}_{ac}\nabla\cdot\vec{u}_{ac}>\,, \tag{2-8}$$

where μ_b is the bulk viscosity coefficient, $\vec{u}_{ac}$ is the oscillatory velocity due to

acoustic wave propagating in a fluid, and p_2 and $\vec{u}_2$ are time-independent terms of the second-order approximations. The second-order time-independent term $\vec{u}_2$ is the streaming velocity.

The acoustic wavelength is much smaller than the transverse dimension of the system. Using a plane wave approximation and $p \approx u_{ac} \rho_0 c_0$ [3], the volume force is written as [4]

$$F = \frac{2\alpha}{\rho_0 c_0^{\,2}} | p |^2 \quad . \tag{2-9}$$

In our calculation of fluid flow, the volume force is expressed by Eq. (2-9).

The geometry with boundary conditions for calculation of flow field is shown in Fig. 2-1(b). In the same way of pressure field calculations, the fluid flow field in the right half of the reactor was calculated since the acoustic pressure field above the transducer governed the liquid flow distribution. The axial symmetry boundary eliminates the liquid velocity in the *r*-axis and the stresses in the *z*-axis direction at the centre of transducer.

The no slip wall was used as the boundary condition to specify a stationary solid wall and transducer surface. This boundary condition is prescribed as

$$\vec{u} = 0 . \tag{2-10}$$

At the liquid surface, the slip wall has been used to specify no viscous effects at the liquid surface. This boundary condition is prescribed as:

$$\vec{u} \cdot \vec{n} = 0 , \tag{2-11}$$

$$\vec{t} \cdot (-p\vec{I} - \tau))\vec{n} = 0 , \tag{2-12}$$

where $\vec{t}$ is the tangential vector of the boundary. Eq. (2-11) states that there is no flow across the boundary. Eq. (2-12) ensures no viscous stress in the tangential direction.

Regarding the subdomain setting, density (1000 kg/m^3), viscosity (0.001 Pa·s) and sound velocity (1500 m/s) were set as water. The initial liquid velocity in water was set as 0 and the thermal convection effect has not been taken into account.

Calculations were carried out by COMSOL Multiphysics^{TM} (COMSOL AB, Stockholm, Sweden). The calculation image is shown in Fig. 2-1 (c), and the experiment apparatus is shown in Fig. 2-1 (d). The element size has been decided to become the same results as those with finer element size. In calculations, the element size was decided as 0.5 mm. Triangle element has been employed. For liquid height of 0.100 m and reactor diameter of 0.200 m, the calculation area consists of about 100,000 elements in the reactor and in calculation the degree of freedom is about 450,000.

Firstly acoustic pressure distributions by numerical simulation were used to obtain the volume force in Eq. (2-9) and the liquid velocity distribution were calculated by using the momentum transport equation in Eq. (2-5). The calculation results have been compared with experimental results reported by Kojima et al. [1].

2.3 Results and discussion

2.3.1 Acoustic pressure distribution

Figure 2-2(a) shows the simulation result of acoustic pressure distribution in the right half of the reactor with high acoustic power. The absorption coefficient was set as 1 m^{-1}. The ordinate and abscissa in the figure indicate the space position in reactor. The acoustic pressure magnitude is indicated by the color scale. A high pressure field is observed just above the transducer surface and just below the liquid surface in the vicinity of transducer centre. Since the high ultrasonic power induces cavitation bubble, it is considered that ultrasonic pressure was absorbed rapidly in a short distance from the transducer. At the liquid surface, the high pressure field is formed

due to the ultrasound reflection. The superposition of the propagation wave and the reflective wave forms the high pressure field. Since the ultrasound at 490 kHz has high directivity, the pressure field outside of transducer area (r>0.025 m) decreases to very low value.

For comparison, Fig. 2-2(b) shows the experiment result of acoustic pressure distribution (input power to transducer at 50 W) reported by Kojima et al. [1]. To measure the acoustic pressure distribution, a rod sensor (ONDA Model HNR-1000, EASTEK CORPORATION) having a diameter of 1 mm with piezoelectric ceramics at the upper part was used. It can be observed from figure that the numerical simulation result agrees well with the experimental result. However, standing wave with intervals of about 1.5 mm is observed in the pressure distribution for simulation results. While in experiment results, the intervals can not be observed. This is because the acoustic pressure was measured by using a rod sensor with a diameter of 1 mm. For low and middle acoustic power, simulation results also agree well with the experimental results at 10 and 30 W, respectively.

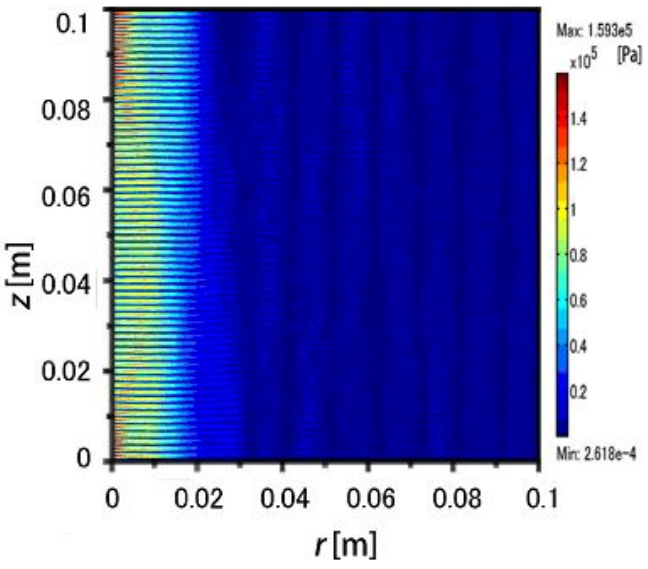

(a)

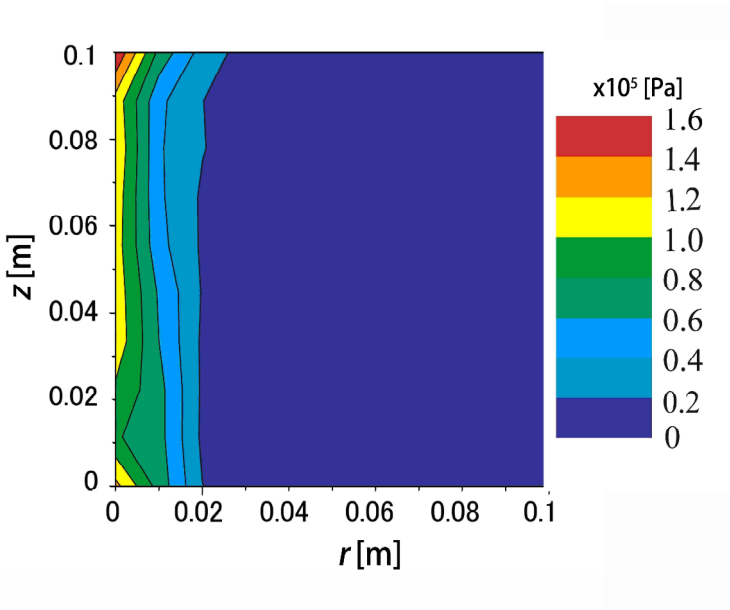

(b)

Figure 2-2 Pressure field distributions with input power of 50 W. (a) simulation and (b) experiment results.

2.3.2 Liquid velocity distribution

(1) Evaluation of absorption coefficient

In order to calculate the liquid velocity field, the absorption coefficient should be decided. High acoustic power was utilized. Figures 2-3(a) and (b) show the simulation results of the liquid velocity distribution in the right half of the sonochemical reactor when the absorption coefficients were 0.005 m^{-1} and 1 m^{-1}, respectively. For comparison, Fig. 2-3(c) shows the experiment result (input power to transducer at 50 W) reported by Kojima et al. [1]. They measured the distribution of liquid velocity at the vertical and horizontal intervals of 10 mm by a laser Doppler velocimeter. The experimental setup of the Laser Doppler Velocimeter consists of an argon ion laser (INNOVA 70, Coherent Inc.), a multicolor beam separator (Model 9201, TSI Incorporated), a probe (Model 9832, TSI, Inc.), a traverse apparatus

(KANOMAX Japan Inc.), a pulse controller (SHOT-204MS, SIGMA KOKI Co., Ltd.) and a PC. The nylon powders having the mean particle diameter of 4 μm and specific weight of 1.02 were employed as a tracer of flow. The filled color in the figure infers the velocity magnitude, and the arrow indicates the direction of fluid velocity. The velocity magnitude is explained in color scale. The ordinate and abscissa indicate the space position in reactor. In Fig. 2-3(a), when the absorption coefficient is 0.005 m^{-1} (the absorption coefficient measured by Burton [5]), the velocity magnitudes in flow field are much lower than experimental result in Fig. 2-3(c). While the absorption coefficient increases to 1 m^{-1}, the velocity magnitude in flow field is very close to the experimental result. This result indicates that the absorption coefficient in the sonochemical rector becomes much higher than the classic absorption value. The classic absorption coefficient was measured in degassed water without cavitation. However, for a sonochemical reactor, the dissolved gas and cavitation bubbles in water absorb and reflect the sound wave. Therefore, it is considered that the absorption value is increased. From Eq. (2-9), it could be inferred that the increase of absorption coefficient increases the volume force, and further enhances the liquid flow. Dähnke et al. [6] considered that the absorption coefficient is about 0.5-5 m^{-1} in simulation. Moreover, Yasui et al. [7] also considered that the absorption coefficient should be 5 m^{-1} in pressure field simulation due to the cavitation bubbles effect.

Nevertheless, compared Figs. 2-3(b) with (c), the upward flow tendencies at the transducer centre near the liquid surface are different. According to results by Kojima et al. [1], the area near the liquid surface above transducer centre is main sonochemical reaction area. In our simulation result, the upward velocity is zero at liquid surface while in experiment result the upward velocity at liquid surface has the

maximum value. In our previous experiments [8], it was found that for middle or high acoustic power (input power to transducer at 30 or 50 W), a fountain occurred at the liquid surface. Thus, the formation of fountain changes the flow field near the liquid surface.

(2) Setting of fountain

In order to reproduce the experiment result near liquid surface above transducer, the fountain formation has been taken into account in model. In our previous experiment, the fountain on the liquid surface was observed when the input power of transducer was beyond 10 W. The fountain size has been experimentally measured [8]. The shape of the fountain was defined as cone. According to experiment results, the fountain height increases linearly with ultrasonic power. The fountain radius firstly increases with increasing ultrasonic intensity and then becomes a constant value with approximately half of the transducer radius. Therefore, we added the fountain in calculation geometry, and the fountain boundary was set as the slip boundary at wall (Fig. 2-1(b)), the definition of slip boundary was described as Eqs. (2-11) and (2-12). The extended line at the transducer centre was set as axial symmetry.

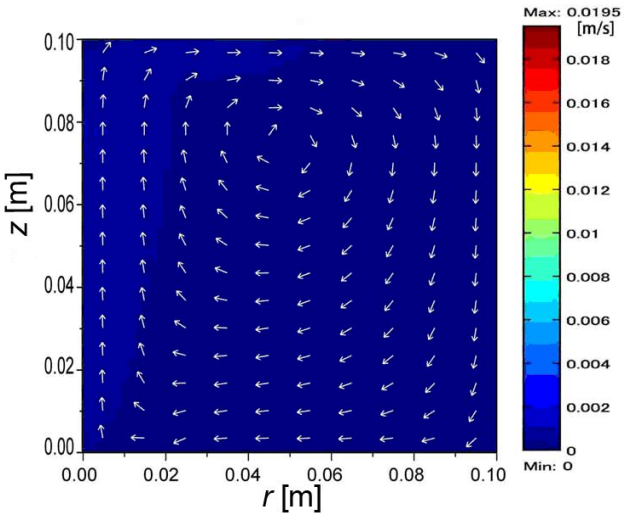

(a)

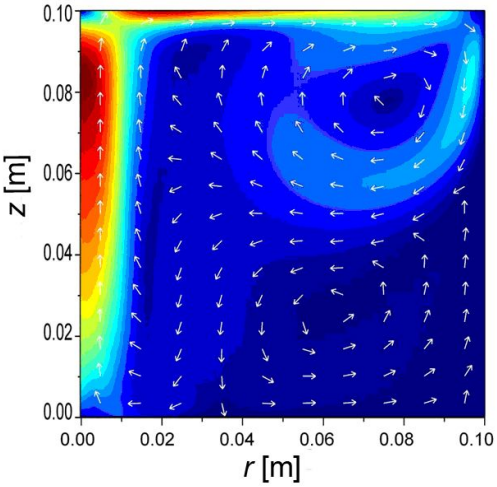

(b)

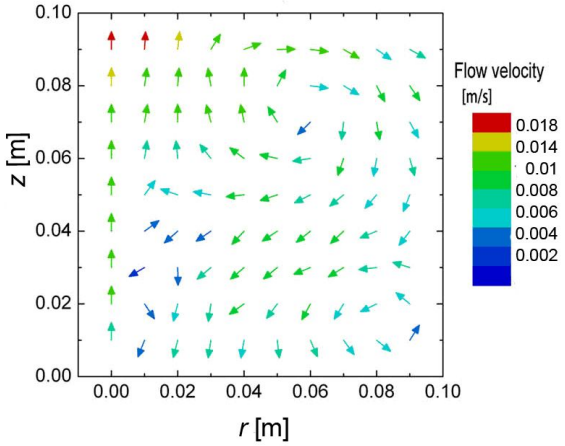

(c)

Figure 2-3 Liquid velocity distributions in sonochemical reactor. Simulation results with absorption coefficient of (a) 0.005 m^{-1} and (b) 1 m^{-1}, (c) experiment result.

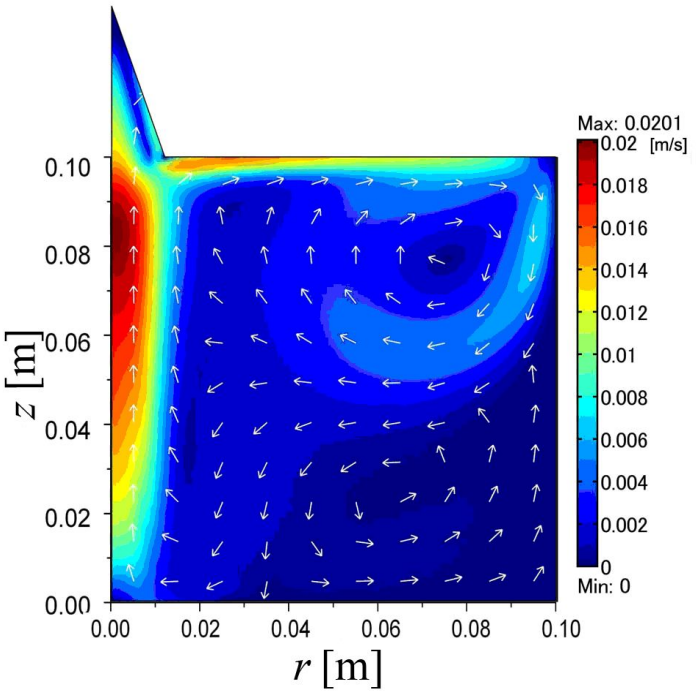

Figure 2-4 Liquid velocity distributions in sonochemical reactor. The fountain has been taken into account.

Figure 2-4 shows the simulation result of liquid velocity distribution with fountain. At z = 0.09 m above transducer centre, the liquid velocity is almost maximum. This tendency is same as that in Fig. 2-3(c). From these results, it is obvious that the setting of fountain is necessary to simulate liquid velocity field in a sonochemical reactor.

(3) Effect of input power

Figure 2-5 shows the liquid velocity distributions in the right half of the sonochemical reactor under low, middle and high acoustic power. For low acoustic power irradiation (Fig. 2-5(a)), the relative high velocity field is assembled in the centre of the transducer and orientated towards acoustic propagation direction. This is because the flow field is driven by the acoustic volume force. At the transducer centre, the velocity firstly increases in z axis and the maximum velocity can be

observed at z = 0.07 m. Then velocity decreases until liquid surface. In the fluid far from the transducer (r > 0.025 m), the liquid velocity decreases to very low values.

For the middle acoustic power irradiation (Fig. 2-5(b)), the liquid velocity tendency at transducer centre in z axis is similar to the case for the low acoustic power. The velocity magnitude is higher than that at low acoustic power, since the higher acoustic power further increases the volume force driven the flow field. Two circulations form in the sonochemical reactor, one is the main circulation and another exists at the bottom corner of the reactor. It is considered that the minor circulation is formed by the high downward velocity at z = 0.07 m close the right wall. The flow separates into two parts: one remains clockwise to form the main circulation, and another becomes anti-clockwise at the corner of the reactor and forms the minor circulation.

For the high acoustic power irradiation (Fig. 2-5(c)), at the centre of transducer, the fluid velocity tendency along z axis is different from low and middle acoustic power case. The velocity magnitude increases until z=0.09 m. This is due to the fountain formed at the liquid surface: the boundary has been reshaped, and the liquid height is higher than that for the low and middle acoustic powers. The velocity rapidly decreases in fountain. In the reactor, two circulations form as the same as the case of middle acoustic power irradiation.

For comparison, the experiment results carried out by Kojima et al. are shown in Fig. 2-5(d), (e) and (f).The experimental measurements were carried out by Kojima et al. [1]. It is found that for the middle and high acoustic power irradiation, the simulation results agree well with experiment results when the input powers to transducer were 30 and 50 W. For the low acoustic power irradiation, the upward velocity tendency above transducer centre (r=0) is almost same as the experimental

ones. However, the circulation can not be observed. Instead, the flow far from transducer is slow and random. It is considered that at low input power, the fluid velocity outside of the ultrasound irradiation area was too low to measure. Furthermore, the experiment result was influenced by thermal convection.

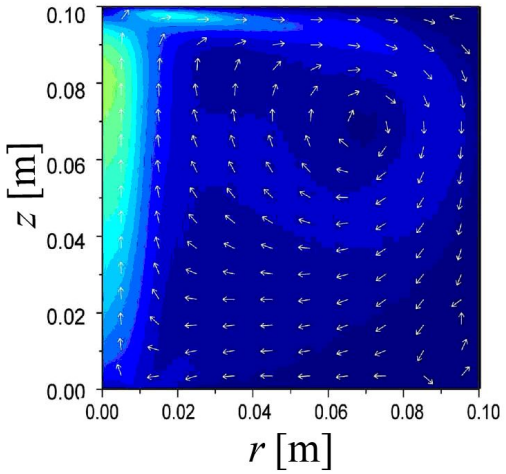
z [m]
r [m]
0.00
0.02
0.04
0.06
0.08
0.10

(a)

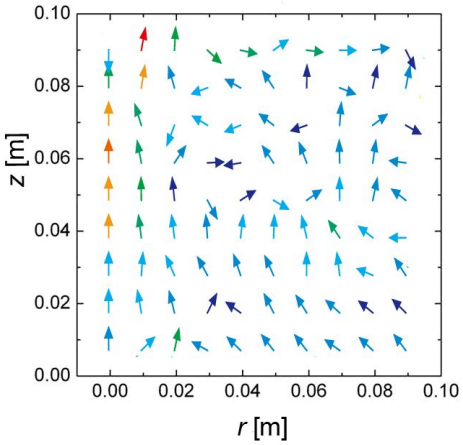
z [m]
r [m]
0.00
0.02
0.04
0.06
0.08
0.10

(d)

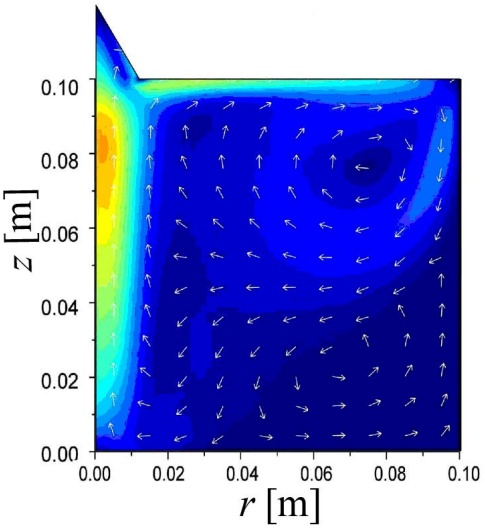
z [m]
r [m]
0.00
0.02
0.04
0.06
0.08
0.10

(b)

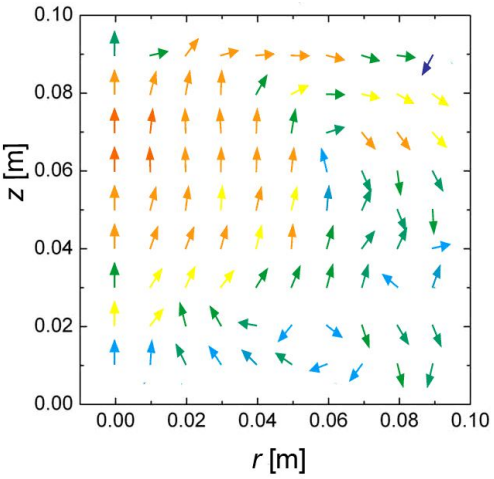
z [m]
r [m]
0.00
0.02
0.04
0.06
0.08
0.10

(e)

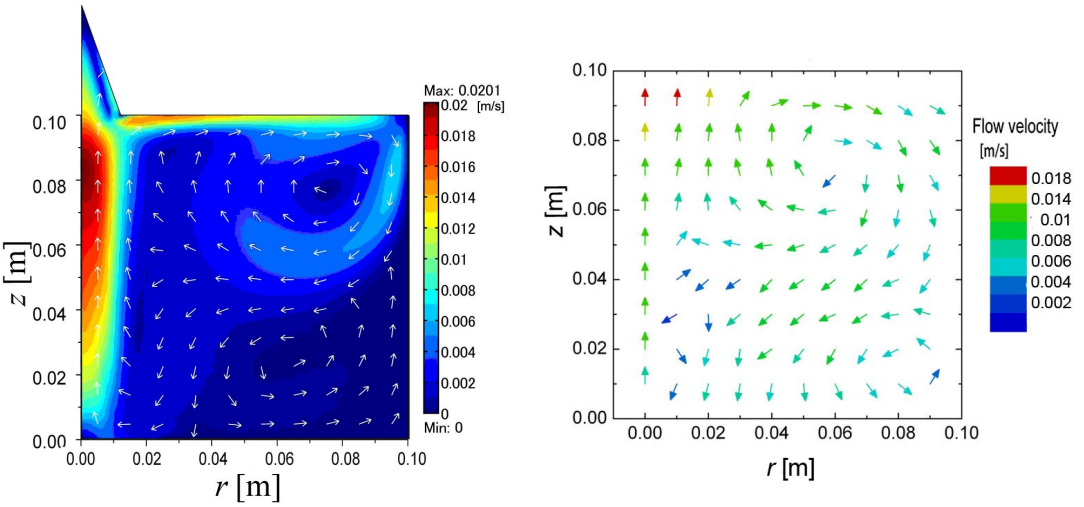

(c) (f)

Figure 2-5 Simulation results of liquid velocity distributions in sonochemical reactors with input power of (a) low (10 W), (b) middle (30W) and (c) high (50 W). (d), (e) and (f) are the experiment results carried out by Kojima et al.

(4) Effect of liquid height

The effect of liquid height on flow field has been investigated. Middle acoustic power was utilized. Figure 2-6 shows the liquid velocity distribution for liquid heights *h* of (a) 0.10 m, (b) 0.20 m, (c) 0.30 m, (d) 0.40 m and (e) 0.50 m. The maximum velocities in each reactor are 0.015, 0.019, 0.022, 0.025 and 0.016 m/s, respectively. Thus, the maximum velocity has the greatest value against liquid height. It is considered that the pressure field in the reactor becomes weak due to the ultrasonic absorption in liquid as the liquid height becomes higher. However, the flow acceleration length increases with increasing the liquid height. From these two phenomena, the liquid height has an optimum value for flow field in the reactor.

In the previous work by Asakura et al. [9], the effect of the liquid height on the sonochemical efficiency (SE) in oxidation of potassium iodide has been examined using the frequency at 490 kHz and input power to transducer at 30 W. It was found that the SE value decreased by the increase of the liquid height from 0.1 to 0.2 m.

When the liquid height increased from 0.2 to 0.4 m, the SE value increased to a maximum value. And the liquid height increased from 0.4 to 0.5 m, the SE value decreased. In order to consider this experiment result from the flow field calculated by simulation, the mean velocity, which represents the space average velocity above transducer centre (r = 0), has been calculated. Figure 2-7(a) shows the effect of the liquid height on the mean velocity above transducer center. For comparison, the experiment results carried out by Asakura et al. are shown as Fig. 2-7(b). The tendency of mean velocity for the variation of liquid height agrees well with that of the SE value. Thus, the sonochemical reaction efficiency is related to the liquid velocity magnitude. The increase of liquid velocity enhances the mass transport of reactant. Furthermore, the increase of flow field prevents the active bubbles from aggregating in the standing wave field and additionally supplies the acoustic field with reactant and the nuclei required for the formation of the active bubbles [1,10,11]. Therefore, the reaction performance is enhanced.

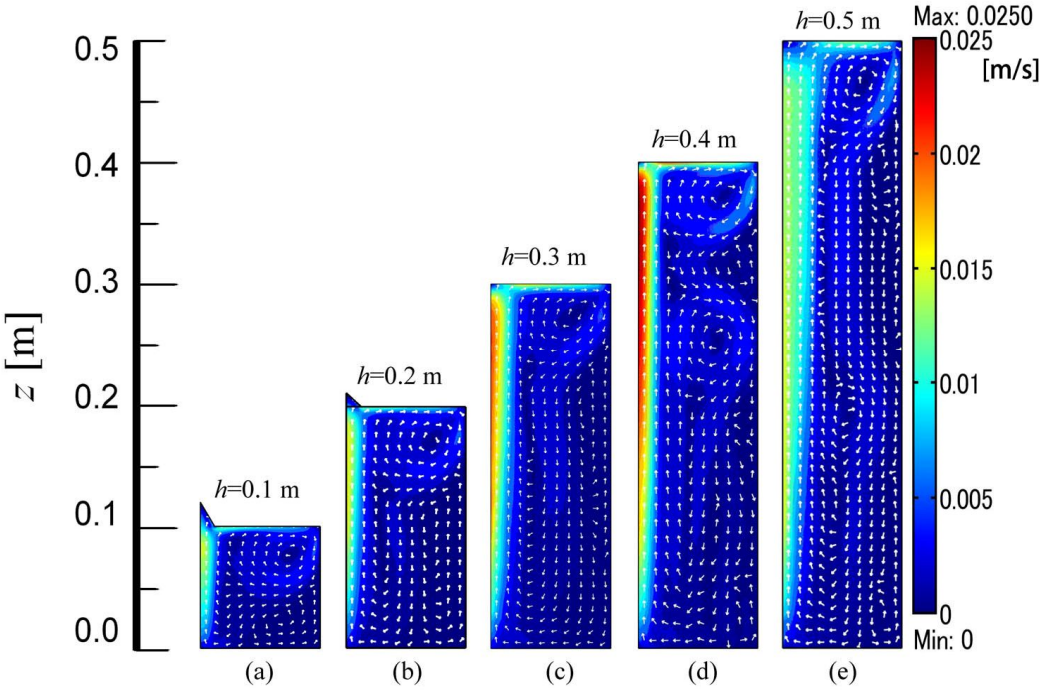

Figure 2-6 Liquid velocity distributions with different reactor height.

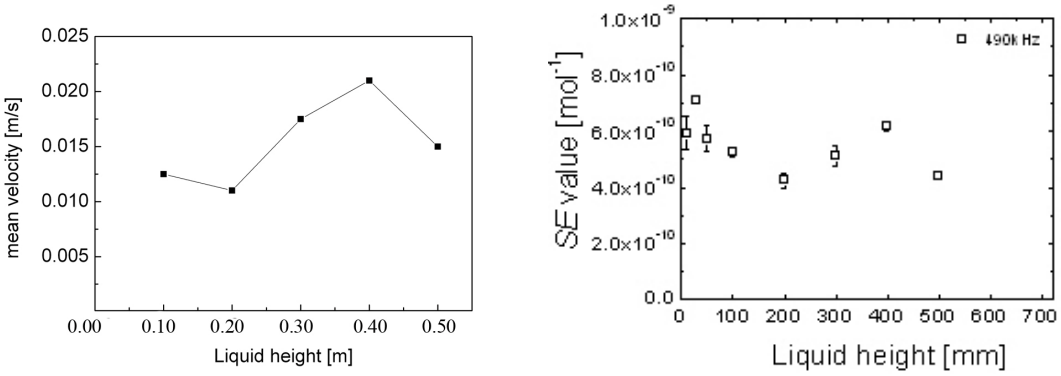

(a) (b)

Figure 2-7 Mean velocities in sonochemical reactor with the change of liquid height. (a) Simulation results. (b) Experiment results by Asakura et al.

(5) Effect of transducer radius

To scale-up the sonochemical reactor, the effect of transducer radius has been investigated. Figure 2-8 shows the velocity distributions in the reactor with transducer radiuses r_p of (a) 0.05 m and (b) 0.075 m, respectively. Acoustic powers from each oscillation plate were same and the high acoustic power was used. Compared with the result of Fig. 2-5(c), the velocity magnitude decreases with increasing transducer radius. For a further understanding, the pressure field for different transducer radius has also been simulated. Figure 2-9 shows the pressure field in the sonochemical reactor with r_p at (a) 0.05 m and (b) 0.075 m. Compared with Fig. 2-2, the pressure field decreases. Since the ultrasonic power per unit area of transducer decreases, the pressure amplitude becomes lower. Therefore, the volume force decreases and further, the flow field becomes lower. From these results we understand that the flow field decreases with increasing transducer radius. However, a variation of transducer radius also influences the pressure field: for the directivity of high frequency transducer, the increase of transducer radius will diminish the high pressure field area (reaction area).

From this chapter, it became evident that the flow field influences the

sonochemical reaction. By this method, it is able to calculate the pressure and flow field by a known input pressure distribution at a transducer plate.

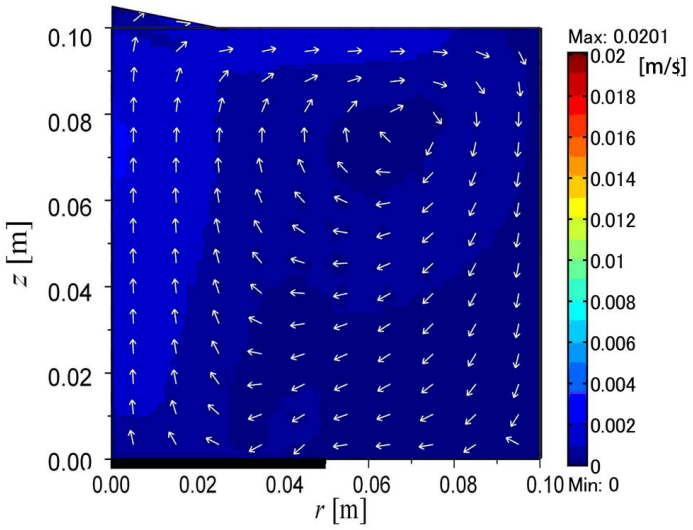

(a)

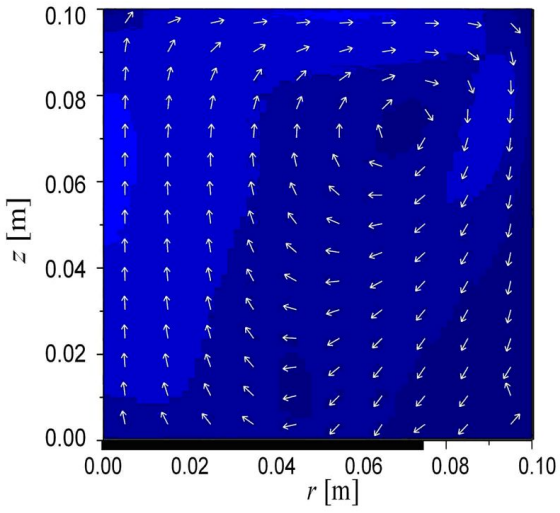

(b)

Figure 2-8 Simulation results of liquid velocity distributions in sonochemical reactors with transducer radius of (a) r_p=0.05 m and (b) r_p=0.075 m.

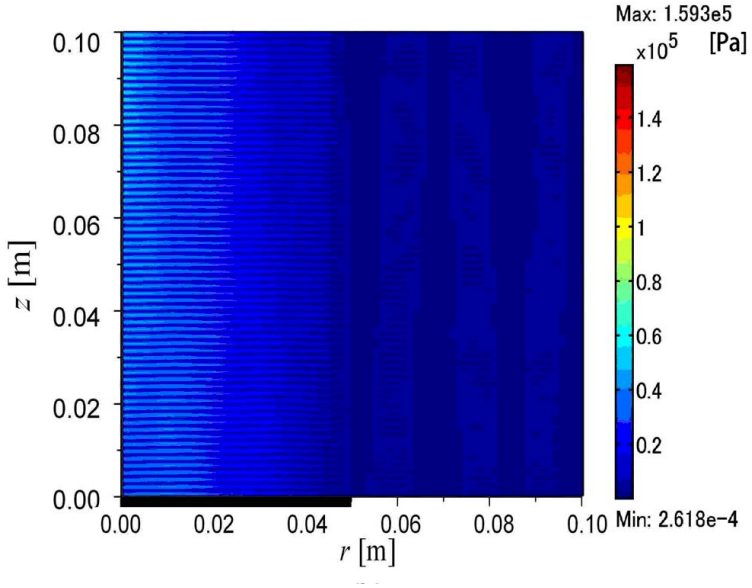

(a)

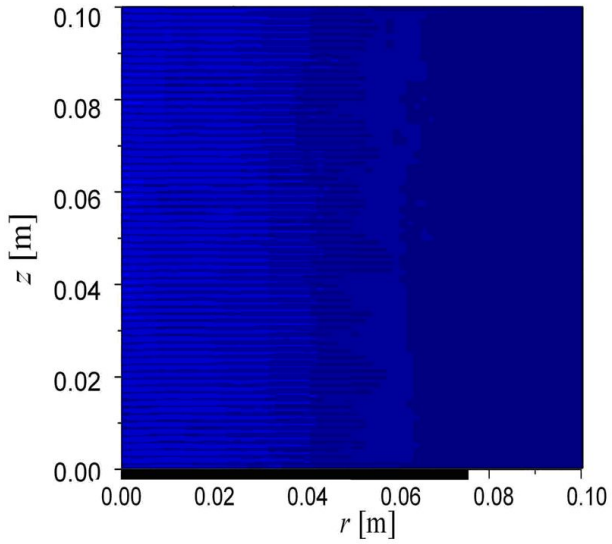

(b)

Figure 2-9 Simulation result of pressure field distributions in sonochemical reactors with transducer radius of (a) r_p=0.05 m and (b) r_p=0.075 m.

2.4 Conclusions

For a sonochemical reactor at high frequency, the liquid flow distribution has been investigated by numerical simulation. The results indicate that the absorption coefficient is 1 m^{-1}, which is different from classical one. The fountain has also been taken into account in our model. The effects of input power, liquid height and plate

radius have been investigated. The fluid velocity increases with increasing input power and decreasing plate radius. The liquid height also influences the fluid velocity. The tendency of mean velocity for the variation of liquid height agrees well with that of the SE value. The increase of fluid velocity further enhances the sonochemical reaction efficiency.

References

[1] Y. Kojima, Y. Asakura, G. Sugiyama, S. Koda, The effects of acoustic flow and mechanical flow on the sonochemical efficiency in a rectangular sonochemical reactor. *Ultrason. Sonochem.*, **17**, 978-984 (2010).

[2] J. Wu, G. Du, Acoustic streaming generated by a focused Gaussian beam and finite amplitude tonebursts. *Ultrasound Med. Biol.*, **19**, 167-176 (1993).

[3] S. I. Aanonsen, T. Barkve, J. N. Tjøtta, S. Tjøtta, Distortion and harmonic generation in the nearfield of a finite amplitude sound beam. *J. Acoust. Soc. Am.*, **75**, 749-768 (1984).

[4] K. R. Nightingale, G. E. Trahey, A finite element model for simulating acoustic streaming in cystic breast lesions with experimental validation. *IEEE T. Ultrason. Ferr.*, **47**, 201-214 (2000).

[5] J. Burton, A study of ultrasonic velocity and absorption in liquid mixtures. *J. Acoust. Soc. Am.*, **20**, 186-199 (1948).

[6] S. Dähnke, K. M. Swamy, F. J. Keil, Modeling of three-dimensional pressure fields in sonochemical reactors with an inhomogeneous density distribution of cavitation bubbles: comparison of theoretical and experimental results. *Ultrason. Sonochem.*, **6**, 31-41 (1999).

[7] K. Yasui, T. Kozuka, T. Tuziuti, A. Towata, Y. Iida, J. King, P. Macey, FEM calculation of an acoustic field in a sonochemical reactor. *Ultrason. Sonochem.*, **14**, 605-614 (2007).

[8] K. Yasuda, H. Honma, Z. Xu, Y. Asakura, S. Koda, Ultrasonic atomization amount for different frequencies. *Jpn. J. Appl. Phys.*, **50**, 07HE23-07HE23-5 (2011).

[9] Y. Asakura, T. Nishida, T. Matsuoka, S. Koda, Effects of ultrasonic frequency

and liquid height on sonochemical efficiency of large-scale sonochemical reactors. *Ultrason. Sonochem.*, **15**, 244-250 (2008).

[10] K. Yasuda, M. Tachi, Y. Bando, M. Nakamura, Effect of liquid mixing on performance of porphyrin decomposition by ultrasonic irradiation. *J. Chem. Eng. Jpn.*, **32**, 347-349 (1999).

[11] S. Hatanaka, H. Mitome, K. Yasui, S. Hayashi, Multibubble sonoluminescence enhancement by fluid flow. *Ultrasonics*, **44**, e435-e438 (2006).

Chapter 3

Numerical simulation of sonochemical reaction field in a sonochemical reactor

3.1 Introduction

To design and produce a high performance sonochemical reactor, an understanding of acoustic pressure distributions is the most important. Corresponding to a given distribution of nuclei sizes there is minimum acoustic pressure amplitude, called the threshold pressure amplitude, necessary to produce transient cavitation [1]. The transient cavitations oscillated in pressure field, and implode at the final stage. The implosion of cavitation yields OH radicals which react with solution, and contribute to sonochemical reaction performance. Due to the inhomogeneous distribution of ultrasonic pressure, the reaction occurs only at field where pressure amplitude above sonochemical reaction threshold. This field is defined as reaction field. Furthermore, the oscillation of cavitation bubbles becomes more intensive with the increase of pressure amplitude. The intensity of the oscillation of cavitation bubbles determines the heat release during its implosion, and influences the sonochemical reaction performance by the generation of OH radical. Physical effects like liquid flow, also increases by the increase of pressure amplitudes, as we discussed in Chapter 2. The intensity of an imploded cavitation increases the impulse waves which stir the solution to homogeneous as we will discuss in Chapter 5. Hence, as the acoustic pressure is increased, the sonochemical reaction performance will increase.

However, calculations of pressure distributions taking into account the transient pressure threshold of the sonochemical reaction has never been carried out. The fountain effect induced by bottom transducer irradiation has never been considered. A comparison of calculated pressure field to the experiment results of reaction field has never been checked.

In this chapter, pressure distributions in a large sonochemical reactor with

optimum ultrasonic frequencies for sonochemical reaction (ca. 400-500 kHz) have been calculated. To simulate sonochemical reaction field, which indicates the field reaction happens; pressure magnitudes above the sonochemical reaction threshold value have been depicted. With bottom transducer irradiation, the fountain effect has been considered. The pressure distribution above threshold value was compared to the sonochemical reaction areas in two dimensions. Simulation results agree well with experiment results reported in our previous paper [2]. Furthermore, the superposition of dual-transducer and the influence of reflection plate have been studied.

3.2 Calculation modeling

To calculate the acoustic pressure distribution, the time harmonic wave equation (inhomogeneous Helmholtz equation) was used. It is written as

$$\nabla(-\frac{1}{\rho_c}\nabla p)-\frac{\omega^2}{\rho_c c_c^{\,2}}p=0 \quad . \tag{3-1}$$

Here p and t represent acoustic pressure and time, respectively. The angular frequency ω, is defined as $\omega = 2\pi f$, where f is the ultrasound frequency.

The absorption coefficient is not directly related to the fluid's physical properties. In order to express attenuation in the wave equation, the complex density ρ_c and complex sound speed c_c are written as

$$\rho_c = \frac{Z_c k_c}{\omega}, \quad c_c = \frac{\omega}{k_c}, \tag{3-2}$$

respectively. The coefficient k_c and Z_c are expressed as

$$k_c = \frac{\omega}{c_s} - i\alpha \quad , \quad Z_c = \rho_0 c_s, \tag{3-3}$$

respectively. Where α is the absorption coefficient, c_s and ρ_0 denote the sound speed in media and the density of the media, respectively.

The subdomain condition of the reactor modeling is shown as Fig. 3-1(a). The experiment apparatus is shown in Fig. 3-1(b).

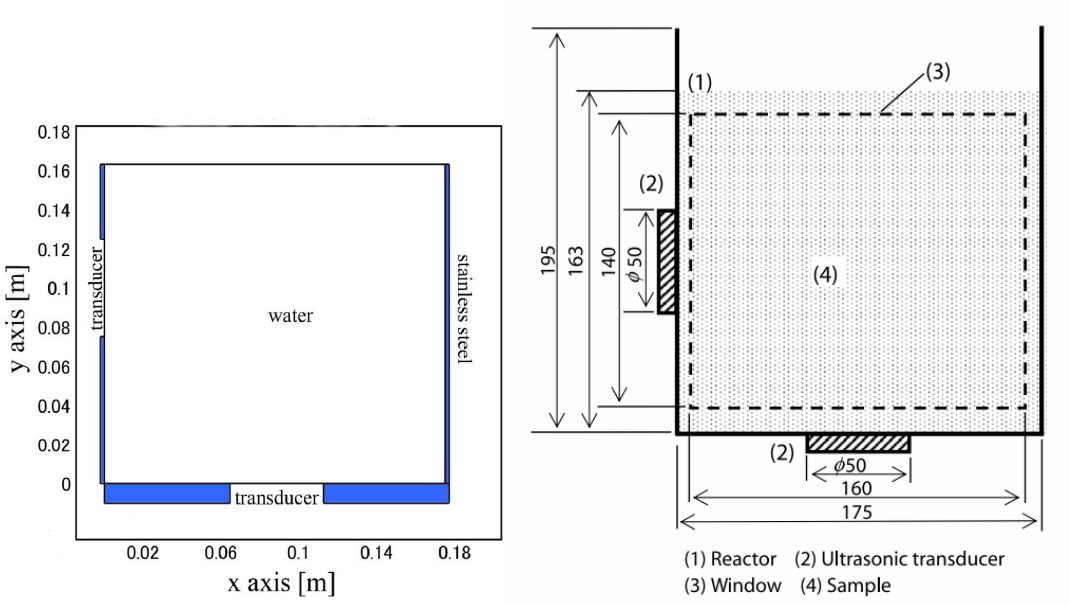

(a) (b)

Fig. 3-1 Simulation and experiment geometry of sonochemical reactor. (a) Subdomain condition of modeling and (b) Experiment apparatus.

In Fig. 3-1, transducer surface is specified as a homogeneous normal acceleration:

$$-\vec{n}\cdot(-\frac{1}{\rho_0}\nabla p)=a_n. \tag{3-4}$$

The value of acceleration has been adjusted according to previous experiment results [2]. For input power of 60 W, acceleration value is set as 0.85×10^5 m·s^{-2}.

The impedance boundary condition is used between all the boundaries (stainless steel and liquid surface) and air, which indicates the reflection property between stainless steel, water and air. The impedance boundary is written as

$$\vec{n}\frac{1}{\rho_c}\nabla p+\frac{1}{Z}\frac{\partial p}{\partial t}=0. \tag{3-5}$$

Here, Z is the acoustic input impedance of the external domain. It can be expressed in a terms of the characteristic impedance inside the domain: $Z = \rho_a c_a$. In our cases, the impedance ($Z = \rho_a$ (= 1.25 kg/m^3) × c_a(= 343 m/s)) is specified as air.

For setting of subdomain, the coefficient of water (ρ_c=1000 kg/m^3 and c_s=1500 m/s), stainless steel (ρ_t=8000 kg/m^3 and c_t=5900 m/s) have been utilized. The thickness of stainless steel at side and bottom has been set as the same as experiment apparatus in previous paper (0.002 and 0.010 m), respectively [2].

The absorption coefficient in water has been discussed in the following part.

The reaction field in sonochemical reaction is in three dimensions. However, due to the limitations of computer, calculations were carried out in two dimensions, and the results have been compared with experiment results in photographs. A sonochemical reactor with the inner size of 0.175 (width) × 0.163 (height) was used. Transducer radii are 0.025 m, one was attached at the center of the bottom wall and the other was attached at the center of the left-hand side wall in the reactor. The emission of plane wave was assumed in two dimensions. The emitted ultrasonic frequency was adjusted until the reflection wave is in maximum. The element size was set as 0.1 to the acoustic wavelength. For experiment condition, the maximum mesh size is limited at 0.3 mm for 472 and 422 kHz. Triangle element has been employed in the model. In calculation, about 18 gigabyte memory was used (peak value), and the calculation time was about 200 seconds.

3.3 Results and discussion

3.3.1 The threshold of a transient cavitation bubble

Reaction areas are important in the evaluation of a sonochemical reaction performance. To compare simulation results to experiment ones carried out in previous paper [2], the threshold of the pressure amplitude to form cavitation

bubbles should be fixed. Šponer [3] theoretically calculated threshold pressure amplitudes for transient caviations with an assumed equilibrium radius of bubbles. From his paper, thresholds of pressure amplitude for transient cavitations at 472 kHz and 422 kHz were about 0.8×10^5 Pa. Since the sonochemical reaction is achieved during the generation of OH radical, the threshold for the transient cavitation is regarded as the threshold for sonochemical reaction. Therefore, pressure amplitudes below 0.8×10^5 Pa are homogenously filled with white in Fig. 3-2. For pressure amplitudes higher than 0.8×10^5 Pa, filled colors corresponding pressure values were expressed in color bar. The maximum of pressure amplitude in the color bar is set as 6×10^5 Pa.

3.3.2 The absorption coefficient

To calculate pressure distributions, the absorption coefficient in water with cavitations should be decided. The side transducer was utilized. Simulation results with absorption coefficients of 0.005, 1 and 3 m^{-1} are plotted in Fig. 3-2(a), (b) and (c), respectively. Experiments for visualization of sonochemical reaction areas were carried out by using luminal aqueous solution. For comparison, the experiment result [2] was shown in Fig. 3-2(d). Compared Fig. 3-2(a) with (d), it is found that reaction areas in Fig. 3-2(a) is more extensive than that in (d). In Fig. 3-2(d), reaction areas are approximately the same as the horizontal areas from the transducer: the vertical width of the reaction areas is close to the diameter of the transducer plate. In Fig. 3-2(a), reaction areas are larger: the width is greater than the diameter of transducer plate. Therefore, an absorption coefficient equals 0.005 m^{-1} is not proper for this calculation. When the absorption coefficient was set as 1 m^{-1}, it can be observed from Fig. 3-2(b) that reaction areas are very close to the experiment result. As the absorption coefficient increases to 3 m^{-1}, it can be observed from Fig. 3-2(c) that

reaction areas become too small and only areas near the transducer center remains reaction areas. Apparently, absorption coefficient equals 1 m^{-1} is most close to experiment result. This result is the same as we discussed in Chapter 2.

Burton [4] experimentally measured the water absorption by using the optical diffraction method. From his results, the absorption of water at acoustic frequency of 500 kHz was 0.005 m^{-1}. However, measurements were carried out by using pulsed waves in a low ultrasonic power. In these cases, absorption of acoustic energy is mainly due to the heat conduction and shear viscosity [5]. Nevertheless, cavitation bubbles formed in our cases due to high acoustic power. The absorption of acoustic pressure is ascribed to the oscillation of bubbles: it transfers the acoustic power into heat and pressure inside the cavitation, and induces the reaction. In addition, the oscillation of cavitation bubbles reflects or scatters the acoustic wave. Therefore, the absorption coefficient is greater than experiment result carried out by Burton. The increase of absorption coefficient has been considered by many researchers: Dähnke et al. [6] considered that the absorption coefficient is about 0.5-5 m^{-1} for pressure area simulation. Yasui et al. [7] also considered that the absorption coefficient should be 5 m^{-1} in pressure field simulations due to cavitation bubbles effect.

3.3.3 Setting of liquid surface

As described in Chapter 2, a fountain forms on liquid surface if a bottom transducer was used. Rough results of pressure distributions have been carried out in Chapter 2: the fountain was not taken into account in simulations. Liquid surface was set as an impedance boundary, which indicates the reflection ratio between the impedance of water and air. However, the fluctuation of fountain disperses and dissipates acoustic energy.

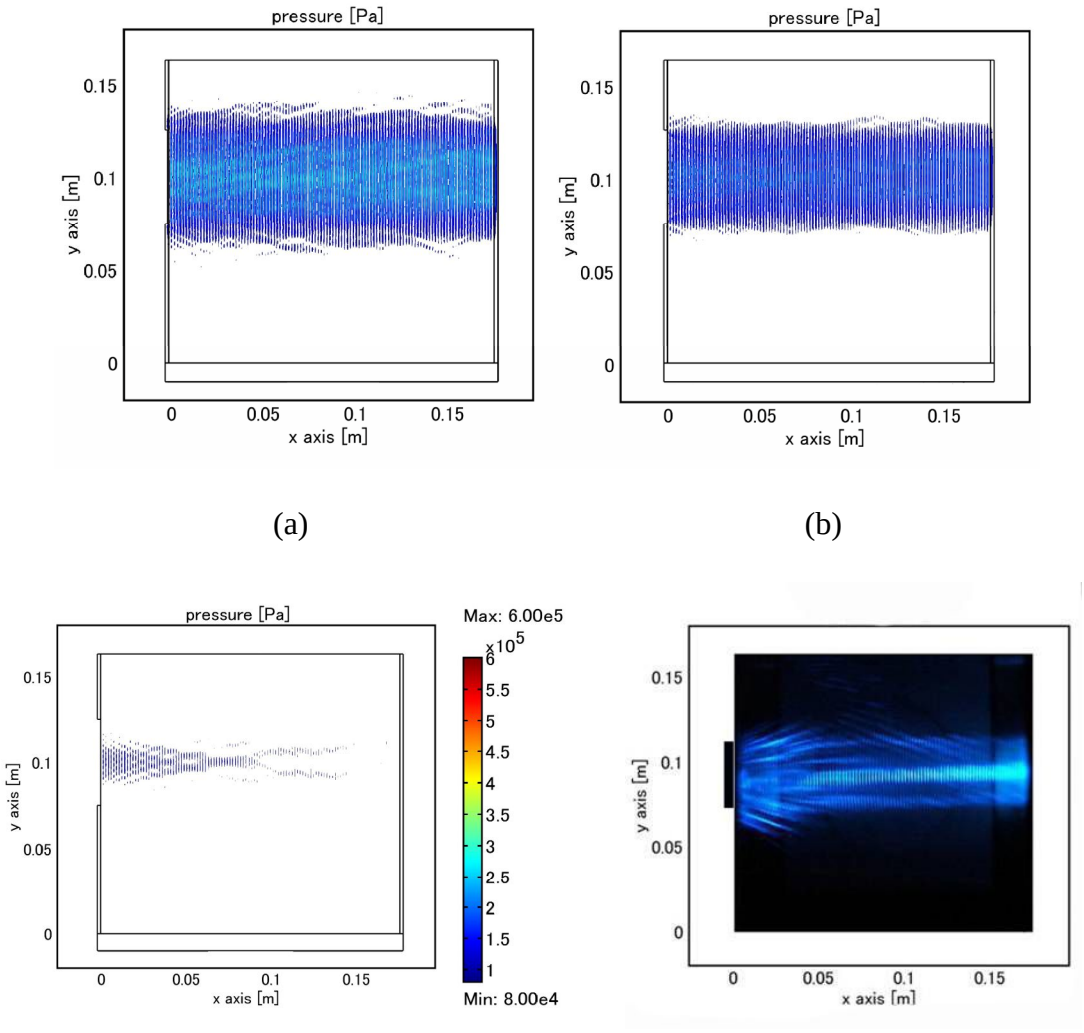

Fig. 3-2 Reaction areas in a sonochemical reactor with 472 kHz side transducer irradiation. The absorption coefficient is set as (a) 0.005, (b) 1 and (c) 3 m^{-1} in simulations. (d) The experiment result for visualization of sonochemical reaction areas by using luminol aqueous solution.

Figure 3-3 shows simulation results with liquid surface set as (a) the impedance boundary, the impedance is set as air (343×1.25 $Pa{\cdot}s{\cdot}m^{-1}$), (b) 0.3 of the incident pressure reflection, (c) 0.8 of the incident pressure reflection, and (d) the experiment result [2]. Compared Fig. 3-3(a) with (d), it is considered that reaction areas is more extensive than that for the experiment result. Therefore, the impedance boundary is not proper in setting of liquid surface when a fountain occurs. A setting of reflecting ratio is necessary in simulating of pressure areas with bottom transducer irradiation.

Compared Fig.3-3(b) with (d), it could be observed that reaction areas with 0.3 of the incident pressure reflection are smaller than the experiment result. When the reflection ratio increases into 0.8, reaction areas (Fig. 3-3(c)) are approximately the same as those in experiment result.

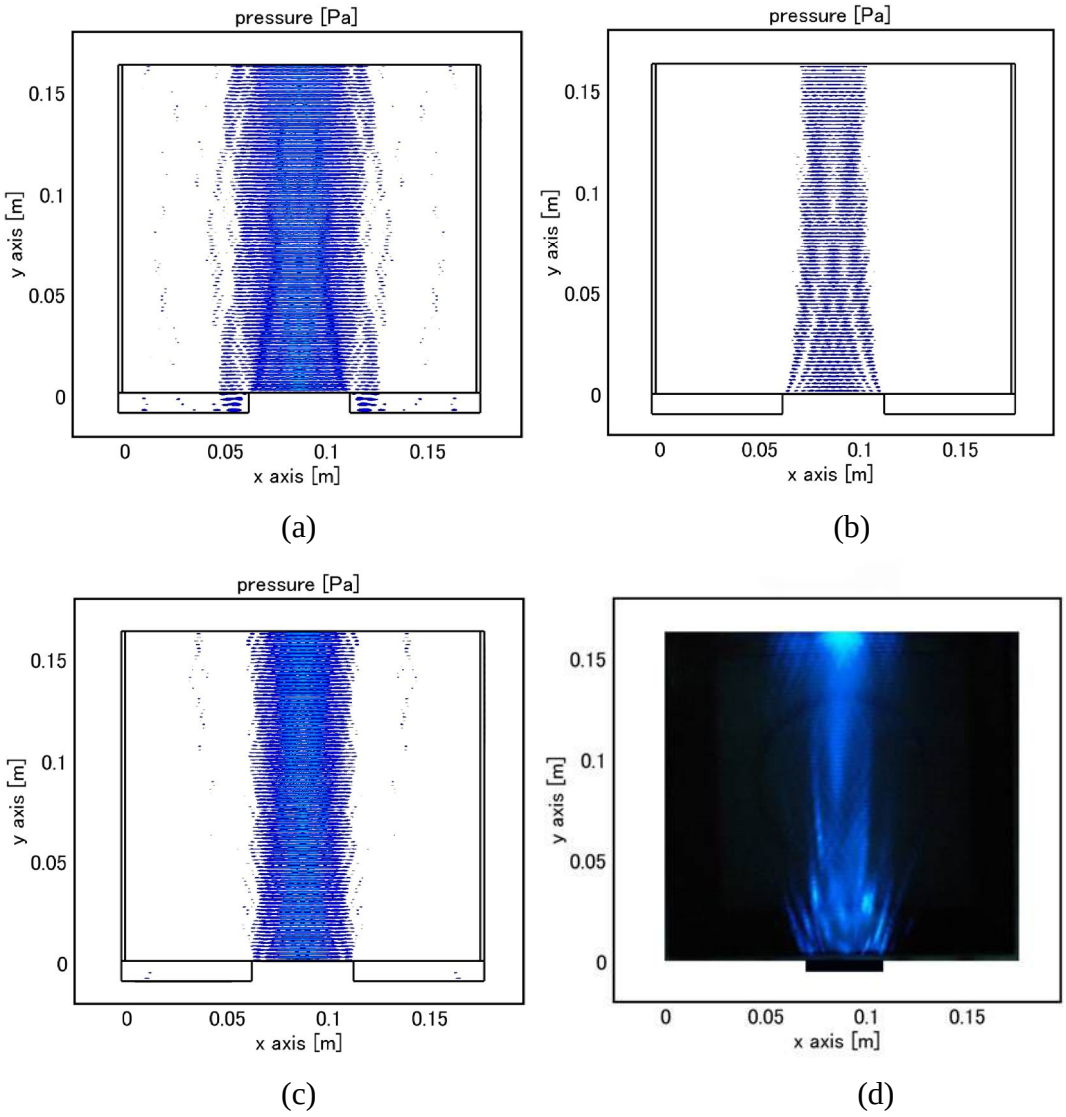

Fig. 3-3 Reaction areas in a sonochemical reactor with bottom transducer irradiation. Liquid surface is set as (a) impedance boundary, (b) 0.3 reflection of incident pressure, and (c) 0.8 reflection of incident pressure. (d) Experiment result for visualization of sonochemical reaction areas by using luminol aqueous solution.

It is considered that the fountain fluctuation disperses and dissipates the acoustic energy, and decreases the reflection wave. In experiment cases, the reflection of incident pressure by liquid surface is about 0.8 of incident acoustic pressure. This value should be changed by the size of fountain and the acoustic frequency.

3.3.4 Dual transducer irradiation

Dual transducer irradiation was numerically simulated. The frequency of bottom and side transducers is set as 422 and 472 kHz, respectively. The result is shown in Fig. 3-4(a). For comparison, experiment result [2] is shown in Fig. 3-4(b). Reaction areas with dual transducer irradiation are more extensive than those with single transducer irradiation, numerically and experimentally. By dual transducer irradiation, some of the unreacted areas become reaction areas due to the superposition of acoustic pressure. Furthermore, it is observed from Fig. 3-4(a) that the pressure amplitude at the cross region becomes very high. It indicates implosion of the cavitation becomes more violent. Therefore, the reaction becomes more intensive. From the experiment result, the cross region also becomes very bright which indicates the reaction becomes more intensive. The simulation result agrees well with the experiment result.

To check the reaction areas quantificationally, the reaction areas for experiment and simulation results have been calculated. Since the photograph has a background color, the blue color value greater than 50 is considered as the reaction areas. In simulation, the pressure amplitude higher than sonochemical reaction threshold (0.8×10^5 Pa) is considered as reaction areas. The calculation results are shown in Tab. 3-1.

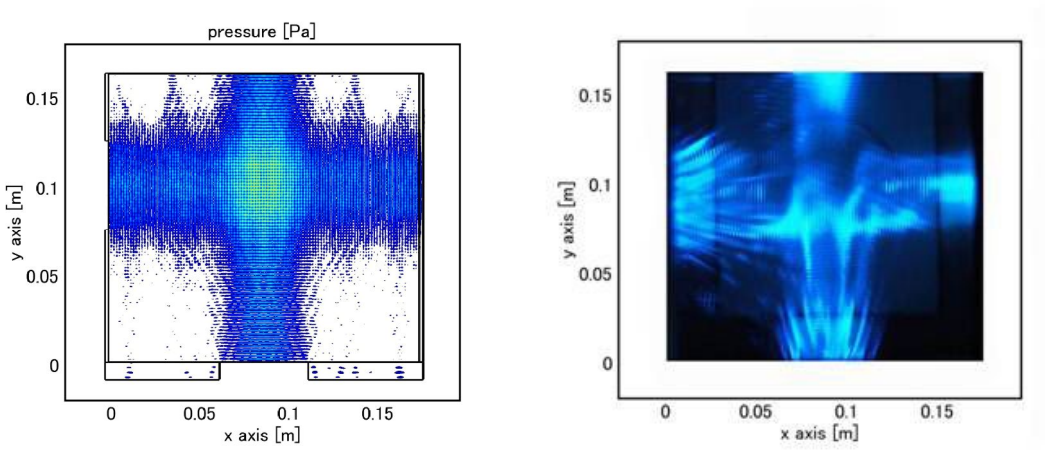

(a) (b)

Fig. 3-4 Reaction areas in reactor with superposed 472 (side) and 422 (bottom) kHz ultrasound irradiation. (a) Simulation result and (b) experiment result.

Table 3-I Simulation and experiment results of reaction areas in a sonochemical reactor with side, bottom and dual transducer irradiation. The results are expressed as (Reaction areas) / (Reactor areas) [-]

	Side	Bottom	Side + Bottom	Dual
Experiment results	0.34	0.29	0.63	0.77
Simulation results	0.36	0.31	0.67	0.77

From Tab. 3-I, it is observed that the simulated results agree well with the experiment results. Furthermore, the dual transducer irradiation induces reaction areas more extensive than the addition of reaction areas induced by bottom and side transducer, respectively. This is one of the origins of the synergistic effect. Another consideration is the intense of reaction areas: The pressure amplitude controls the intensity of bubble oscillation, and further influences the released temperature and pressure during cavitation implosion. In previous experiment result [2], it was found that by use of dual transducers, the sonochemical reaction performance increase almost 100% compared with respective use of bottom and side transducer.

3.3.5 Influence of reflection plate

In Chapter 5, a reflection plate has been used in a sonochemical reactor; the results indicate that the sonochemical reaction is enhanced with the placement of a reflection plate. Here, we numerically calculated the reflection plate influence on reaction areas. Figure 3-5(a) and (b) show the simulation results of reaction areas with a reflection plate at a distance of 0.06 and 0.12 m from transducer, respectively. The maximums of pressure in the reactor for a reflection plate at 0.06 (Fig. 3-5(a)), 0.12 m (Fig. 3-5(b)) and without reflection plate (Fig. 3-2(b)) are 4.19×10^5, 2.68×10^5 and 2.40×10^5 Pa, respectively. From these results, it is considered that the pressure area in the left side is enhanced by the placement of a reflection plate. This is because the pressure is attenuated by the medium during propagation. By the decrease of propagation pathway, the attenuated pressure becomes smaller. The reflection times increase, and the pressure area is enhanced.

In the experiment (Chapter 5), it is found that with the placement of a reflection plate, the sonochemical reaction is enhanced. The luminescence is more intensive than that without reflection plate. Therefore, though the reaction areas are decreased, the increase of the reaction intensity also increases the sonochemical reaction performance.

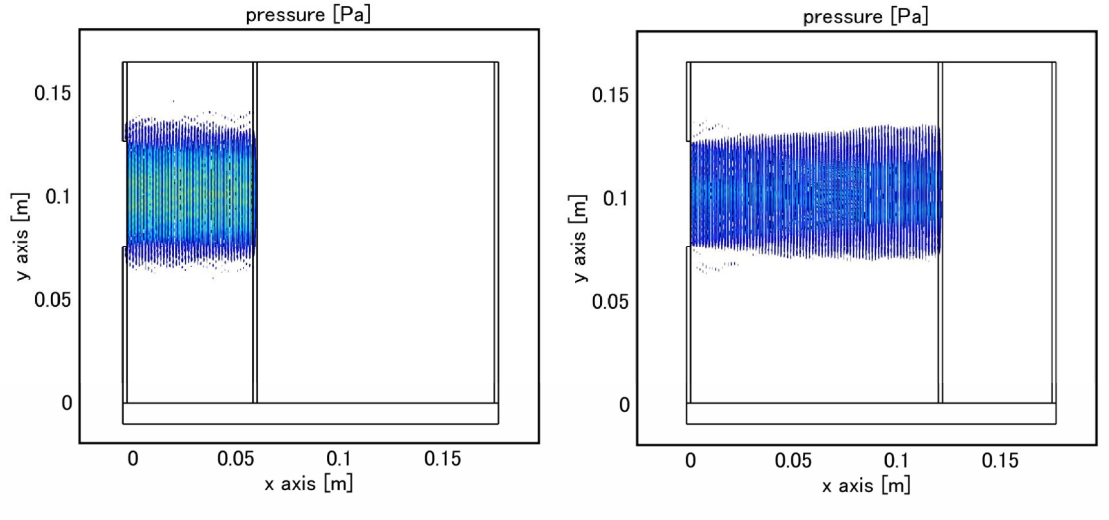

(a) (b)

Fig. 3-5 Reaction areas in a sonochemical reactor with 472 kHz side transducer irradiation. A reflection plate placed at (a) 6 cm and (b) 12 cm from the side transducer is used.

3.4 Conclusions

The sonochemical reaction areas have been studied numerically. The simulation results indicate absorption coefficient in a sonochemical reactor is greater than the experiment measured value due to the existence of cavitation bubble. When using bottom transducer, the fluctuation of liquid surface should be considered in simulation. Dual-transducer enhances sonochemical reaction performance by the enlargement of reaction areas and the enhancement of reaction intensity. The reflection plate enhances the reaction intensity between the transducer and reflection plate.

References

[1] P. Chendke, H. Fogler, Second-order sonochemical phenomena-extensions of previous work and applications in industrial processing. *Chem. Eng. J.*, **8**, 165-178 (1974)

[2] K. Yasuda, T. Torii, K. Yasui, Y. Iida, T. Tuziuti, M. Nakamura, Y. Asakura, Enhancement of sonochemical reaction of terephthalate ion by superposition of ultrasonic fields of various frequencies. *Ultrason. Sonochem.*, **14**, 699-704 (2007).

[3] J. Šponer, Dependence of the cavitation threshold on the ultrasonic frequency. *Czech. J. Phys.*, **40**, 1123-1132 (1990).

[4] J. Burton, A study of ultrasonic velocity and absorption in liquid mixtures. *J. Acoust. Soc. Am.*, **20**, 186-199 (1948).

[5] L. Hall, The origin of ultrasonic absorption in water. *Physical Review*, **73**, 775-781 (1948).

[6] S. Dähnke, K. M. Swamy, F. J. Keil, Modeling of three-dimensional pressure fields in sonochemical reactors with an inhomogeneous density distribution of cavitation bubbles: comparison of theoretical and experimental results. *Ultrason. Sonochem.*, **6**, 31-41 (1999).

[7] K. Yasui, T. Kozuka, T. Tuziuti, A. Towata, Y. Iida, J. King, P. Macey, FEM calculation of an acoustic field in a sonochemical reactor. *Ultrason. Sonochem.*, **14**, 605-614 (2007).

Chapter 4

Enhancement of sonochemical reaction by dual-pulse ultrasound

4.1 Introduction

To enhance sonochemical reaction performance, dual-pulse ultrasound has been checked. In this chapter, the effects of dual-pulse ultrasound on the oxidation of KI and the degradation of acid orange 7 solutions have been investigated. The reactor with two transducers attached at the bottom, the reflective surface of which was free (liquid surface), and at the side, the reflective surface of which was rigid (stainless steel), was used. The ultrasonic signal from the two transducers was modulated into continuous or pulsed waves. It was observed that both dual transducers and pulsed waves enhanced the sonochemical reaction rate. The amounts of enhancement sonochemical reaction originating from the application of the dual transducers and the pulsed wave were estimated separately and both enhancement mechanisms were discussed.

4.2 Experiment methods

4.2.1 Apparatus

Figure 4-1 shows the outline of the experimental apparatus. The reaction vessel was made of transparent acrylic resin [120×120×350 mm^3 (in height)]. A reflection plate made of stainless steel was fixed on the right-side wall of the reactor. Two transducers of 50 mm diameter, operated at 490 kHz, were attached on the bottom and the side wall of the rectangular vessel. The transducers were driven by two power amplifiers and a signal generator with two channels to emit sinusoidal signals with the selected frequency. The effective electric power input to the transducer was calculated from the voltage at the transducer and the current measured by an

oscilloscope (Tektronix TDS3014B) and a current probe (Tektronix TCP202). The ratio of the ultrasonic power to the effective electric power input to the transducer was 80 % as determined by the measurement by the calorimetry method.

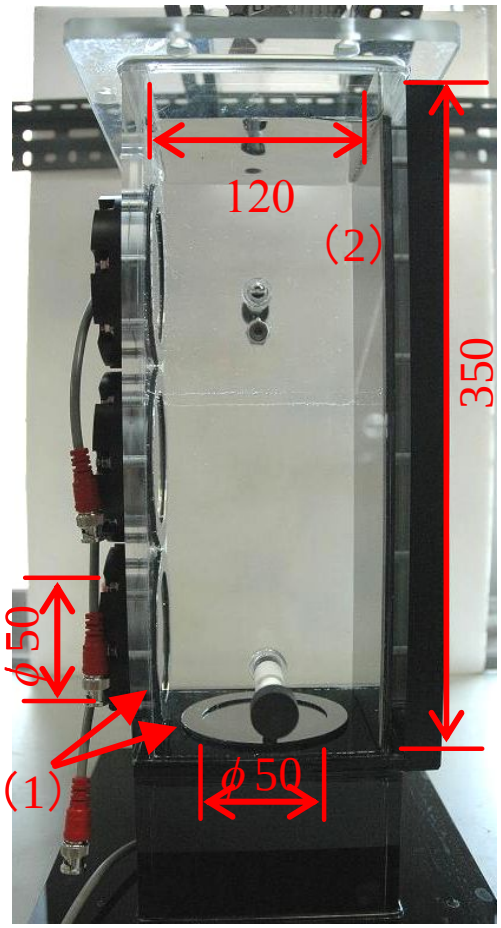

(1) Transducers (2) Reflection plate

Figure 4-1 Experimental apparatus.

4.2.2 Sample

KI and acid orange 7 [AO7, 4-(2-hydroxy-1-naphthylazo) benzenesulfonic acid, sodium salt, also known as orange II] aqueous solution, were used as samples. The initial concentrations of KI and AO7 solution were fixed at 100 and 2.85×10^{-2} mol/m^3, respectively. The sample volume was 3 L. In order to diminish the influence of the initial gas content, air was sparged into solution by air pump for 15 min before

the experiment. The sample temperature was within 293 – 295 K. After 30 min of reaction, the amount of I_3^- formation or AO7 degradation was measured using a UV spectrometer.

4.2.3 Visualization

The sonochemical reaction fields were visualized using sonochemical luminescence. The concentrations of luminal solution and sodium hydroxide were 30 and 0.72 mM, respectively. The luminal (3-aminophthalhydrazide) reacts with hydroxyl radicals, which are produced by sonolysis of water, to generate luminescence. The luminal image was recorded for an exposure time of 45 s using a digital camera (Nikon D70) in a dark room.

4.2.4 Power-modulated pulsed wave

In previous studies, researchers used time-modulated pulsed ultrasound, it was found that the sonochemical yield was never better than under CW conditions [1]. Therefore, a power-modulated pulsed wave was used to balance the overall energy between pulsed and continuous waves in chapter. In order to obtain the same total ultrasonic energy over a given time period by the following expression, analogous to that for irradiation time [1]:

$$P_{pw} = P_{cw} (1 + 1 / R). \quad (4\text{-}1)$$

R is calculated by

$$R = t_{on} / t_{off}, \quad (4\text{-}2)$$

where P_{pw} and P_{cw} are ultrasonic powers for the pulsed wave at the pulse on time and for the continuous wave, respectively. The t_{on} and t_{off} represent pulse on time and

off time, respectively. In our experiment, t_{on} and t_{off} were set to be equal (R = 1) and this condition was the same as that reported by Casadonte et al [1]. The input power of the transducer for continuous wave irradiation was 25 W. Thus, when utilizing pulsed waves, the input power at the pulse on time was 50 W. The ultrasonic irradiation time was fixed at 30 min.

4.3 Results and discussion

4.3.1 Oxidation of KI solution

(1) Pulsed wave by single transducer

Figure 4-2 shows the effect of pulse on time on I_3^- ion concentration for irradiation from the bottom transducer. The concentration for continuous-wave irradiation is also represented in the figure by the horizontal line. In the case of t_{on} = 0.001 s, the I_3^- ion concentration for the pulsed wave is lower than that for the continuous-wave. According to the discussion by Henglein et al. [2], transient cavitation is regarded as being the most efficient in producing chemical reactions. The implosion of transient cavities releases high temperature and high pressure as well as violently reactive free-chemical radicals such as OH radicals in the liquid. These free radicals can react with solutes in solution. However, a pulse on time with short period (t_{on} = 0.001 s) decreases the possibilities for a transient bubble to implode. Since few implosions occur, most of the cavities remain in existence at the end of the pulse on time. During the pulse off time, the ultrasonic pressure attenuates to 0, and the remaining bubbles relax. Thus, higher ultrasonic pressure is required to induce implosion during the next pulse on time. According to the decrease of implosion bubbles, the

reaction performance became lower compared with the case of continuous-wave irradiation. In the case of t_{on} = 0.04 s, the I_3^- ion concentration for the pulsed wave is higher than that for the continuous wave. The enhancement ratio is calculated as the ratio of I_3^- ion concentration for the pulsed wave to that for the continuous wave, and the value is 26%.

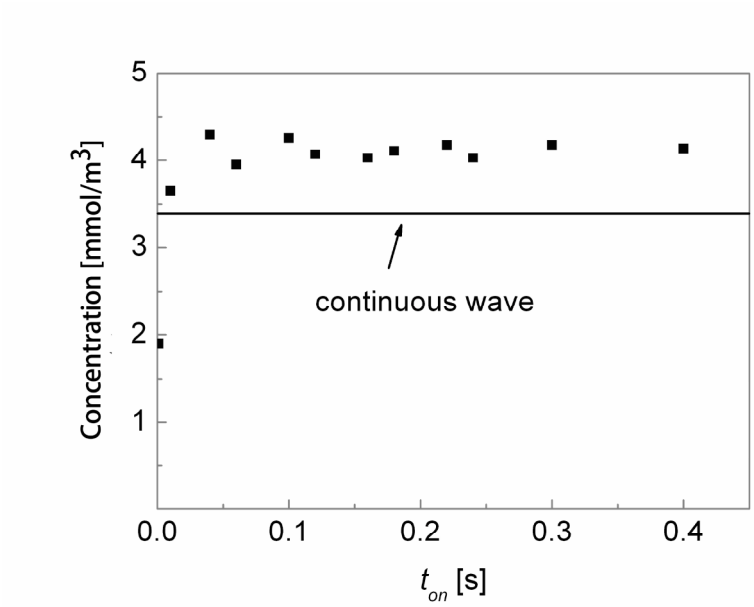

Figure 4-2 Effect of pulsed on time on I_3^- ion concentration for irradiation from bottom transducer.

Figure 4-3 shows the effect of input power to the transducer on I_3^- ion concentration for the continuous-wave. The bottom transducer was used and the input power was below 25 W since the fountain, which disturbs sonochemical reaction [3], was observed on the liquid surface when the input power was above 25 W. Linear fitting is used and the fitted line with the threshold value is also represented in the figure. Entezari and Kruus [4] also reported a linear relationship with a reaction threshold between I_3^- ion concentration and input ultrasonic frequency of 900 kHz. Because of the existence of the reaction threshold for KI

oxidation, none of the I_3^- ion is formed below the threshold. Furthermore, as I_3^- ion concentration was proportional to irradiation time [5], at the same input power, the I_3^- ion concentration for irradiation over 30 min will be doubled compared with the case of irradiation for over 15 min. The I_3^- ion concentration for continuous wave at 50 W over 15 min calculated from data in Fig. 4-2 is 4.0 mmol/m^3, and this value is 18% higher than that for the continuous wave at 25 W over 30 min. From these results, it is considered that the main mechanism of reaction enhancement for the power-modulated pulsed wave is the reduction of the reaction threshold effect. However, the enhancement ratio of the reduction of the reaction threshold effect (18%) is lower than that for pulsed wave at t_{on} = 0.04 s in Fig. 4-2 (26%). It is considered that the difference in the enhancement ratio can be ascribed to the residual sound pressure and the removal of large bubbles impedes implosion during the pulse off time. The residual acoustic amplitude is effective for reuse of the seed bubbles for pulsation [6].

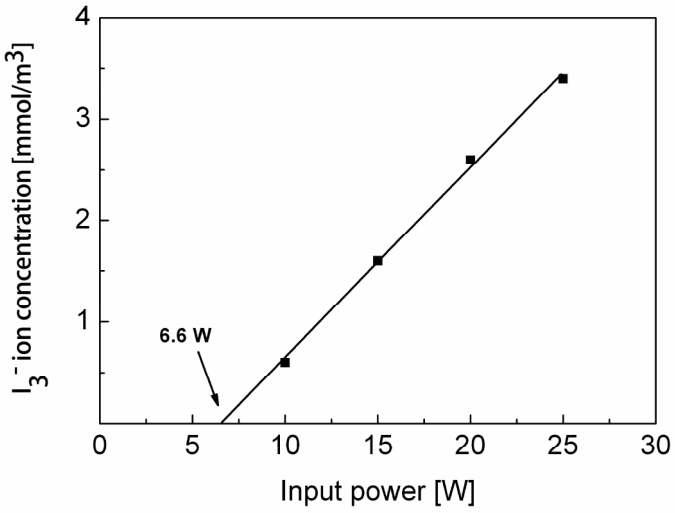

Figure 4-3 Relationship between ultrasonic power and I_3^- ion concentration for irradiation from bottom transducer.

In the case of t_{on} > 0.04 s in Fig. 4-2, the I_3^- ion concentration fluctuates against the pulse on time. A fountain began to form at the liquid surface at t_{on} = 0.06 s, and the fountain height and shape fluctuated with changes in pulse on time. From these results, the fluctuation of I_3^- concentration is due to the formation behavior of the fountain at the liquid surface.

Figure 4-4 shows the effect of pulse on time on I_3^- ion concentration for irradiation from the side transducer. The concentration for continuous-wave irradiation is also represented in the figure by the horizontal line. The I_3^- ion concentrations for irradiation from the side transducer are higher than those from the bottom transducer in Fig. 4-2. This is because the region of standing waves for irradiation from the side wall was expanded by the reflection plate, compared with that for irradiation from the bottom, and the sonochemical reaction effectively proceeds in the ultrasonic field, forming standing waves [7].

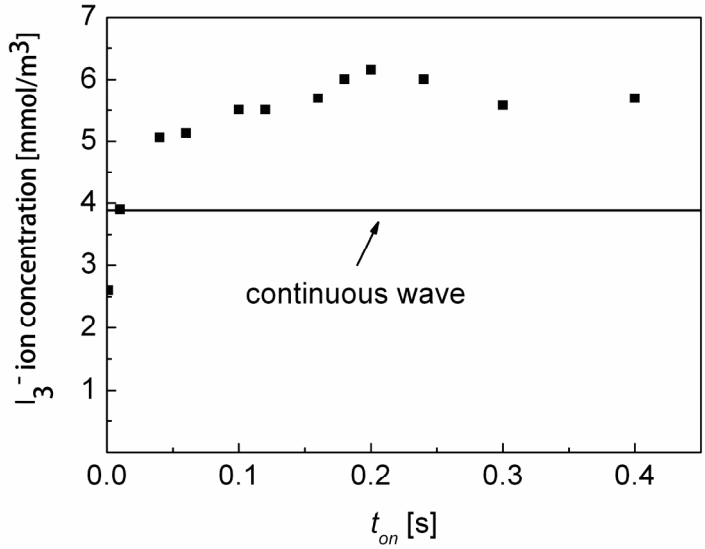

Figure 4-4 Effect of pulsed on time on I_3^- ion concentration for irradiation from side transducer.

In the case of t_{on} = 0.001 s, the I_3^- ion concentration for the pulsed wave is lower than that for the continuous wave. It is considered that a pulse on time with a short period does not satisfy the required period for the oscillation and implosion of a transient cavity. After the rapid increase of the I_3^- ion concentration at t_{on} = 0.04 s, which is due to the reduction of the reaction threshold effect, the I_3^- ion concentration increases with pulse on time until $t_{on} = t_{off}$ = 0.24 s. The enhancement can be ascribed to the residual sound pressure and the removal of large bubbles without implosion during the pulse off time. The number of large bubbles removed increases as the pulse off time becomes longer. Large bubbles that remain without imploding disturb the sonochemical reaction. The enhancement ratio at $t_{on} = t_{off}$ =0.24 s is 58% and this value is higher compared with that when using the free surface (bottom transducer). The ultrasonic field with a fixed surface has a large standing-wave area and many unimploded large bubbles remain in the case of the continuous wave. The pulsed wave removes such large bubbles and the sonochemical reaction is greatly enhanced. In the case of $t_{on} = t_{off} > 0.24$ s, the I_3^- ion concentration becomes lower. It is considered that the residual acoustic pressure cannot maintain the necessary number of pulsating bubbles when the pulsed off time is long.

(2) Dual-pulse irradiation

The effect of dual-transducer irradiation on the oxidation of KI solution using pulsed waves was experimentally investigated. The I_3^- ion concentrations after ultrasonic irradiation by continuous and/or pulsed ultrasonic waves from side and

bottom transducers are listed in Table 4-I. The pulse on time of 0.24 s was chosen in all pulsed cases because the sonochemical reaction performances were high for single irradiation from the bottom or side transducer. In the case of dual pulsed irradiation, the phases of pulsed waves were same. In order to clarify the mechanism, the enhancement by dual-pulse irradiation has been separated into two parts: the dual-transducer enhancement E_{dual} and pulsed wave enhancement E_{pw}. The definitions are

$$E_{dual} = C(\mathrm{S\&B}) / [C(\mathrm{S}) + C(\mathrm{B})] - 1, \quad (4\text{-}3)$$

$$E_{pw} = C(\mathrm{S\&B}) / [C(S_{cw} \,\&\, B_{cw})] - 1, \quad (4\text{-}4)$$

where S, B, and S&B in eqs. (4-3) and (4-4) denote ultrasound irradiations from side, bottom, and dual transducers, respectively. The subscripts cw and pw indicate continuous and pulsed waves, respectively.

Table 4-I I_3^- ion concentration and amount of enhancement with dual transducer.

	C (mmol/m^3)	E_{dual} (%)	E_{pw} (%)
S_{cw} & B_{cw}	7.83	7.9	-
S_{cw} & B_{pw}	8.63	9.1	10.2
S_{pw} & B_{cw}	10.65	8.5	35.9
S_{pw} & B_{pw}	11.60	13.0	48.1

In the case of dual continuous-wave irradiation, the dual-transducer enhancement is 7.9%. The reaction enhancement due to dual transducers is a result of the enlargement of reaction fields: the area where the acoustic pressure amplitude is above the reaction threshold becomes more extensive in the reactor with dual-transducer irradiation [7]. When utilizing dual pulsed waves, the dual-transducer enhancement is 13%. It is considered that dual-transducer

enhancement becomes higher as the ultrasonic power from dual transducers becomes higher.

Furthermore, when the pulsed wave is superposed on the continuous wave, the pulsed wave enhancements for pulsed wave irradiation from bottom and side transducers are 10.2% and 35.9%, respectively. In the case of pulsed wave irradiation from the side transducer, the enhancement of the I_3^- ion concentration is more obvious compared with pulsed wave irradiation from the bottom transducer.

Moreover, when dual-pulse ultrasound is utilized, the reaction performance is higher than those for any other irradiation conditions. The enhancement was ascribed to the effects of both the pulsed wave and dual transducers. The pulsed wave reduces the effect of the reaction threshold. The residual acoustical pressure at the pulse off time and the removal of large bubbles also influence the reaction. The dual-transducer effect enlarges the reaction areas by the superposition of the ultrasonic field. Thus, utilizing a dual pulse produces the best environment for the sonochemical reaction.

To check the enlargement of the reaction areas when utilizing dual pulsed waves, sonochemical luminescent images were taken, as shown in Fig. 4-5. Figures 4-5(a), 4-5(b), 4-5(c) and 4-5(d) are images of the pulsed wave produced by the bottom transducer, the pulsed wave produced by the side transducer, dual pulsed wave and dual continuous waves, respectively. Upon comparing Figs. 4-5(a), 4-5(b) and 4-5(c), it can be found that dual pulsed irradiation enlarges the reaction field around the crossing area of the propagation of two ultrasonic waves (outlined by red circle),

which indicates that dual pulsed waves enlarge the reaction area, as in explanation. A comparison of dual-pulsed-wave (c) and dual-continuous wave (d) reaction areas also shows that utilizing pulsed waves enlarges the reaction areas. As described, pulsed wave irradiation enhances the reaction via the reduction of the cavitation threshold effect, which results in the enlargement of reaction areas and intensive reaction areas. In a comparison of Figs. 4-5(c) and 4-5(d), the intensive reaction areas cannot be observed in Fig. 4-5(c). However, from the observation by the naked eyes, the sonochemical luminescent field produced by dual-pulsed wave was found to be brighter than that produced by dual continuous wave. These differences may due to the recording system of the camera. The camera recorded the information of pulse on and off times together during the exposure time. As a result, the image for dual pulsed irradiation became dimmer than that for continuous-wave irradiation.

Superposition modes have been experimentally investigated. The signal trigger of a signal generator with two channels was modulated; two superposition modes were formed at the center of the reaction vessel. The first was the superposition of two pulsed on cycles (on phase). The other was the superposition of the pulsed on cycle and off cycle together (out of phase). The results are listed in Table 4-II. The superposition of pulsed waves of the on phase generates many more I_3^- ions during reaction compared with the out of phase. This is because the superposition of pulsed waves of the on phase creates higher ultrasonic pressure fields compared with the out of phase. Furthermore, the center of the vessel, as reaction areas, can be enhanced by on phase superposition but not by out of phase superposition.

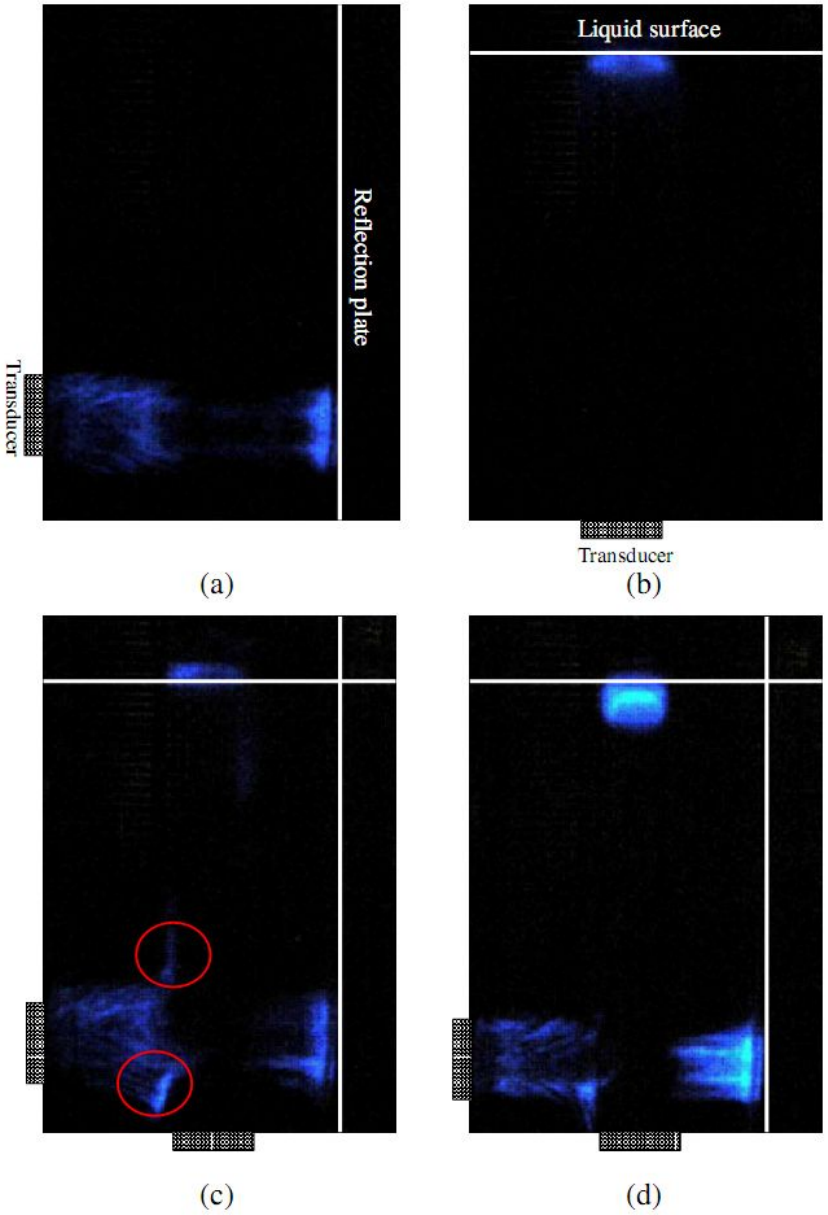

Figure 4-5 Luminal images for irradiation of pulsed and continuous waves (pulsed wave: 50 W, 490 kHz, t_{on}=t_{off}=0.24 s. continuous wave: 25 W, 490 kHz).
(a) Irradiation from side transducer (pulsed wave).
(b) Irradiation from bottom transducer (pulsed wave).
(c) Irradiation from both transducers (pulsed wave).
(d) Irradiation from both transducers (continuous wave).

Table 4-II I_3^- ion concentration for different superposition modes.

	I_3^- ion concentation ($mmol/m^3$)
On phase	11.60
Out of phase	9.31

4.3.2 Degradation of AO7 solution

The degradation of AO7 solution was investigated. The results of pulsed and/or continuous ultrasound irradiation on the degradation ratio (D) of AO7 are listed in Table 4-III. The ultrasound conditions were the same as those in Table 4-II. It is observed that pulsed wave enhancement for the degradation of AO7 is lower than that for the oxidation of KI. The degradation of AO7 in the case of irradiation from the bottom transducer occurred when the input power to the transducer was over 4.4 W, which is lower than that for KI solution. From these results, it is considered that the pulsed wave enhancement becomes more obvious as the reaction threshold becomes higher.

On the other hand, the dual-transducer enhancement is higher than that of the oxidation of KI. In utilizing dual transducers, the enhancement is ascribed to the enlargement of reaction areas and the increase of reaction intensity. Due to the decrease of reaction threshold, the pressure distribution in sonochemical reactor is easy to exceed the reaction threshold by dual-transducer irradiation. Therefore, the enhancement ratio by dual-transducer irradiation increases.

Table 4-III Degradation ratio and enhancement amount for dual transducer in degradation of AO7.

	Degradation ratio	E_{dual} (%)	E_{pw} (%)
S_{cw}&B_{cw}	0.106	15.8	-
S_{cw}&B_{pw}	0.106	19.0	0.03
S_{pw}&B_{cw}	0.108	20.7	1.9
S_{pw}&B_{pw}	0.119	23.1	9.3

4.4 Conclusions

The oxidation of KI and degradation of AO7 solution have been investigated under the irradiation from dual transducers. Pulsed and continuous waves have been modulated to study the mechanism of pulsed waves and dual transducers in the sonochemical reaction. When the pulse on time was sufficiently long, utilizing pulsed wave was more efficient in the reaction than using continuous waves. The effect of the superposition of pulsed wave on reaction performance has also been studied. The best reaction condition can be achieved by utilizing dual pulsed waves. The enhancement was separately calculated. Enhancement by pulsed waves was ascribed to the increase in ultrasound power diminishing the effect of the reaction threshold and the residual acoustical pressure. Enhancement by dual transducers was ascribed to the enlargement of reaction areas. Furthermore, we investigated the superposition of pulsed phases; on phase superposition is more efficient in the reaction than out of phase superposition.

References

[1] D. J. Casadonte Jr, M. Flores, C. Petrier, Enhancing sonochemical activity in aqueous media using power-modulated pulsed ultrasound: an initial study. *Ultrason. Sonochem.*, **12**, 147-152 (2005).

[2] A. Henglein, R. Ulrich, J. Lilie, Luminescence and chemical action by pulsed ultrasound. *J. Am. Chem. Soc.*, **111**, 1974-1979 (1989).

[3] Y. Asakura, K. Yasuda, D. Kato, Y. Kojima, S. Koda, Development of a large sonochemical reactor at a high frequency. *Chem. Eng. J.*, **139**, 339-343 (2008).

[4] M. H. Entezari, P. Kruus, Effect of frequency on sonochemical reactions II. Temperature and intensity effects. *Ultrason. Sonochem.*, **3**, 19-24 (1996).

[5] Z. Xu, C. Y. Ma, J. Y. Xu, X. J. Liu, Dynamical properties of iodine release in potassium iodide solution under combination of ultrasound and light irradiations. *Ultrason. Sonochem.*, **16**, 475-480 (2009).

[6] T. Tuziuti, K. Yasui, J. Lee, T. Kozuka, A. Towata, Y. Iida, Mechanism of enhancement of sonochemical-reaction efficiency by pulsed ultrasound. *J. Phys. Chem. A*, **112**, 4875-4878 (2008).

[7] K. Yasuda, T. Torii, K. Yasui, Y. Lida, T. Tuziuti, M. Nakamura, Y. Asakura, Enhancement of sonochemical reaction of terephthalate ion by superposition of ultrasonic fields of various frequencies. *Ultrason. Sonochem.*, **14**, 699-704 (2007).

Chapter 5

Advanced oxidation processes for wastewater treatment

5.1 Introduction

Advanced oxidation processes (AOPs) refers to a set of chemical treatment procedures to remove organic and inorganic materials in wastewater by oxidation. It constitutes a promising technology for the treatment of wastewater containing non-easily removable organic compounds. Contaminants are oxidized by reagents as ozone, hydrogen peroxide, oxygen, and Fenton. These procedures may also be combined with light or ultrasound irradiations.

In some cases, sonochemical treatment is low efficiency for practical use. Therefore, a combination of sonochemical with any other AOPs is necessary. In this chapter, we investigated the combined use of ultrasound and light irradiations, and combined use of ultrasound and ozone microbubbles. The synergistic effect was obtained in experiment and the mechanism has been discussed.

5.2 Dynamical properties of iodine release under combination of ultrasound and light irradiations

5.2.1 Introduction

To enhance sonochemical reaction performance, we combined ultrasound irradiation with light irradiation to oxidize potassium iodide. We focus on the kinetics of iodine release under ultrasound and light irradiations. It was found that the efficiency for iodine release increases exponentially with irradiation time under combined irradiation of ultrasound and visible light, suggesting the pseudo-first order kinetics. From Chapter 2, it becomes clear that the flow mixing enhances sonochemical reactions. The kinetics analysis indicates that the synergistic effect under combined irradiation of ultrasound and visible light may be due to the well-mixed condition in the photochemical reactor with the applying simultaneous ultrasound.

5.2.2 Apparatus and methods

In experiments, a test solution was prepared by dissolving potassium iodide with analytical purity in 100 ml deionized distilled water, resulting in various concentrations of materials. The apparatus employed in the experiment was consisted of a 200 ml cubic reactor made by quartz glass, which is surrounded by a water-cooling jacket to keep the material solution room temperature. An ultrasonic transducer (20 kHz, 0-30 W/cm^2) made by HuaNeng electron Inc in China was used as the ultrasonic energy source. The transducer probe with radius of 1 cm was immerged in the center of the potassium iodide aqueous solution, as shown in Fig. 5-1. In the experiments, a high-pressure xenon lamp was used as the irradiated light, which transmitted through the material solution from one side of the reactor. The intensity of the irradiated light was adjusted by optical attenuator and measured by the light power-meter. All of the experiments were performed in the darkroom and at room temperature.

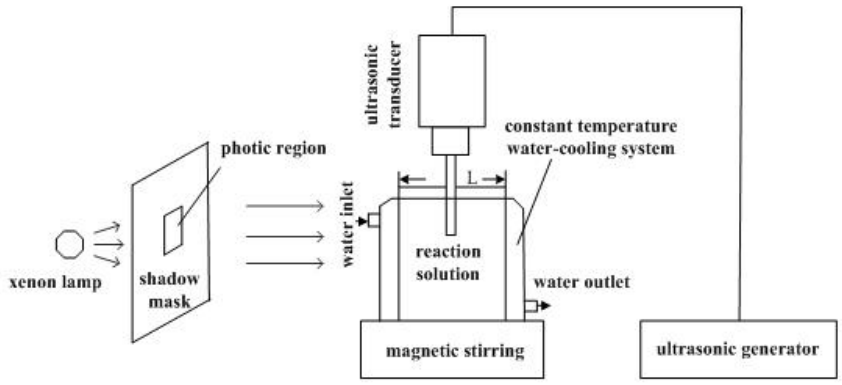

Figure 5-1 Experimental apparatus for iodine release in potassium iodide solution by combination of ultrasound and visible light irradiations.

The amount of iodine release in potassium iodide solution was detected with a UV-Vis spectrophotometer. The absorption spectra of KI solution with various ultrasonic irradiation times are shown in Fig. 5-2. With increasing the irradiation

time, an absorption peak appears at 354 nm, and becomes strong with time. The absorption peak is ascribed to the electron transfer within the I_3^- ions [1]. Under ultrasonic irradiation, I^- ions are oxidized to give iodine. When excess I^- ions are present in solution, iodine will react with the I^- ions, and form I_3^- ions [1]

$$I_2 + I^- \longleftrightarrow I_3^- \tag{5-1}$$

The intensity of absorbance at 354 nm is proportional to concentration of I_3^- ions, which obeys to Lambert-Beer Law [2]. In addition, the amount of iodine release is proportional to concentration of I_3^- ions. Thus, the amount of iodine release can be described with the absorbance $[I]_{abs}$ of I_3^- ions at 354 nm. In our experiments, the efficiency for iodine release r_{KI} in potassium iodide solution is defined as

$$r_{KI} = \frac{[I]_{abs} - [I]_{abs,in}}{[I]_{abs,max} - [I]_{abs,in}} \quad , \tag{5-2}$$

where $[I]_{abs,\,in}$ and $[I]_{abs,\,max}$ are the optical absorbance at 354 nm before irradiation and after reaction saturation, respectively.

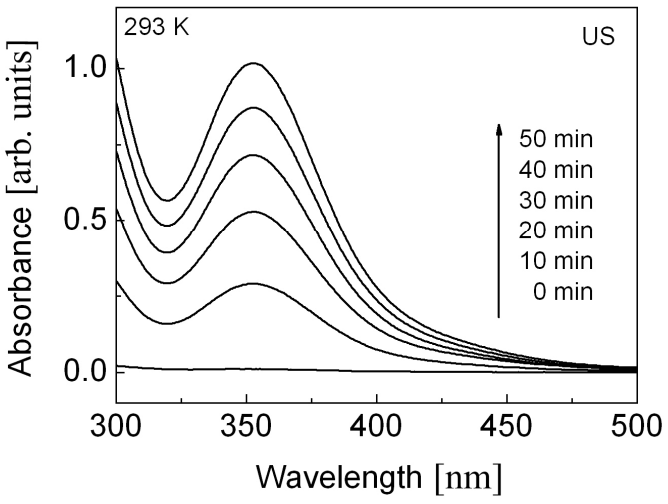

Figure 5-2: Temporal evolution of absorption spectra for potassium iodide solution under irradiation of ultrasound (20 kHz, 1.5 W/cm^2).

5.2.3 Results and discussion

(1) Kinetics for the oxidation of potassium iodide under respective irradiations of ultrasound and visible light

It was found that the amount of iodine release under the combined irradiation of ultrasound and visible light is larger than the sum of those under the respective irradiations of ultrasound and visible light, indicating a synergistic effect of ultrasound and visible light irradiations on the iodine release in potassium iodide solution [3]. Here, we focus on the kinetics of iodine release in potassium iodide solution under combination of ultrasound and light irradiations. Figure 5-3 shows the temporal evolution of iodine release with initial concentration of 0.5 mol/L under irradiation of ultrasound and visible light respectively and simultaneously: A, B and C show the results under ultrasound irradiation (20 kHz and 1.5 W/cm^2), xenon light irradiation (7.6 mW/cm^2) and simultaneous irradiations of ultrasound (20 kHz and 1.5 W/cm^2) and xenon light (7.6 mW/cm^2), respectively. With increasing the irradiation time, A can be fitted with a linear line, while B and C can be fitted with an exponential function.

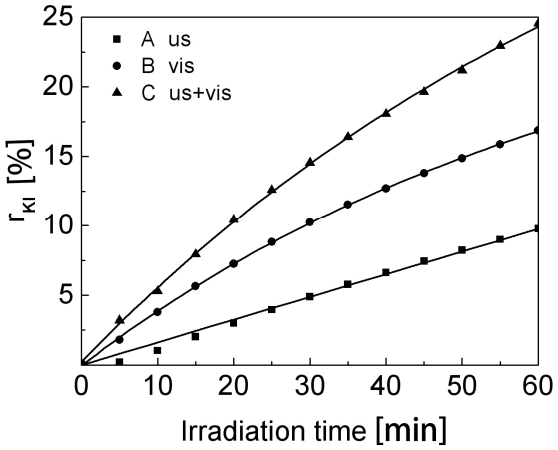

Figure 5-3: Temporal evolution of reaction efficiency for iodine release under irradiation of ultrasound (20 kHz, 1.5 W/cm^2) and visible light (7.6mW/cm^2) respectively and simultaneously.

Recently, Brown et al. [4] have investigated the oxidation of KI by using oxygen and ozone. Ozone oxidation of KI leads to the formation of IO_3^-, which can induce the iodine release in the present of water, while no reaction is found between oxygen and KI in the absent of the irradiation of ultrasound. Under ultrasonic irradiation, the oxidation of potassium iodide can be attributed to the sonochemical reaction due to ultrasonic cavitation [5]. Implosion of cavity bubbles in sonicated water containing dissolved gases can result in the generation of hydrogen (H·) and hydroxyl radicals (·OH) due to fragmentation of water molecules, which should combine and further generate other oxidative species such as hydrogen peroxide (H_2O_2). The hydrogen peroxide generated during the sonochemical cavitation can react with potassium iodide, which results in the increase of the iodine release. The oxidation of potassium iodide can be expressed as

$$2I^- +))) \xrightarrow{k_{us}} I_2, \tag{5-3}$$

where k_{us} is the reaction rate constant under ultrasonic irradiation, and))) denotes the ultrasonic irradiation. The efficiency for iodine release under ultrasonic irradiation increases linearly with the irradiation time (see A in Fig. 5-3), indicating the fact of the zero-order reaction [6]. Then, the formation rate $v_{I_3^-,us}$ can be given as following

$$v_{I_3^-,us} = k_{us}. \tag{5-4}$$

Under light irradiation, the electrons are excited from the ground state to the excited state within potassium iodide, which results in the production of I·. I· reacts with each other to form iodine [7]. The mechanism of oxidation of potassium iodide is expressed as

$$2I^- + h\nu \xrightarrow{k_{vis}} I_2, \tag{5-5}$$

where k_{vis} is the reaction rate constant under light irradiation, and $h\nu$ denotes the light irradiation. The efficiency for iodine release under light irradiation increases exponentially with the irradiation time (see B in Fig. 5-3), indicating the pseudo first-order reaction [6]. The reaction rate of the oxidation of potassium iodide $v_{I_3^-,vis}$ can be given by the following equation [8]

$$v_{I_3^-,vis} = k_{vis} I_{abs} \tag{5-6}$$

where I_{abs} and k_{vis} are the quantity of photons absorbed by a unit volume of solution and first-order constant, respectively.

Normally, the light power cannot be equally absorbed by the medium with the common mechanical stirring in the photochemical reaction system. The absorbed light power is much more intensive near the walls of reactor than that inside the reactor. Thus, the quantity of photons absorbed by a unit volume of solution is related to the path length between the unit volume and the light irradiation surface, indicating a nonhomogeneous photochemical reaction. The $V=SL$ is defined as the solution volume, where S is the irradiation area and L is the path length in the solution. If the light power is equally absorbed in a unit volume of the solution V_{dl} ($V_{dl} = S\mathrm{d}l$; here l is the path length of light), the quantity of photons absorbed by a unit volume at l is expressed as [2]

$$I_{abs,l} = \frac{(I_{l,0} - I_{l,t})S}{S\mathrm{d}l} = I_{l,0}\alpha[\mathrm{KI}], \tag{5-7}$$

where $I_{l,0}$, $I_{l,t}$ are the light intensities at the path length l and $l + dl$, respectively, and α, [KI] are the absorption coefficient and the concentration of potassium iodide solution, respectively.

In the nonhomogeneous system, the photon density should decrease exponentially with the path length l. The light intensity at l can be expressed as

$$I_{l,0} = I_0 \exp(-\alpha[\mathrm{KI}]l). \tag{5-8}$$

Thus, the reaction rate under light irradiation at l can be described as

$$v_{\mathrm{I_3^-},l} = k_{vis} I_{abs,l} = k_{vis} I_0 \alpha[\mathrm{KI}] \exp(-\alpha[\mathrm{KI}]l), \tag{5-9}$$

and the average reaction rate can be obtained by the following equation

$$\overline{v_{\mathrm{I_3^-},vis}} = \frac{1}{L}\int_0^L v_{\mathrm{I_3^-},l}\,\mathrm{d}l. \tag{5-10}$$

The rate equation of oxidation of potassium iodide is obtained by substituting Eq. (5-9) into Eq. (5-10), which is expressed as

$$\overline{v_{\mathrm{I_3^-},vis}} = \frac{k_{vis}}{L} I_0[1-\exp(-\alpha[\mathrm{KI}]L)]. \tag{5-11}$$

In this reaction system, the amount of iodine released is proportional to the amount of potassium iodide consumed in the reaction. Therefore, the concentration of potassium iodide can be presented as follows at the irradiation time t

$$[\mathrm{KI}] = [\mathrm{KI}]_0 - A[\mathrm{I_3^-}] \tag{5-12}$$

where $[\mathrm{KI}]_0$ is the initial concentration of potassium iodide, $[\mathrm{I_3^-}]$ is the amount of iodine release during the reaction, and A is the proportionality coefficient.

The average reaction rate of iodine release in the nonhomogeneous photochemical reaction can be described as

$$\overline{v_{\mathrm{I_3^-},vis}} = \frac{k_{vis}}{L} I_0[1-\exp(-\alpha[\mathrm{KI}]_0 L + A\alpha[\mathrm{I_3^-}]L)] \tag{5-13}$$

Thus, the photochemical reaction rate decreases exponentially with the increase of the amount of the iodine release.

On the other hand, the photochemical reaction system with well-mixed condition can be considered as a homogeneous system. With well-mixed condition, the quantity of photons absorbed by each part of solution can be considered to be the same, and then the quantity of photons absorbed by a unit volume is expressed as

$$I_{abs} = \frac{(I_0 - I)S}{SL} = I_0 \alpha [\mathrm{KI}], \tag{5-14}$$

where I and I_0 are the transmitted and incident intensities of light, respectively. Thus, the reaction rate for oxidation of potassium iodide in the homogeneous system can be obtained from Eq. (5-6)

$$v_{\mathrm{I_3^-},vis} = k_{vis} I_0 \alpha [\mathrm{KI}]. \tag{5-15}$$

Therefore, the relationship between the reaction rate $v_{\mathrm{I_2},vis}$ and the amount of iodine release can be described as

$$v_{\mathrm{I_3^-},vis} = k_{vis} I_0 \alpha [\mathrm{KI}]_0 - A k_{vis} I_0 \alpha [\mathrm{I_3^-}]. \tag{5-16}$$

The reaction rate of photochemical reaction should decrease linearly with the amount of iodine release.

(2) Kinetics for the oxidation of potassium iodide under combined irradiation of ultrasound and light

As shown in curve C of Fig. 5-3, the temporal evolution of iodine release under combined irradiation of ultrasound and visible light indicates an exponential increase with irradiation time. The exponential behavior shows a typical pseudo first-order reaction [6]. The mechanism of oxidation of potassium iodide can be described as

$$2\mathrm{I^-} +))) + h\nu \xrightarrow{k_{us+vis}} \mathrm{I_2}, \tag{5-17}$$

where $k_{\mathrm{us+vis}}$ is the reaction rate constant. Thus, the reaction rate $v_{\mathrm{I_3^-},us+vis}$ can be expressed as

$$v_{\mathrm{I_3^-},us+vis} = k_{us+vis} [\mathrm{KI}], \tag{5-18}$$

which is further expressed by the amount of iodine release as

$$v_{I_3^-,us+vis} = k_{us+vis}[\mathrm{KI}]_0 - Ak_{us+vis}[I_3^-]. \tag{5-19}$$

If the reaction kinetics under the combined irradiation of ultrasound and light is the sum of kinetics under the respective irradiations of ultrasound and light, the reaction rate $v_{I_3^-,us+vis}$ can be obtained through Eqs. (5-4) and (5-11)

$$\begin{aligned} v_{I_3^-,us+vis} &= v_{I_3^-,us} + \overline{v_{I_3^-,vis}} \\ &= k_{us} + \frac{k_{vis}}{L} I_0[1-\exp(-\alpha[\mathrm{KI}]_0 L + A\alpha[I_2]L)] \end{aligned}. \tag{5-20}$$

Thus, the reaction rate should change exponentially with the amount of iodine release in the hypothesis. We have investigated the variation of the reaction rate with the amount of the iodine release under the combined irradiation of ultrasound and light. According to the curve C in Fig. 5-3, we can obtain the variation of the reaction rate though fitting the slope of the curve C with irradiation time *t*. We have found that the reaction rate decreases linearly with the efficiency for iodine release r_{KI}, as shown in Fig. 5-4, which is not consistent with the reaction kinetics as the sum of kinetics under the respective irradiations of ultrasound and light.

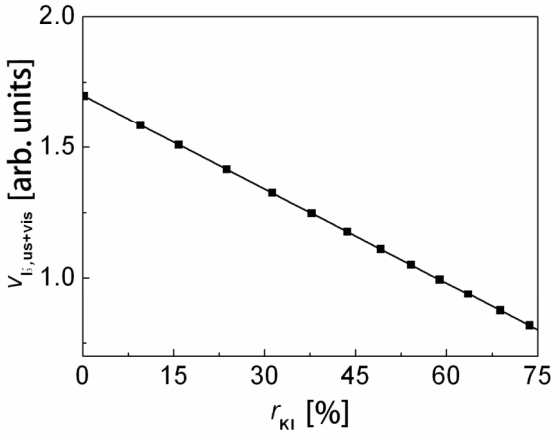

Figure 5-4: Reaction rate vs iodine release during the process of oxidation of potassium iodide under combined irradiation of ultrasound (20 kHz, 1.5 W/cm^2) and visible light (7.6 mW/cm^2).

Here, we have ascribed it to the synergistic effect for the combined irradiation of ultrasound and visible light. It is well known that the well-mixed condition can be produced during the process of bubble formation, growth and sudden collapse under ultrasound irradiation, which can produce more chances for the molecule to absorb light power and drive the photochemical system homogeneous [8,9]. As a result, the reaction rate and efficiency can be improved and the reaction kinetics may be changed. If so, the reaction system can be as the homogeneous system for the potassium iodide solution under combined irradiation of ultrasound and light. The kinetics can be expressed through Eqs. (5-4) and (5-16)

$$\begin{aligned} v_{I_3^-,us+vis} &= v_{I_3^-,us} + v_{I_3^-,vis} \\ &= k_{us} + k_{vis} I_0 \alpha [\mathrm{KI}]_0 - A k_{vis} I_0 \alpha [\mathrm{I_3^-}] \end{aligned} . \qquad (5\text{-}21)$$

In this situation, the reaction rate decreases linearly with the amount of iodine release, which is in accordance with the experiment result.

(3) Influence of initial concentration of potassium iodide on synergistic effect

Figure 5-5(a) shows the time dependence of the efficiency for iodine release r_{KI} with various initial concentrations of potassium iodide under irradiation of ultrasound (20 kHz, 8.0 W/cm^2): A, B, C and D represent the data obtained with the initial concentrations of 0.25, 0.5, 0.75, and 1 mol/L, respectively. When the irradiation time reaches to 50 min, the efficiency for iodine release r_{KI} are 62 %, 33 %, 25 % and 20 % for the initial concentrations of 0.25, 0.5, 0.75, and 1 mol/L, respectively. The respective oxidation ratio to time K_{us}, calculated as the slope of the fitted line, are obtained as 0.01833, 0.00842, 0.00599, and 0.00465 for 0.25, 0.5, 0.75, and 1 mol/L, which are listed in Table 5-I. With increase of the initial concentration, the decrease of r_{KI}-value and suppression of K_{us}-value can be ascribed to the limit of available bubble-water interfacial area: both pyrolysis and

free radical reactions can occur in the interfacial area [10]. Also, the reaction radicals are constant at the fixed ultrasonic power. Thus, the iodine released amounts at different initial concentrations are approximately the same, which results in the decrease of decomposition ratio while increasing initial concentration.

Figure 5-5(b) shows the time dependence of the r_{KI}-value with various initial concentrations under irradiation of visible light (10 mW/cm^2): A, B, C and D show the results under irradiation of visible light with initial concentrations 0.25, 0.5, 0.75, and 1 mol/L, respectively. After 50 min of reaction, the value of r_{KI} for initial concentrations 0.25, 0.5, 0.75, and 1 mol/L are 17.4%, 16.5%, 16 % and 13.7%, respectively. The respective oxidation ratio to time K_{vis}, defined as $K_{vis} = \frac{1}{t}\ln(\frac{r_{KI,t}}{r_{KI,0}})$, are obtained as 0.00320, 0.00285, 0.00274, and 0.00268 for 0.25, 0.5, 0.75, and 1 mol/L, as shown in Table 5-I. Senthilkumaar *et al.* [11] also observed the decrease of r_{KI}-value and suppression of K_{vis}-value with increase of the initial concentration in methylene blue solution under photo-irradiation. They explained the behavior by the decrease of the path length for the photon absorption in the case of the high initial concentration.

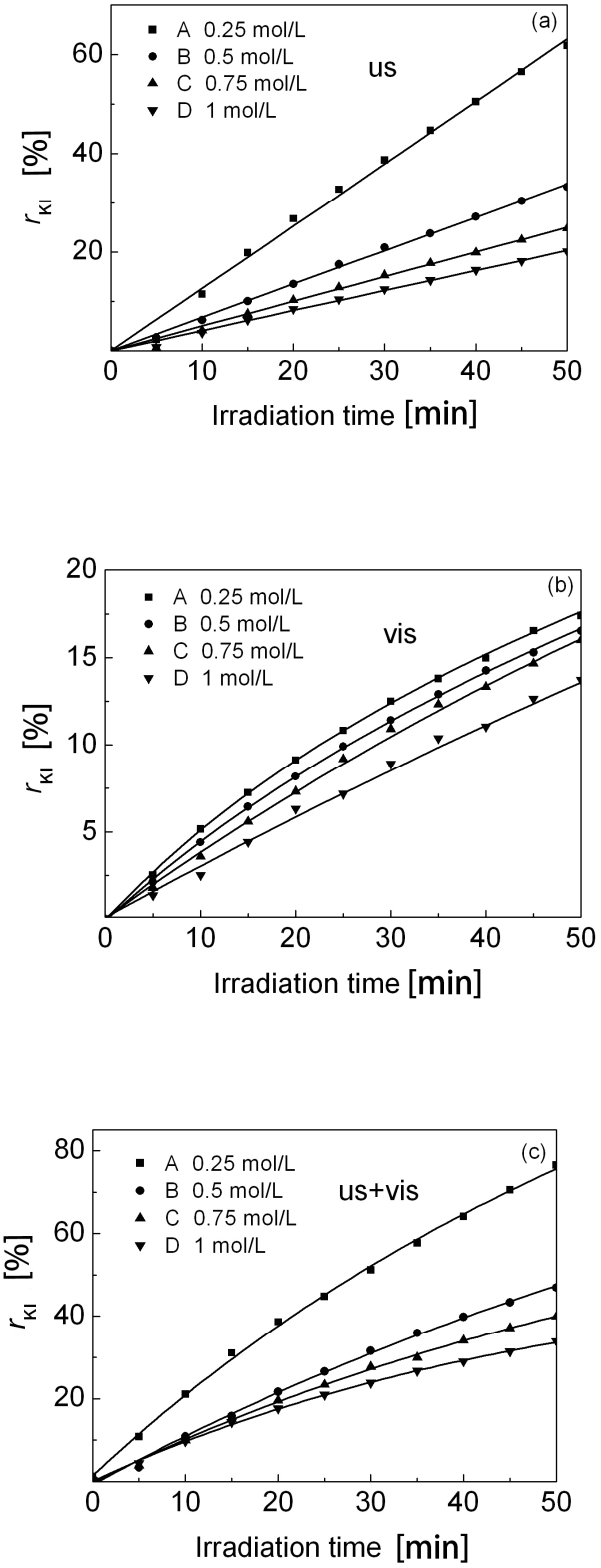

Figure 5-5: Temporal evolution of decomposition ratio for potassium iodide under irradiation of (a) ultrasound (20 kHz, 8.0 W/cm^2), (b) visible light (10 mW/cm^2), and (c) ultrasound (20 kHz, 8.0 W/cm^2) combined with visible light (10 mW/cm^2).

Figure 5-5(c) shows the time dependence of the r_{KI}-value with various initial concentrations under combined irradiation of ultrasound (20 kHz, 8.0 W/cm^2) and visible light (10 mW/cm^2): A, B, C and D show the results with initial concentrations 0.25, 0.5, 0.75, and 1 mol/L, respectively. After 50 min of reaction, the r_{KI}-value for initial concentrations 0.25, 0.5, 0.75, and 1 mol/L are 77%, 47%, 40% and 34%, respectively. The respective oxidation ratio to time $K_{US+vis} = \frac{1}{t}\ln(\frac{r_{KI,t}}{r_{KI,0}})$ are obtained as 0.02762, 0.01355, 0.01002, and 0.00818 for 0.25, 0.5, 0.75, and 1 mol/L, as shown in Table 5-I. It is noted that the K_{us+vis}-value is larger than the sum of the respective K_{us}-value and K_{vis}-value, suggesting the significant synergistic effect of the combined irradiation of ultrasound and visible light.

Table 5-I: Oxidation ratio to time corresponding to the sonolysis, photolysis and sonophotolysis of potassium iodide in various concentrations.

$[KI]_0$ [mol/L]	K_{us}	K_{vis}	K_{us+vis}
0.25	0.01833	0.0032	0.02762
0.5	0.00842	0.00285	0.01355
0.75	0.00599	0.00274	0.01002
1	0.00465	0.00268	0.00818

5.2.4 Conclusions

The oxidation of potassium iodide has been investigated under the irradiations of ultrasound and visible light respectively and simultaneously. We have observed that the amount of iodine liberated under the combined irradiation of ultrasound and visible light is larger than the sum of that under irradiations of ultrasound and visible

light, respectively, indicating a synergistic effect of ultrasound and visible light irradiations. The analysis of reaction kinetics indicates that the ultrasound irradiation can result in the homogenization of the primary light effect in the reaction medium, which may change the kinetics of the photochemical reaction and hence improve the reaction rate and yield. The well-mixed condition under ultrasound irradiation is probably the origin of the synergistic effect.

5.3 Effects of operational conditions on 1,4-dioxane degradation by combined use of ultrasound and ozone microbubbles

5.3.1 Introduction

1,4-Dioxane ($C_4H_8O_2$, dioxane) is widely used in the industry as a solvent for many organic and inorganic compounds. It is a known carcinogen to animals and a suspected carcinogen to human. Furthermore, it is resistant to both aerobic and anaerobic biological processes. Hence, it is classified as a hazardous compound and a priority pollutant. Distillation treatment is not feasible for this compound because of the high boiling point of dioxane (101 °C). Other methods, including activated carbon treatment, and air stripping, enable inefficient removal due to the high aqueous solubility and low vapor pressure of dioxane [12-16]. Therefore, the development of a new dioxane degradation process is necessary.

Microbubbles are bubbles smaller than one millimeter in diameter, but larger than one micrometer [17]. They have a large specific interfacial area, a low rising velocity, a high inner pressure, and high electricity on the surface [18]. Recently, they have been applied in various fields, such as wastewater treatment [19-22], aquafarming, cleaning processes, and production of fine particles. In previous study [21], the decomposition performance of dimethyl sulfoxide was found to be much higher for ozone microbubbles than for ozone millimeter-sized bubbles (millibubbles).

The purpose of this section is to investigate the effect of ultrasound at 490 kHz and its combination with ozone microbubbles (or millibubbles) for the degradation of dioxane solution. The effects of ultrasonic intensity and ozone concentration on the degradation performance are examined and the mechanism of the synergistic effect is discussed.

5.3.2 Experimental procedure

(1) Apparatus

Figure 5-6 shows the outline of the experimental apparatus. The vessel was made of transparent acrylic resin and has the following dimensions: 160 mm length, 100 mm width, and 600 mm height. The ultrasonic transducers were made of PZT (Honda Electronics) and had a diameter 50 mm. Five transducers were attached to one side of the vessel wall. The ultrasonic frequency was 490 kHz. A signal generator (NF WF1974) was used to emit a continuous sinusoidal wave signal. The signal was amplified by a power amplifier to simultaneously drive the five transducers. The reflection plate was made of stainless steel with 3 mm thickness and set perpendicularly to the direction of ultrasonic propagation. The distance between the transducers and the reflection plate was changed to 40, 80, 120, and 160 mm.

The microbubble generator utilizing liquid shear stress (NITTA Awataro) was attached to the lower side of the vessel wall to generate microbubbles. The diameters of microbubbles ranged from 5 to 50 μm, and the median diameter was within 10 – 20 μm. For comparison, a sintered glass gas sparger was used to generate millibubbles, (1 – 5 mm in median diameter) and inserted near the vessel bottom. Ozone gas was supplied by an ozone generator (Okitoronikusu OZM-1200M) from pure oxygen. The ozone concentration in the gas was measured by an ozone meter (Nippon Ozone OMD-100HPF). The gas flow rate of ozone was fixed at 30 ml/min.

(2) Sample and measurement

The initial concentration and volume of dioxane aqueous solution were 10 mg/L and 10.25 L, respectively. The dioxane concentration after the experiment was measured by gas chromatography with a flame ionization detector (GL Science

GC-4000).

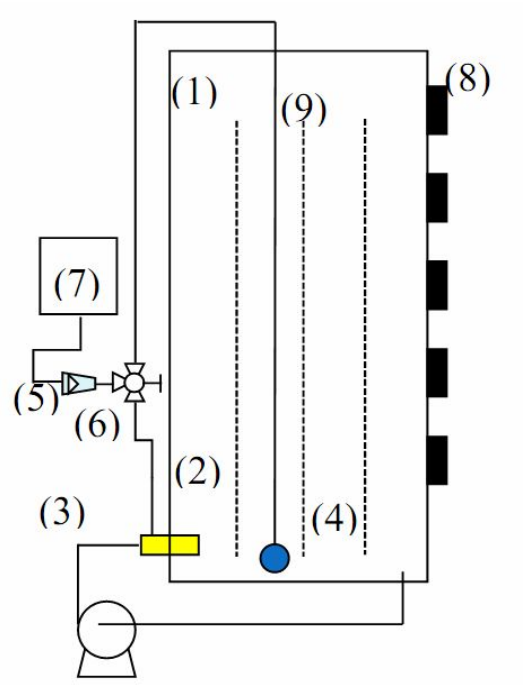

Figure 5-6 Experimental apparatus: (1) reactor, (2) microbubble generator, (3) pump, (4) sintered glass sparger, (5) gas flowmeter, (6) triple valve, (7) ozone generator, (8) ultrasound transducer, and (9) reflection plate.

The sonochemical reaction fields were visualized using the sonochemical luminescence of luminal solution. The concentrations of luminal (3-aminophthalhydrazide) and sodium hydroxide solutions were 30 and 0.72 mM, respectively. The luminal image was recorded for an exposure time of 45 s with a digital camera (Nikon D70) in a dark room. The change in ozone concentration in water with time was measured using an ozone detector (Kasahara Chemical Instruments O3-3F). The concentration of hydrogen peroxide produced in water by ultrasound and/or ozone was determined as follows. After the experiment, the solution was mixed with solutions A and B in a water:solution A:solution B ratio = 2:1:1, where solution A was prepared by dissolving NaOH (1 g), KI (33 g), and $(NH_4)_6Mo_7O_24H_2O$ (1 g) in 500 ml of water, and solution B was prepared by dissolving potassium hydrogen phthalate (10 g) in 500 ml of water. The

concentration of hydrogen peroxide produced by ultrasound and/or ozone was measured by a UV spectrometer (λ_{max} = 350 nm).

5.3.3 Results and discussion

(1) Ultrasound

The efficiency of energy conversion from electric input power to ultrasonic intensity was 80% as measured by a calorimetric method. To optimize the configuration of a sonochemical reactor, the effect of the distance between the transducers and reflection plate on the sonochemical reaction performance was investigated. As reported by Beckett and Hua [13], dioxane degradation by ultrasonic irradiation follows first-order reaction kinetics. Figure 5-7 shows the change in dioxane concentration with time for different distances between the transducers and the reflection plate. The reflection plate was made of stainless steel, and set 4, 8, 12 and 16 cm from transducer. The ordinate indicates the ratio of the present dioxane concentration to initial dioxane concentration. The total input power for the transducers here and elsewhere was fixed at 150 W. The reaction rate constant increases with decreasing distance between the transducers and the reflection plate.

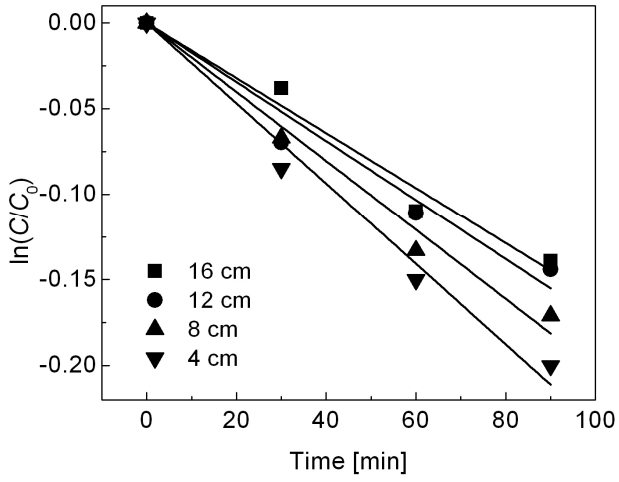

Figure 5-7 Change in dioxane concentration with time by ultrasonic irradiation for different distances between transducers and reflection plate.

Figure 5-8 shows photographs of the sonochemical luminescence of the luminal solution for different distances between the transducers and the reflection plate. The bright area is due to sonochemical luminescence. For a distance of 40 mm [Fig. 5-8(a)], stripes of intense luminescence are observed from the transducer to the reflection plate. Since the interval of stripes corresponds to half the wavelength of ultrasound (ca. 1.5 mm), these stripes represent the formation of standing waves in the reactor. On the other hand, in the case of a distance of 160 mm [Fig. 5-8(b)], the sonochemical luminescence is mostly observed near the reflection surface. From these results, it can be inferred that standing waves with a high acoustic pressure become easier to form as the distance decreases. As we discussed in Chapter 3, since the attenuation of the acoustic pressure field in the sonochemical reactor is large owing to cavitation bubbles, a decrease in the distance of ultrasonic propagation reduces the acoustic energy loss of incident waves at the reflection plate results in a increase of reflection times. Thus, the sonochemical reaction performance increased. The rest of the experiment result was obtained with a distance between the transducers and the reflection plate of 40 mm.

Figure 5-9 shows the effect of total input power to five transducers on reaction rate constant. Linear fitting is utilized to describe the relation between input power and reaction rate constant, and the fitting line is also plotted in figure. As we discussed in Chapter 3, there exists a threshold power for exciting the sonochemical reaction. For the degradation of dioxane with our apparatus, the threshold power is 58 W for ultrasonic irradiation by five transducers (11.6 W each). Therefore, the following empirical relation was obtained:

$$k_{US} = 2.6\times10^{-5}(P–58), \qquad (5\text{-}22)$$

where k_{US} ($=\frac{1}{t}\ln(C_0 / C)$) is the reaction rate constant by ultrasonic irradiation and P (W) is the total input power to five transducers.

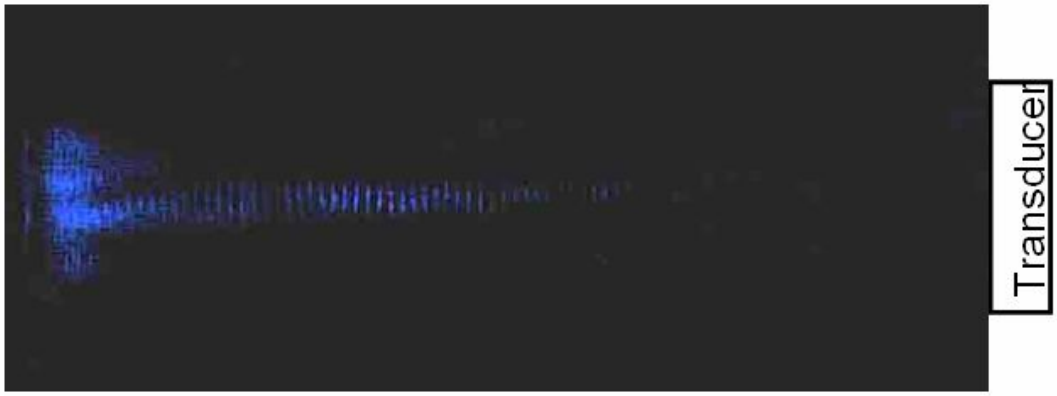

(a)

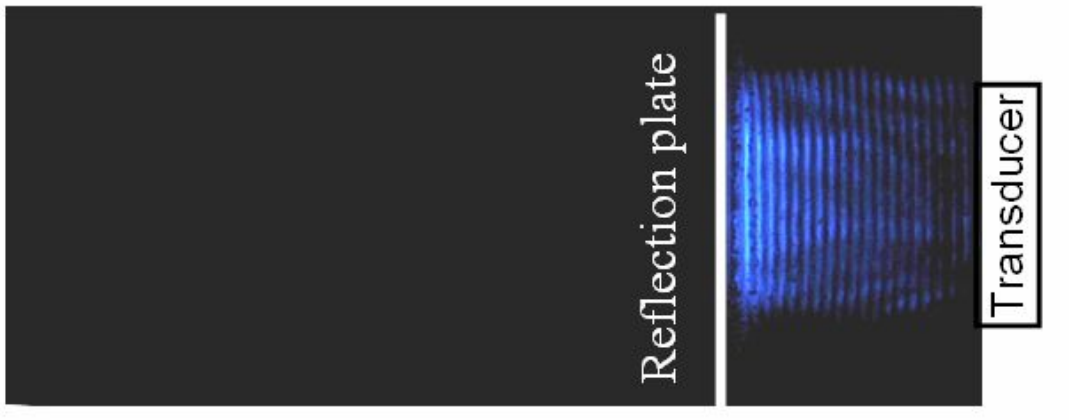

(b)

Figure 5-8 Photographs of sonochemical luminescence of luminol solution for different distances between transducers and reflection board. The distances are (a) 40 and (b) 160 mm.

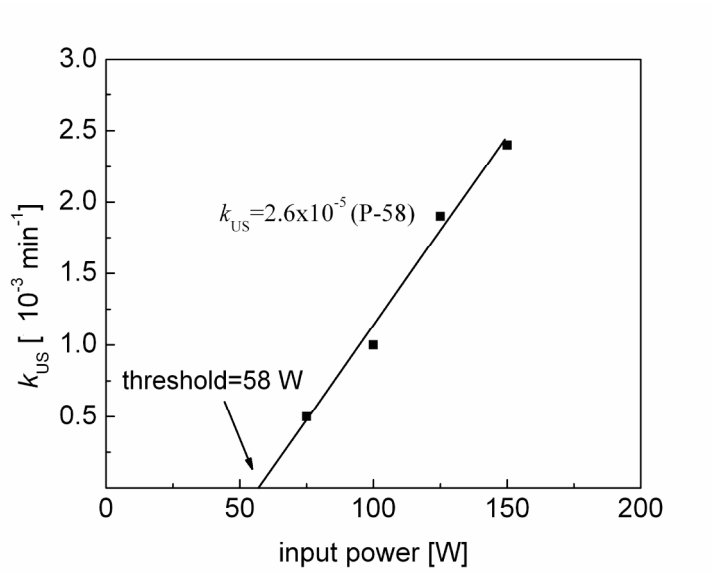

Figure 5-9 Effect of total input power to five transducers on reaction rate constant.

(2) Ozone microbubbles

The effect of bubble size on the ozonolysis of dioxane solution was examined. Figure 5-10 shows the change in dioxane concentration with time for ozone millibubbles and microbubbles. The ordinate indicates the ratio of the present dioxane concentration to the initial dioxane concentration. The ozone concentration in gas was fixed at 101.5 mg/L. The dioxane degradation by ozone obeys the first-order reaction kinetics, as reported by Suh and Mohseni [16]. The reaction rate constant for microbubbles is higher than that for millibubbles.

To discuss the difference in reaction rate constant between microbubbles and millibubbles, the ozone concentration in water was measured. Figure 5-11 shows the changes in the dissolved ozone concentration in water with time for ozone millibubbles and microbubbles, respectively. Compared with ozone millibubbles, ozone microbubbles dissolve rapidly, that is, their volumetric mass transfer coefficient is large. Their maximum ozone concentration is also high. This means that their volumetric mass transfer coefficient is large since the maximum ozone concentration increases with the volumetric mass transfer coefficient [23]. From

these results, it is clear that microbubbles with a large specific interfacial area and a low rising velocity enhance ozone dissolution from the gas phase to the liquid phase and show a high degradation rate for dioxane in water.

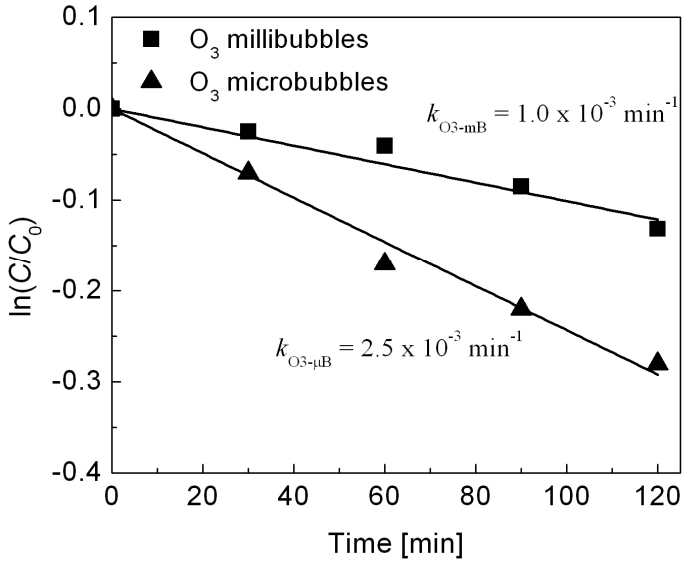

Figure 5-10 Changes in dioxane concentration with time for ozone millibubbles and microbubbles.

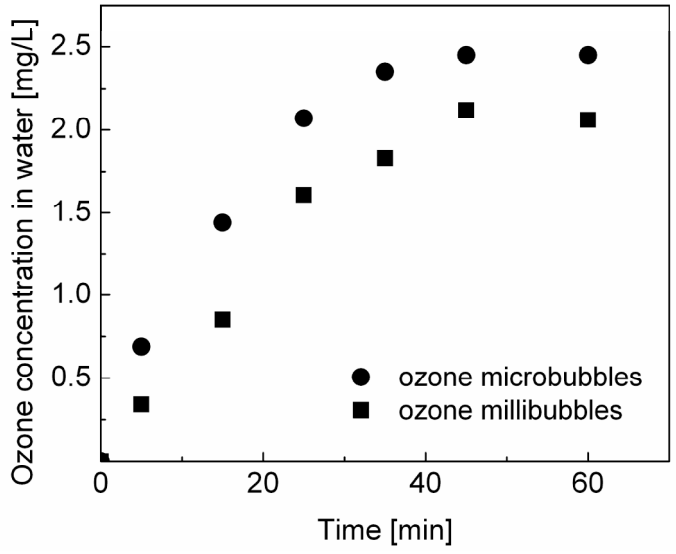

Figure 5-11 Changes in dissolved ozone concentration in water with time by ozone millibubbles and microbubbles.

Figure 5-12 shows the effect of ozone concentration for microbubbles on the reaction rate constant of dioxane degradation. The reaction constant for microbubbles is proportional to ozone concentration. For the millibubbles, Suh and Mohseni showed that dioxane degradation rate is proportional to ozone concentration [16]. Linear fitting is utilized to describe the relation between ozone concentration and reaction rate constant, and the fitting line is also plotted in figure. The following empirical relation was obtained:

$$k_{O3\text{-}\mu B} = 2.2 \text{ x } 10^{-5}\, G, \tag{5-23}$$

where $k_{O3\text{-}\mu B}$ (min^{-1}) is reaction rate constant by ozone microbubbles and G (mg/L) is the ozone concentration.

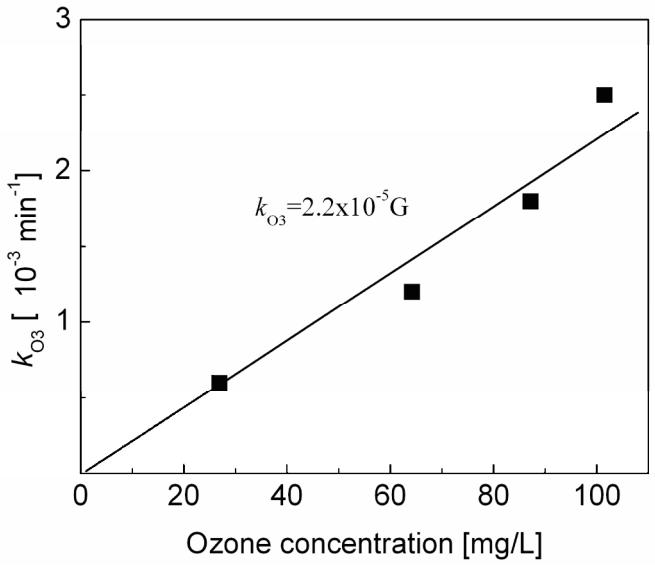

Figure 5-12 Effect of ozone concentration on reaction rate constant.

(3) Combination of ultrasound and ozone microbubbles

Ultrasound and ozone were simultaneously utilized and an experiment on dioxane degradation was carried out. Figure 5-13 shows the change in dioxane concentration with time for ultrasound, ozone microbubbles, and their combination. Total input

electrical power and ozone concentration were fixed at 150 W and 101.5 mg/L, respectively. For the combination of ultrasound and ozone microbubbles, the degradation of dioxane follows first-order reaction kinetics. The reaction rate constant for the combination of ultrasound and ozone microbubbles is 6.3×10^{-3} min^{-1} (which is higher than that for the combination of ultrasound and ozone millibubbles, 4.2×10^{-3} min^{-1}). However, the sum of reaction rate constants for ultrasound and ozone microbubbles is 4.9×10^{-3} min^{-1}. Therefore, these results indicate that a synergistic effect exists in the combination of ultrasound and ozone microbubbles.

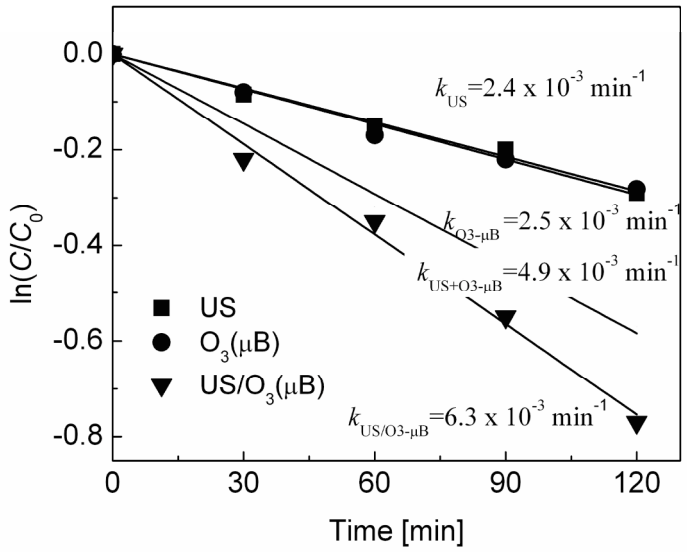

Figure 5-13 Changes in dioxane concentration with time for ozone microbubbles, ultrasound, and their combination.

To clarify the mechanism of the synergistic effect by the combination of ultrasound and ozone microbubbles, *tert*-butanol (t-BuOH) was added to dioxane solution as a radical trap agent. The dioxane degradation with t-BuOH addition by ultrasound, ozone microbubbles, and their combination was carried out. The initial t-BuOH concentration was 84 mg/L, which almost completely quenched the reaction between OH radicals and dioxane. Hence, the reaction rate constant with t-BuOH addition is regarded as the reaction rate constant by the direct reaction except for OH

radicals. Table 5-II shows the reaction rate constants of dioxane degradation by direct reaction (with t-BuOH) for ultrasound, ozone microbubbles, and their combination. For comparison, the table also shows the total reaction rate constant (without t-BuOH) and the reaction constant for OH radicals, which is estimated from the difference in reaction constant between the total (without t-BuOH) and direct (with t-BuOH) reactions.

Table 5-II. Reaction rate constants of dioxane degradation with and without t-BuOH addition for ultrasound, ozone microbubbles, and their combination.

(units: 10^{-3} min^{-1})

	Direct reaction	Total	OH radical reaction (Total-Direct reaction)
US	0.7	2.4	1.7
$O_{3\text{-}\mu B}$	1.0	2.5	1.5
Sum	1.7	4.9	3.2
$US/O_{3\text{-}\mu B}$	0.9	6.3	5.4

The reaction constant by the direct reaction for the combination (0.9×10^{-3} min^{-1}) is smaller than the sum of the reaction constants for ultrasound and ozone (1.7×10^{-3} min^{-1}). By contrast, the reaction constant for OH radicals for the combination (5.4×10^{-3} min^{-1}) is larger than the sum of the reaction constants for ultrasound and ozone (3.2×10^{-3} min^{-1}). For the combined use of ultrasonic irradiation and ozone sparging in water, it is considered that ozone is decomposed thermolytically by sonolysis as follows [12]:

$$O_3(g) +))) \rightarrow O_2(g) + O(^3P)(g), \quad (5\text{-}24)$$

$$O(^3P)(g) + H_2O(g) \rightarrow 2\cdot OH(g), \quad (5\text{-}25)$$

$$\cdot OH + \cdot OH \rightarrow H_2O_2. \quad (5\text{-}26)$$

The synergistic effect of dioxane degradation can be ascribed to Eqs. (5-24)-(5-26). By ultrasonic irradiation, ozone does not only directly react with dioxane solution but also reacts with ultrasonic cavitation and releases OH radicals. OH radicals react with dioxane and enhance the reaction performance. Moreover, they react with each other and form hydrogen peroxide. This hydrogen peroxide formed further enhances the reaction performance. Therefore, the reaction constant for the direct reaction decreased owing to the ozone decomposition. On the other hand, the reaction constant for the OH radical reaction and the total reaction constant increased.

To confirm the above mechanism of the synergistic effect, the concentrations of ozone and hydrogen peroxide in water were measured. The saturated ozone concentration in water for ozone microbubbles decreased from 2.5 to 1.5 mg/L with ultrasonic irradiation. This is because of ozone decomposition. The hydrogen peroxide concentrations after 30 min for ultrasound and ozone microbubbles were 4.07 and 8.27 μM, respectively. The hydrogen peroxide concentration for their combination was 15.24 μM, which was higher than the sum of the concentrations for ultrasound and ozone microbubbles.

Figure 5-14 shows the effect of total input power to transducers on reaction rate constant for the combination of ultrasound and ozone microbubbles. Ozone concentration was fixed at 101.5 mg/L. The sums of the reaction constants for ultrasound and ozone microbubbles [US+O_3(μB)] are also plotted in the figure. The reaction constant for the combination increases with increasing input power and is higher than the sums of the reaction constants for ultrasound and ozone

microbubbles. Furthermore, the difference between the reaction constant for the combination and the sum of the reaction constants for ultrasound and ozone microbubbles, which indicates the amount of synergistic effect, increases nonlinearly with increasing input power. It is considered that ozone decomposition enhances the generation of OH radicals at a high temperature induced by intensive cavitation collapse.

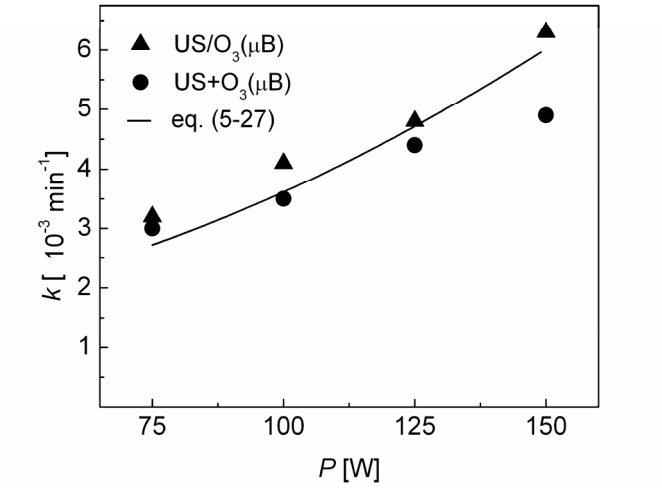

Figure 5-14 Effect of total input power to transducer on reaction rate constant for combination of ultrasound and ozone microbubbles.

Figure 5-15 shows the effect of ozone concentration on reaction rate constant for the combination of ultrasound and ozone microbubbles. The total input power to the transducers was fixed at 150 W. The sums of the reaction constants for ultrasound and ozone microbubbles are also plotted in Fig. 5-15. The reaction constant for the combination increases with increasing ozone concentration and is higher than the sums of the reaction constants for ultrasound and ozone microbubbles. Furthermore, the amount of synergistic effect increases nonlinearly with increasing ozone concentration. It is considered that the number of OH radicals due to ozone decomposition increases as ozone concentration increases.

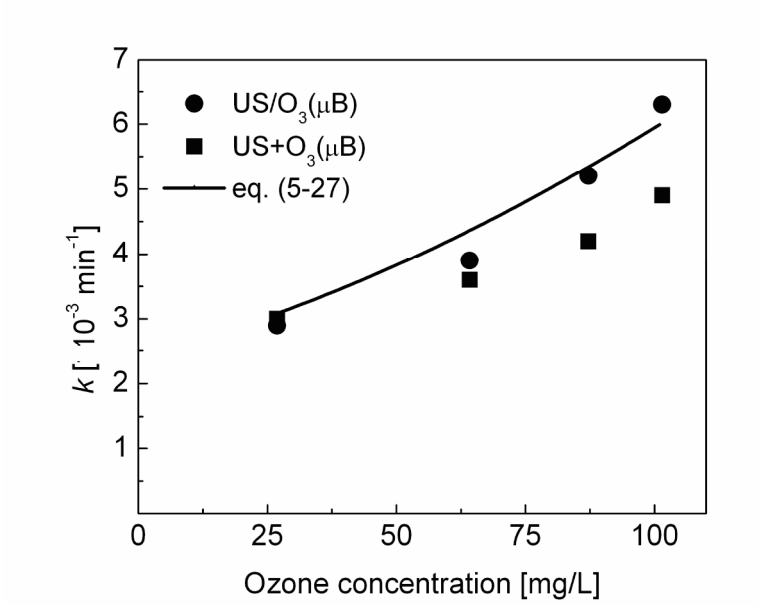

Figure 5-15 Effect of ozone concentration on reaction rate constant for combination of ultrasound and ozone microbubbles.

The results in Figs. 5-14 and 5-15 indicate that the synergy effect for the combination of ultrasound and ozone microbubbles is enhanced nonlinearly as the input power to the transducers and ozone concentration increase. We simply expressed the reaction rate constant of dioxane degradation for the combination as the following empirical relation developed using Eqs. (5-22) and (5-23):

$$k_{\mathrm{US/O3\text{-}\mu B}} = k_{\mathrm{US}} + k_{\mathrm{O3\text{-}\mu B}} + k_{\mathrm{synergy}}$$

$$= 2.6\times10^{-5}(P-58)+2.2\times10^{-5}\,G+1.6\times10^{-11}G^{2}\,(P-58)^{2} \qquad (5\text{-}27)$$

$$0 < G < 101.5 \text{ mg/L}, \; 58 < P < 150 \text{ W},$$

where k_{synergy} (min^{-1}) is the difference between the reaction constant for the combination and the sum of the rate constants for ultrasound and ozone microbubbles. The calculated results obtained using Eq. (5-27) are also plotted in Figs. 5-14 and 5-15 as curves and they are in good agreement with the experimental results.

From this section, we found out that ozone microbubbles are efficient in dioxane

degradation, especially in combination with ultrasound. The synergistic effect depends on ozone concentration and the input power to the transducers. Empirical equations considering the reaction constants for ultrasound, ozone microbubbles, and their combination has been established, according to the experimental data.

5.3.4 Conclusions

In this section, the degradation of 1,4-dioxane in water by the combined use of ultrasound and ozone microbubbles has been investigated. It is found 1,4-dioxane degradation by ultrasound and/or ozone microbubbles follows a first-order reaction kinetics. A synergistic effect on reaction constant was observed by the combined use of ultrasound and ozone microbubbles. The synergistic effect can be ascribed to the number of OH radicals increased with the sonolysis of ozone. The synergistic effect was enhanced nonlinearly with increasing ultrasound input power and ozone concentration. The empirical relations between ultrasound, ozone, and reaction constant were established and were in good agreement with the experimental data.

References

[1] T. J. Mason, J. P. Lorimer, Sonochemistry: Theory, *Applications and uses of Ultrasound in Chemistry*. Ellis Horwood Limited (1988).

[2] J. M. Coxon, B. Halton, *Organic photochemistry*. Cambridge University Press (1974).

[3] S. Senthilkumaar, K. Porkodi, R. Vidyalakshmi, Photodegradation of a textile dye catalyzed by sol-gel derived nanocrystalline TiO_2 via ultrasonic irradiation. *J. Photoch. Photobio. A*, **170**, 225-232 (2005).

[4] M. A. Brown, J. T. Newberg, M. J. Krisch, B. S. Mun, J. C. Hemminger, Reactive uptake of ozone on solid potassium iodide. *J. Phys. Chem. C*, **112**, 5520-5525 (2008).

[5] A. Weissler, H. W. Cooper, S. Snyder, Chemical effect of ultrasonic waves: oxidation of potassium iodide solution by carbon tetrachloride. *J. Am. Chem. Soc.*, **72**, 1769-1775 (1950).

[6] C. Berberidou, I. Poulios, N. P. Xekoukoulotakis, D. Mantzavinos, Sonolytic, photocatalytic and sonophotocatalytic degradation of malachite green in aqueous solutions. *App. Catal. B: Environ.*, **74**, 63-72 (2007).

[7] A. M. Schllowitz, J. R. Wlesenfeld, State-specific production of electronically excited potassium atoms in the ultraviolet photolysis of potassium iodide. *J. Phys. Chem.*, **87**, 2194-2198 (1983).

[8] A. Gáplovský, J. Oonovalová, Š. Toma, R. Kubinec, Ultrasound effects on photochemical reactions, Part 1: photochemical reactions of ketones with alkenes. *Ultrason. Sonochem.*, **4**, 109-115 (1997).

[9] M. H. Entezari, M. Mostafai, A. A. Sarafraz, Combination of ultrasound and a bio-catalyst: removal of 2-chlorophenol from aqueous solution. *Ultrason.*

Sonochem., **13**, 37-41 (2006).

[10] B. Mohammad, M. Nasser, S. Mohammad, V. Behrouz, Effect of operational parameters on degradation of Malachite Green by ultrasonic irradiation. *Ultrason. Sonochem.*, **15**, 1009-1014 (2008).

[11] S. Senthilkumaar, K. Porkodi, R. Vidyalakshmi, Photodegradation of a textile dye catalyzed by sol-gel derived nanocrystalline TiO_2 via ultrasonic irradiation. *J. Photochem. Photobio. A: Chem.*, **170**, 225-232 (2005).

[12] Z. He, S. Song, H. Zhou, H. Ying, J. Chen, CI reactive black 5 decolorization by combined sonolysis and ozonation. *Ultrason. Sonochem.*, **14**, 298-304 (2007).

[13] M. A. Beckett, I. Hua, Elucidation of the 1,4-dioxane decomposition pathway at discrete ultrasonic frequencies. *Environ. Sci. Technol.*, **34**, 3944-3953 (2000).

[14] M. A. Beckett, I. Hua, Enhanced sonochemical decomposition of 1,4-dioxane by ferrous iron. *Water Res.*, **37**, 2372-2376 (2003).

[15] A. Nakajima, H. Sasaki, Y. Kameshima, K. Okada, H. Harada, Effect of TiO_2 powder addition on sonochemical destruction of 1,4-dioxane in aqueous systems. *Ultrason. Sonochem.*, **14**, 197-200 (2007).

[16] J. H. Suh, M. Mohseni, A study on the relationship between biodegradability enhancement and oxidation of 1,4-dioxane using ozone and hydrogen peroxide. *Water Res.*, **38**, 2596-2604 (2004).

[17] S. Onari, M. Miura, K. Matsuishi, Raman spectroscopic studies on bismuth nanoparticles prepared by laser ablation technique. *Appl. Surf. Sci.*, **197**, 615-618 (2002).

[18] M. Takahashi, ζ potential of microbubbles in aqueous solutions: electrical properties of the gas-water interface. *J. Phys. Chem. B*, **109**, 21858-21864 (2005).

[19] P. Li, H. Tsuge, Ozone transfer in a new gas-induced contactor with microbubbles. *J. Chem. Eng. Jpn.*, **39**, 1213-1220 (2006).

[20] M. Takahashi, K. Chiba, P. Li, Free-radical generation from collapsing microbubbles in the absence of a dynamic stimulus. *J. Phys. Chem. B*, **111**, 1343-1247 (2007).

[21] Y. Bando, T. Yoshimatsu, W. Luo, Y. Wang, K. Yasuda, M. Nakamura, Y. Funato, M. Oshima, Flow characteristics in cocurrent upflow bubble column dispersed with micro-bubbles. *J. Chem. Eng. Jpn.*, **41**, 562-567 (2008).

[22] K. Yasuda, Y. Wang, K. Haneda, T. Naito, Y. Bando, T. Takeyama, Y. Kawase, Development of airlift bubble column dispersed with micro-bubbles. *Can. J. Chem. Eng.*, **88**, 518-522 (2010).

[23] A. K. Bin, Ozone dissolution in aqueous systems treatment of the experimental data. *Exp. Therm. Fluid Sci.*, **28**, 395-405 (2004).

Chapter 6

Conclusions and future works

6.1 Conclusions

The sonochemical reaction phenomena are studied numerically and experimentally in this thesis. The numerical calculations for ultrasound pressure and flow distribution are carried out. The reaction areas can be predicted by our calculations. The flow distribution explains the reaction performance tendency by the change of the parameters of a sonochemical reactor. In addition, sonochemical reaction performance under irradiation of dual-pulse, the combination of ultrasound and ozone or light in sonocemical reaction has been experimentally investigated. In the following, some major points are summarized.

(Numerical work)

[1] From the studies of the flow distribution in a sonoreactor, it becomes clear that:

- For a sonoreactor with frequency of about 500 kHz, the absorption coefficient is 1 m^{-1}. The flow velocity increases with increase of the acoustic input power and decrease of the plate radius.
- The liquid height influences the flow velocity.
- The increase of flow velocity enhances the sonochemical reaction performance.

[2] From the studies of pressure distribution in a sonochemical reactor, it becomes clear that:

- The acoustic induced fountain decreases the reflection wave.
- The set of reflection plate enhances reaction intensity.
- Superposition of pressure field enhances reaction area and intensity.

(Experimental work)

[3] From the studies of enhancement of sonochemical reaction by dual-pulse ultrasound, it becomes clear that:

- When the pulsed on time is sufficiently long, use of pulsed wave is more efficient

in reaction than continuous wave.

- Enhancement by pulsed wave is ascribed to the increase in ultrasound power diminishing the effect of reaction threshold and the residual acoustical pressure.
- Enhancement by dual-transducer is ascribed to the enlargement of reaction sites.
- Same phase superposition is more efficient in reaction than reverse phase superposition.

[4] From the studies of dynamical properties of iodine release under combination of ultrasound and light irradiations, it becomes clear that:

- The amount of iodine liberated under the combined irradiation of ultrasound and visible light is larger than the sum of that under irradiations of ultrasound and visible light, respectively.
- The ultrasound irradiation can result in the homogenization of the primary light effect in the reaction medium, which may change the kinetics of the photochemical reaction and hence improve the reaction rate and yield.
- The well-mixed condition under ultrasound irradiation is probably the origin of the synergistic effect.

[5] From the operational conditions on 1,4-dioxane degradation by combined use of ultrasound and ozone microbubbles, it becomes clear that

- 1,4-Dioxane degradation by ultrasound and/or ozone microbubbles follows a first-order reaction kinetics.
- A synergistic effect on reaction constant was observed by the combined use of ultrasound and ozone microbubbles. The synergistic effect was ascribed to the observation that the number of OH radicals increased with the sonolysis of ozone.
- The synergistic effect is enhanced nonlinearly with increasing ultrasound input power and ozone concentration.

- The empirical relations between ultrasound, ozone, and reaction constant were established.

6.2 Future works

Due to the complexity of a sonochemical reaction, the current study is only one step in an attempt to understand the mechanisms of this phenomenon. It is still a long way to go to reach a full understanding of this phenomenon. To optimize the sonochemical reactor, several issues need to be addressed in future studies.

The relation between flow velocity and sonochemical reaction performance has been qualitatively investigated, but the quantificational calculation is still unclear. We will try to predict the sonochemical reaction performance due to mixing effect.

The fountain has been set in the calculation geometry. However, the size of fountain should be measured by an experiment. It is necessary to predict the fountain size by a calculation in our future work.

Since the acoustic pressure field can be calculated, the sonochemical reaction performance tendency is able to be predicted qualitatively. The quantificational prediction of sonochemical reaction yield is still unclear. Through the pressure field and cavitation bubble dynamics simulation, it is possible to quantify the reaction yields.

The optimized pulse length has been experimentally checked, and the possible mechanism has been listed, but the mechanism in detail is still unclear. We will check the reaction performance by the change of parameters (frequency and pressure) of ultrasound wave. By the change of optimized pulse length with ultrasound frequency

and pressure, the mechanism in detail can be carried out.

The enhancements of dual-transducer and pulsed wave depend on the transducer positions, ultrasonic power and reaction threshold. However, the numerical calculation of reaction field is difficult with pulsed wave irradiation. The pressure field can be calculated in transient mode, but the evaluation of reaction efficiency in a transient pressure field is still remained a problem. Furthermore, the relation between pulse length and reaction threshold is unclear.

The fluid flow distribution with pulsed wave irradiation should also be investigated in future. By the change of pulsed length and pulsed on time power, the liquid flow effect on pulsed wave irradiation could be made clear.

To enhance the reaction performance by combined use of ultrasound with visible lights, the optimized parameter (ultrasound frequency, light wavelength) for reaction should be investigated in our near future.

The empirical equations have been made to predict the tendencies of reaction yield by the change of ultrasound power and ozone concentration. However, the mechanisms in detail remain unknown. It will be considered in future.

Appendix

A.1. Modeling of pressure and flow distribution in a sonochemical reactor

A.1.1 Pressure distribution (Example of Fig. 3-5(a), Version: Comsol 3.5a)

New→2D→Acoustics Module→Pressure acoustics→Time harmonic analysis→OK

Draw mode:

Draw rectangle/square→Width=0.175, Height=0.163, Base x=0, y=0 (Vessel)

Rectangle/square→Width=0.002, Height=0.075, Base x=-0.002, y=0 (stainless steel)

Rectangle/square→Width=0.002, Height=0.038, Base x=-0.002, y=0.125 (stainless steel)

Rectangle/square→Width=0.179, Height=0.01, Base x=-0.002, y=-0.01 (stainless steel)

Rectangle/square→Width=0.002, Height=0.163, Base x=0.175, y=0 (stainless steel)

Rectangle/square→Width=0.002, Height=0.163, Base x=0.06, y=0 (reflection plate)

The geometry is shown in Fig. A-1.

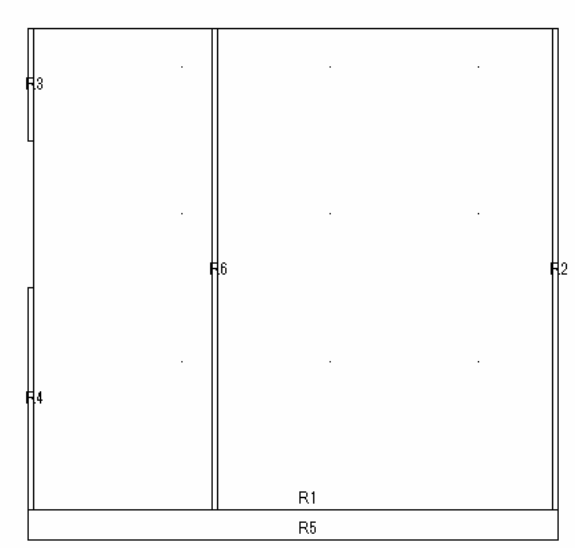

Fig. A-1 Sonochemical reactor geometry

Boundary Mode

Transducer→Normal acceleration a_n=0.85e5 m/s^2 (Color in green).

Liquid surface and boundary of stainless steel→Impedance boundary condition (Fig. A-2 color in red)

Z=1.25*343 Pa·s/m

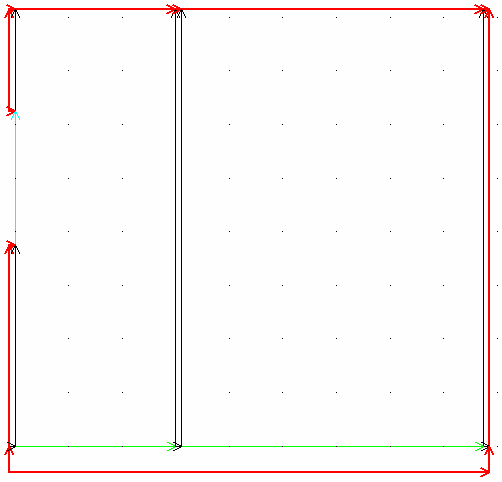

Fig. A-2 Boundary conditions

Subdomain mode

Stainless steel (Include reflection plate) →density 8000 kg/m^3, speed of sound 6000 m/s. (Fig. A-3 color in red)

Solution (water) →density 1000 kg/m^3, speed of sound 1500 m/s, attenuation coefficient 1 m^{-1}. (Fig. A-3 color in blue)

Frequency

The frequency is set as (n+0.5)*λ=propagation length. For frequency near 472 kHz, n=18. Therefore, frequency is set as 462.5 kHz. Physics→scalar variables→freq_acpr →462500 Hz

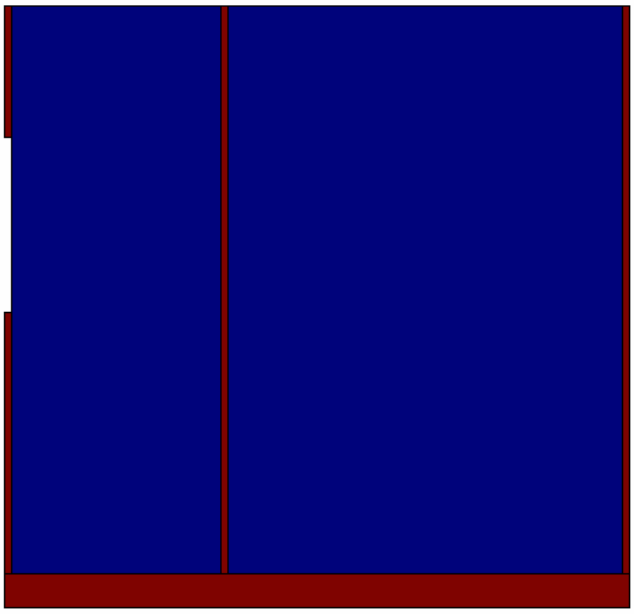

Fig. A-3 Subdomain conditions

Mesh

Mesh→free mesh parameter-Maximum element size: 3e-4 m→remesh

Solve

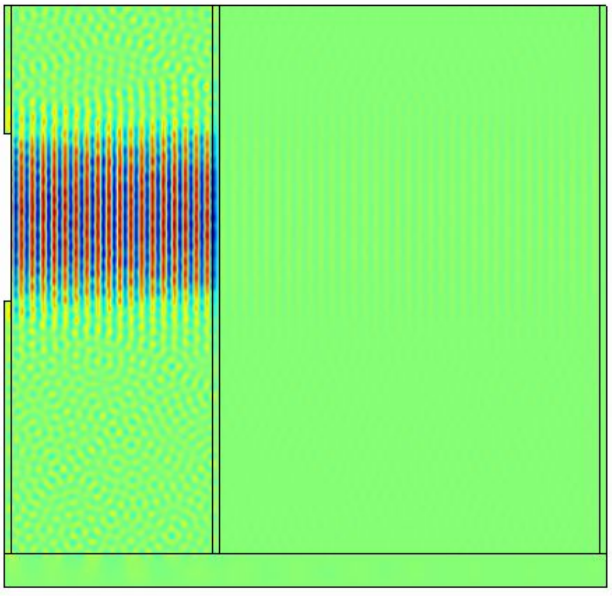

Fig. A-4 Solved result

Postprocessing

Plot parameters→surface→Expression: abs(p), Range: min: 0.8e5, max: 6e5.

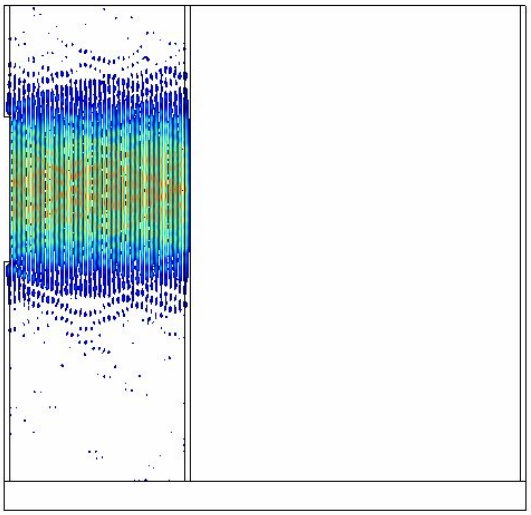

Fig. A-5 The result after postprocessing

Data output

In order to calculate the fluid flow, the pressure data should be used. After we got the pressure distribution data, we continue.

File→Export→post processing data→subdomain→expression: input abs(p). → regular gird→regular grid specification: x points: 100, y points: 100. (The grid is not very important in fluid flow calculation. It is also OK if you input x points: 500, y points: 500).

Go to→general export to file (write to the file name as you like.)

Format of exported data→Coordinate, data.

A.1.2 Fluid flow distribution (Example of Fig. 2-5(a), Version: Comsol 3.5a)

New → Axial symmetry(2D) → COMSOL Multiphysics → Fluid Dynamics → Incompressible Navier-Stokes→Steady→state analysis→OK.

Data import

Option→functions→new→input function name (as you like) →interpolation→Use data from (file) → file name (Generated from the data output) → Use space coordinates as default function arguments (check) →OK.

Draw mode

Draw rectangle/square→Width=0.1, Height=0.1, Base x=0, y=0 (Vessel)

Draw a triangle (fountain) with specify objects (line) →Coordinates (r=0 0 0.012 0, z=0.1 0.12 0.1 0.1).

Shift click the triangle and rectangle, click Union.

Specify a point as (CO3, r=0.025 z=0)

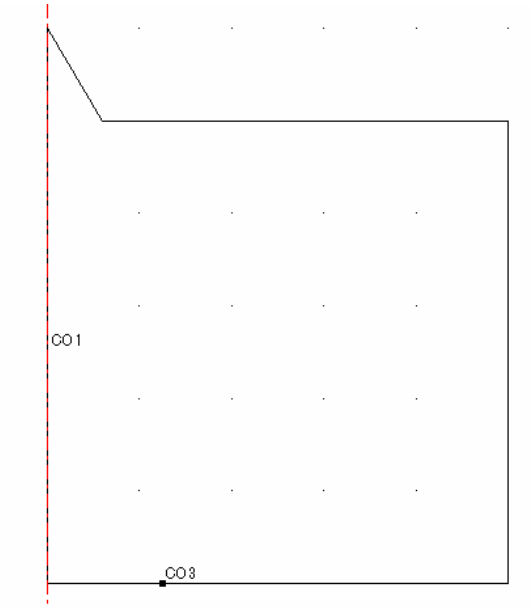

Fig. A-6 Reactor geometry for fluid flow calculation

Boundary conditions

Double click the line in green and red, set as axial symmetry.

Double click the line in aqua blue, set as Wall-slip.

Double click the line in blue, set as Wall-no slip.

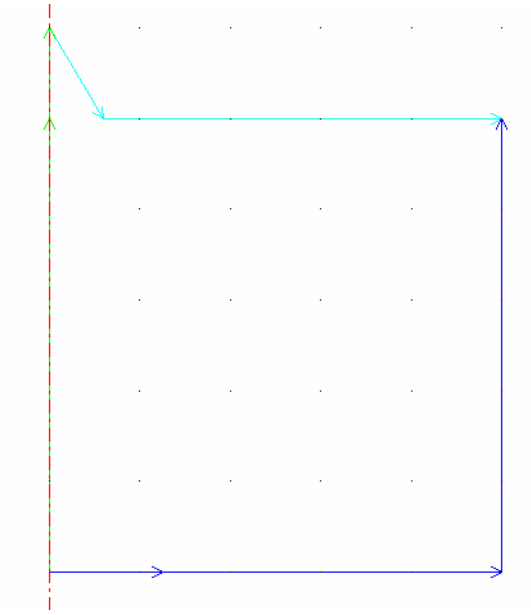

Fig. A-7 Boundary conditions

Subdomain conditions

Solution was set as water (density=100 kg/m^3, viscosity=1e-3 Pa·s, Volume force, r dir=0 N/m^3, Volume force, z dir=1*(the function you defined in import data)^2/(1500^2*1000)).

Mesh

Mesh→free mesh parameter→Maximum element size: 5e-4 m→remesh.

Solve (In solve of fluid flow problem, no convergence is very often to meet. Please decrease the volume force to a very low value until the calculation can be finished, and then increase the volume force, and resolve).

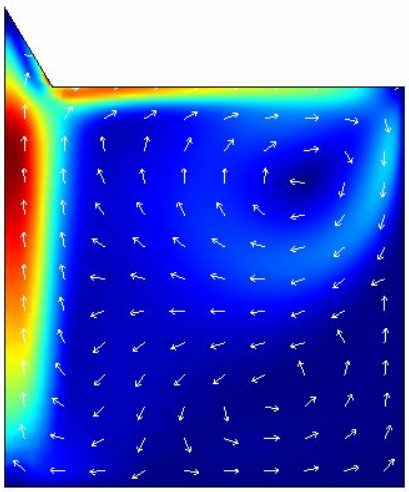

Fig. A-8 The result

List of publications

[1] Z. Xu, K. Yasuda, S. Koda, Numerical simulation of liquid velocity distribution in a sonochemical reactor, *Ultrason. Sonochem.,* (in press).

[2] Z. Xu, K. Mochida, T. Naito and K. Yasuda, Effect of operational conditions on 1,4-Dioxane degradation by combination of ultrasound and ozone microbubbles. *Jpn. J. Appl. Phys.*, (in press).

[3] Z. Xu, K. Yasuda, Enhancement of sonochemical reaction by dual-pulse ultrasound. *Jpn. J. Appl. Phys.,* **50**, 07HE07 1-5, (2011).

[4] K. Yasuda, H. Honma, Z. Xu, Y. Asakura, S. Koda, Ultrasonic atomization amount for different frequencies. *Jpn. J. Appl. Phys.,* **50**, 07HE23 1-5, (2011).

[5] K. Yasuda, D. Kato, Z. Xu, M. Sakka, K. Sakka, Effect of ultrasonic frequency on enzymatic hydrolysis of cellulose. *Jpn. J. Appl. Phys.,* **49**, 07HE08 1-2, (2010).

[6] Z. Xu, C. Ma, J. Xu, X. Liu, Dynamical properties of iodine release in potassium iodine solution under combination of ultrasound and light irradiations. *Ultrason. Sonochem.,* **16**, 475-480, (2009).

Acknowledgements

The completion of my doctoral thesis can be a lonely and isolating experience, yet it is not possible without the personal and practical support of numerous people. Thus my sincere gratitude goes to my parents for their love, support and patience during the last three years.

I wish to thank Prof. Yasuda, for inspiring and encouraging me to pursue a career in sonochemistry studies, and in addition, taking care of me throughout my daily life. I would also like to thank Profs. Koda, Horizoe, Kojima in Nagoya University, and my supervisor during master course, Prof. Liu in Nanjing University, for giving me much advice in research and daily life. I wish to thank Drs. Asakura, Kozuka, and Yasui for giving me much constructive advice in simulation of ultrasound pressure fields.

I would like to thank my colleagues and friends, the all members in Yasuda's and in Horizoe's lab. With their company, I spent a very beatific life in Japan.

At last, I would like to thank China government for giving me this chance to study in Japan.